UiT
THE ARCTIC UNIVERSITY OF NORWAY

Faculty of Science and Technology

Department of Geosciences

Reconstruction of past and present methane emission in the Arctic cold seeps using biogeochemical proxies

—

Haoyi Yao

A dissertation for the degree of Philosophiae Doctor – March 2020

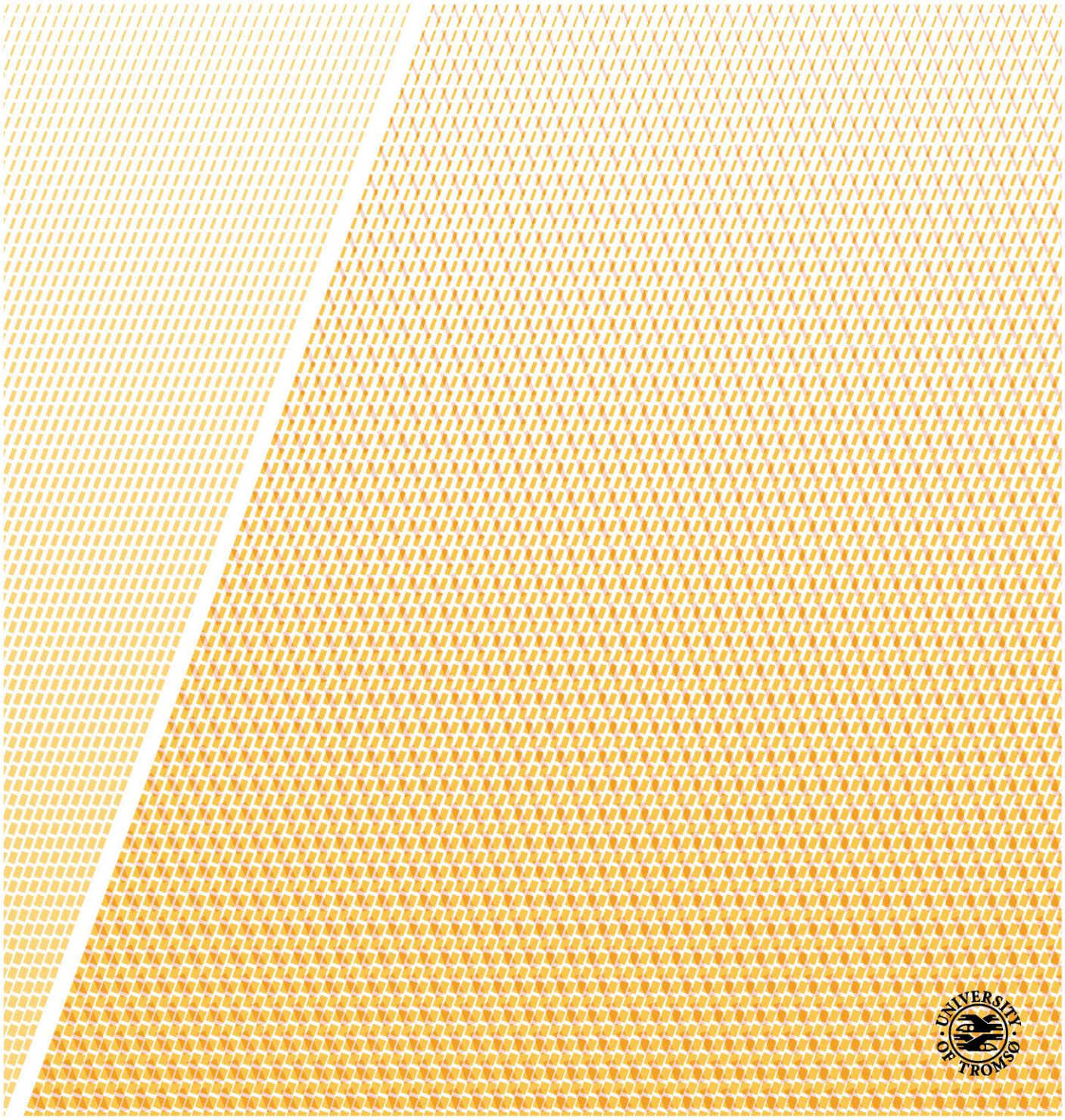

Dissertation for the degree of Philosophiae Doctor

Reconstruction of past and present methane emission in the Arctic cold seeps using biogeochemical proxies

Haoyi Yao

Department of Geosciences, UiT The Arctic University of Norway

Centre for Arctic Gas Hydrate, Environment and Climate (CAGE)

Jan 31st, 2020

Date of public defense: March 26th, 2020

Abstract

Global warming is now highly concerned by society as extreme weather is more often than ever, and the Arctic is experiencing warming twice as fast as the global mean. A large amount of carbon is stored in the forms of methane and methane hydrate in the continental margins worldwide. Methane is the most predominant gaseous compound in natural gas hydrate, which is stable under low temperature and high pressure. With the warming Arctic, methane from gas hydrate dissociation may release into the water column and atmosphere in the future and have positive feedback to the warming as methane is one of the most potent greenhouse gases. Therefore, it is crucial to study and understand the state, the drivers, and the fate of methane hydrate in the Arctic marine sediment.

In this thesis, I study the methane seepage events in both modern and paleo settings. The methane seepage history was studied using authigenic carbonates, foraminifera, molecular fossils such as lipid biomarkers and sedimentary properties. I focus on two methane seepage sites in the Arctic Ocean, Vestnesa Ridge (1200m water depth), and Storfjordrenna (380 meters water depth). The former is characterized by numerous seafloor pockmarks, subseafloor fluid flow system, and gas flares in the water column whereas the latter is characterized by mound features at the seafloor, and gas flares in the water column.

The thesis focused primarily on lipid biomarkers from the anaerobic oxidation of methane (AOM) microbial communities to reconstruct the history of methane seepage. The main research goal is to understand first the cold seep system at the study sites, then the current and paleo drivers of the methane emissions in the Arctic Ocean sediments, whether the discharge was triggered by the warming Arctic or it was a natural process that persists over a long time. Lipid biomarkers is a useful molecular tool to study methane seepage. They are stable over geological time scales and reflect the size as well as the source of the carbon pool based on its concentrations and isotopic signatures. Through these characteristics, they can trace the paleo methane seepage in combination with other methane proxies such as foraminifera and authigenic carbonates. These proxies unravel the history of methane seepage. Lipid biomarkers can also indicate the methane transport modes, diffusion vs. advection when used in combination with other geochemical data in modern settings.

Preface

This doctoral thesis was carried out between June 2015 and February 2020 at the Department of Geosciences at UiT with a nine-month leave. The PhD project was funded by the Research Council of Norway (grant no. 223259) for CAGE, and it is integrated into the methane history working package (WP5) at CAGE. My main supervisor is Prof. Dr. Giuliana Panieri and co-supervised by Prof. Helge Dr. Niemann (NIOZ).

The project aims to use lipid biomarkers from the microbial communities with foraminifera and other geochemical evidence to identify the methane seeping events in modern days and past together. As part of the thesis work, I participated in three CAGE cruises (CAGE 15-6, 16-5 and 17-2), two NORCRUST cruises (P1606 and P1707), and two international cruises together with MARUM (HE450 and MSM57). In these cruises, I have taken roles not only in sampling sediments for my project, but also helping in sampling pore water and onboard analysis, headspace sampling and onboard analysis, and have gained fruitful experience to prepare for and participate in research expeditions.I have participated and presented my research work and findings at several international conferences, including Gordon Research conference for gas hydrate in 2016, Goldschmidt conference in 2017 and 2019, and EGU18 General Assembly. For some of the meetings, I have received travel grants from the Ph.D. school ResClim and UiT. For Goldschmidt 2017, I was the volunteer for the conference for the entire week working on different positions (e.g., in charge of the large lecture room, runners for smaller lecture rooms).

In 2017, I received a ten-month travel grant from UiT, and I visited the University of Plymouth, School of Geography, Earth and Environmental Sciences to learn and apply the sea ice proxy IP_{25}, the rest of the time I visited the University of Basel, Department of Environmental Sciences to finish up the lipid biomarker analyses there.

During the Ph. D., I have duty works in assisting Geo 2008 for three semesters, helping the installation and startup of the stable isotope lab with the new mass spectrometer at UiT. I have served as a reviewer for Eurofleets Plus.

In addition to my thesis project, I have set up a project between CAGE and Oregon State University, Department of Chemistry, Loesgen group to extract and screen natural products from the marine environment for anti-bacterial, anti-cancer activities.

Acknowledgment

I am very grateful to my main supervisor, Giuliana Panieri, for opening up the opportunity for me to start this Ph.D. project. And through all these years, Giuliana was very supportive, providing all she can for me to be able to participate more research cruises, to get the travel grant from the university, to guide me on my research. I started as someone who could not recognize any species in foraminifera, and can pick only eight foraminifera in a day, and finished with identifying the common Arctic species and can pick up to hundreds of foraminifera in a day. Also, my co-supervisor, Helge Niemann, I truly appreciated all the support, guidance, and knowledge you gave me. The dedication and carefulness are something I should always remember to learn from. You are both very engaging and inspiring scientists to work with and to learn from.

I want to thank all the colleagues in CAGE and NGU. Andrea has always been a pioneer in the group to ask experience and advice from. Pierre-Antoine always seems hilarious and can release the pressure. Kasia always has surprising new ideas. Jochen and Aivo at NGU always ask about the progress and share their time to provide guidance and suggestions.

Marta is always there to support and help. I had my first research cruise with Marta and learned all the sampling techniques from you. Also, I would thank Helge and Moritz for hosting the lab use in Basel. The IG lab managers, Trine, Ingrid, and Karina, for providing numerous help on the lab use, equipment, and technical problems. Moreover, all my co-authors providing valuable insights to the manuscripts, and giving me the chance to share my data/knowledge with you.

Last but not least, to my family. Wei-Li, I would not come to Norway without you. I would not get so far in geosciences without you. Helping me to start from scratch in geosciences and taking responsibility for our daughter when I am under stress. It has been eight years since I finished my master thesis, it has been two doctoral programs we have been through, and I thank my parents and my in-laws for understanding the decision and being supportive along the way.

Supervisors

Prof. Dr. Giuliana Panieri

CAGE – Centre for Arctic Gas Hydrate, Environment and Climate,

Department of Geosciences,

UiT- the Arctic University of Norway in Tromsø, Norway

Prof. Dr. Helge Niemann

Department of Marine Microbiology and Biogeochemistry,

NIOZ Royal Institute for Sea Research, and Utrecht University, Texel, The Netherlands

CAGE – Centre for Arctic Gas Hydrate, Environment and Climate,

Department of Geosciences,

UiT- the Arctic University of Norway in Tromsø, Norway

Department of Environmental Sciences,

University of Basel, Switzerland

Table of Contents

1 Introduction

1.1 Methane in marine sediments

It is globally recognized that the Arctic is warming faster than anywhere on our planet. Global warming is now of serious concern by society as we are experiencing extreme weather more often than ever (Trenberth and Fasullo, 2007; Cohen et al., 2014). A huge amount of carbon is stored in the forms of methane and methane hydrate in the continental margins worldwide (Judd and Hovland, 2007). Gas hydrate is an ice-like substance formed primarily with methane gas and water in a clathrate structure. It is stable under low temperature and high pressure. With the continuous warming in the Arctic Ocean, methane may release into the water column and atmosphere in the future and then have further positive feedback to the warming.

Methane is concerned as a powerful greenhouse gas; the greenhouse effect is 25 times stronger (traps 25 times more heat per mass unit) than that of carbon dioxide in a 100-year time frame (Lelieveld et al., 1998). The atmospheric chemistry of methane: as it controls the concentration of tropospheric hydroxyl radicals, adds to the methane radiative forcing thus amplify the impact of methane emissions (Dlugokencky et al., 2011, Holmes, 2018). The contribution of methane in the atmosphere to the current global warming is estimated to be around 15% (Badr et al., 1991). All these factors make methane plays an essential role in the future climate modeling. At the same time, methane from the methane hydrate reservoirs is also a potential energy source. Marine sediments in the Arctic contain three times more energy-equivalent gas than oil (Gautier et al., 2009).

1.1.1 Methane sources

Methane in marine sediment can be produced by three different processes: thermogenic, microbial, and abiotic. Thermogenic methane formation occurs where complex organic molecule kerogen breaks down by a thermocatalytic reaction, which is part of the petroleum generating process. This thermocatalytic reaction develops deep within the sedimentary basins usually at subbottom depths exceeding 1000 m (Floodgate and Judd, 1992; Judd, 2004). Thermogenic methane formation requires temperatures above 80 °C and is the dominant process at temperatures above 150 °C (Clayton, 1991). Microbial methane is produced by methanogenic archaea biologically via methanogenesis (Kvenvolden and Rogers, 2005). Microbial methane formed by reducing CO_2 is the primary microbial process for most methane

formed in marine sediments, which is produced through the remineralization of sedimentary organic carbon (Whiticar, 1999). The rain of phytoplankton to the seafloor in highly productive areas and terrestrial sediment from the continents provide the organic carbon for methane formation to the sediment. The less common microbial methane production process utilizes acetate fermentation; because sulfate-reducing bacteria also use acetate as a substrate, so it is more competitive for acetate to be available for methanogenesis. The temperature for methanogenesis is between 35 °C and 45 °C and can be up to 60 °C (Ferry and Lessner, 2008). As a result, methanogenesis occurs at shallower sediment where organic matter is higher compared to the thermogenic formation in deeper subsurface (Judd, 2000). The least common way of methane formation is abiotic methane through magmatic and gas-water-rock reactions. This methane formation pathway is very rarely observed and poorly understood (Etiope and Sherwood Lollar, 2013). One of the known reactions for abiotic methane formation is Fischer-Tropsch reaction where CO_2 or CO with H_2 and metal catalysts are involved.

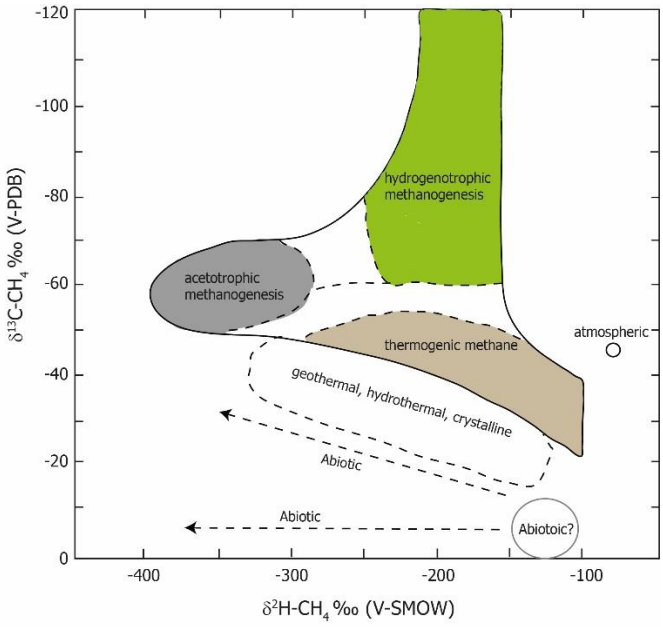

Figure 1. From Whiticar 1999 (modified). Schematic differences between carbon and hydrogen isotopes of different methane formation.

The efficient way to identify the sources of methane is through the isotopic signatures of the methane carbon and hydrogen (Figure 1). During the methane formation, the kinetic isotope effect changes the isotopic composition of the product methane (Judd and Hovland, 2007). The three known methane formation pathways can be differentiated by their stable carbon and hydrogen isotopic signatures, and the relative proportion of methane to other higher

hydrocarbons (i.e., ethane, propane, and butane) (Whiticar, 1999). Extensive isotope fractionation during the microbial methane formation process resulted in a very depleted value of the methane carbon isotope ranging from -100 to -50 ‰. Thermogenic methane carbon is generally enriched in ^{13}C compared to the microbial methane carbon; this is because the precursors are also more enriched in ^{13}C, a smaller isotope fractionation and a higher reaction temperature are involved. Abiotic methane is believed to be the most enriched in ^{13}C with $\delta^{13}C$ values above -25 ‰ (Etiope and Sherwood Lollar, 2013).

1.1.2 Methane sinks in the marine environment

Within the marine sediments, the most persistent biochemical sink of methane is through anaerobic oxidation of methane (AOM) (Barnes and Goldberg, 1976). AOM is carried out by a consortium between methanotrophic archaea and sulfate-reducing bacteria (Knittel and Boetius, 2009), which couple the methane oxidation strongly with sulfate reduction (Reeburgh, 2007). This AOM microbial consortia is estimated to consume up to 80-90 % of the methane produced in the sediment and is termed as the biofilter of methane (Figure 2).

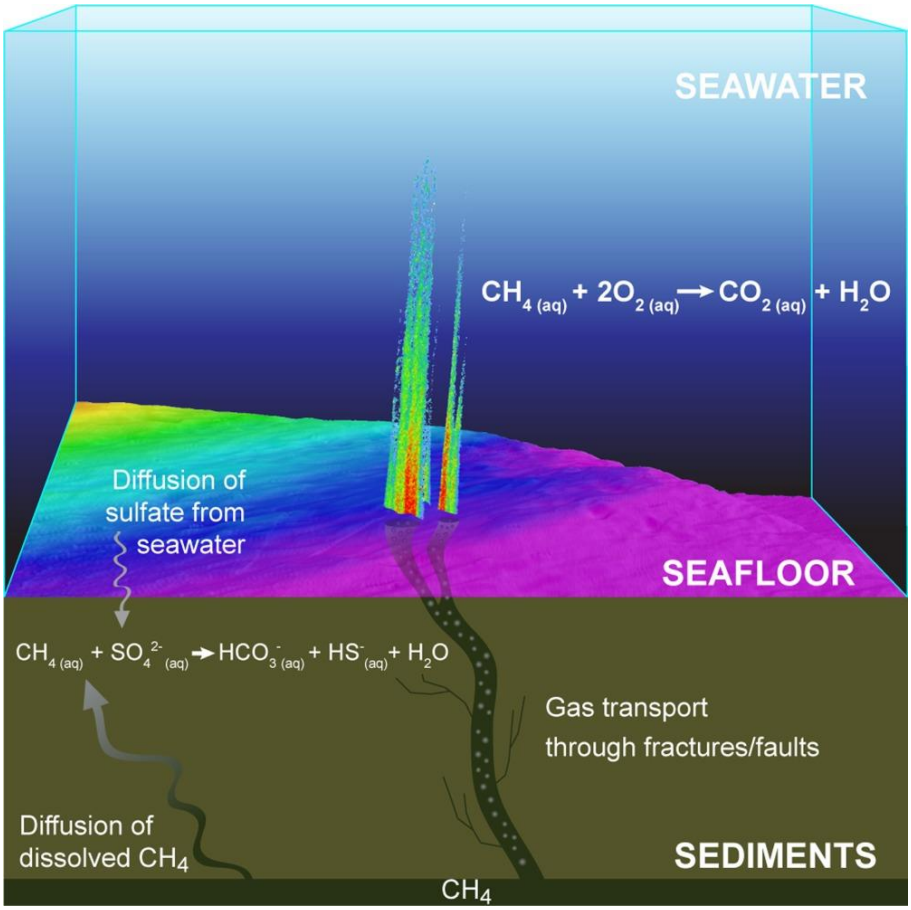

Figure 2. Methane sinks in marine sediments and water column. Figure from James et al., 2016.

AOM is highly efficient when methane is transported by diffusion (Joye et al., 2004). On the other hand, only about 20% of the methane is consumed by AOM at locations where methane migration is dominant by advection (Boetius and Wenzhöfer, 2013). The reduced efficiency of AOM in consuming methane at sites with high advective fluxes is due to that, during the advection, most methane is transported in the form of gas bubbles, which is able to bypass the sediment biofilter and eventually be released to the water column.

When AOM is coupled to sulfate reduction, the lower boundary of sulfate reduction zone is termed as sulfate methane transition zone (SMTZ), which can be centimeters (Fischer et al., 2012) to meters (D'Hondt et al., 2002) below the seafloor. The depth of SMTZ can be used to infer the upward methane flux (Borowski et al., 1996): a deeper SMTZ below the seafloor reflects a lower upward methane flux vs. a shallower SMTZ is translated to a high methane flux. Sometimes the SMTZ can be only centimeters below the seafloor (e.g., Treude et al., 2003; Fischer et al., 2012; Yao et al., 2019) that often indicate a very high methane flux.

After the discovery of AOM coupled to sulfate reduction, recent studies have also provided evidence for other electron acceptors coupled to methane oxidation such as Fe/Mn oxides (Beal et al., 2009; Sivan et al., 2014) and nitrite (Ettwig et al., 2010). However, the environmental significance of these novel electron acceptors in marine sediments is yet to be evaluated as the amount of sulfate is of magnitude higher than these other potential electron acceptors. Therefore, the biofilter efficiency of these newly discovered electron acceptors would be much lower than the sulfate-dependent AOM.

Once methane gas bypasses the sediment-water interface and enters the water column, methane can then be oxidized aerobically (MOx) as oxygen becomes available as the electron acceptor (Hanson and Hanson, 1996). There have been relatively fewer measurements of the strength of this sink compared to that of AOM (Valentine and Reeburgh, 2000; Kessler et al., 2011; Mau et al., 2013). In general, the oxidation rates are mostly affected by temperature, pressure, and methane concentration (Scranton and Brewer, 1978). The MOx studies inoculate seawater samples with radioisotope traces to measure the rate at specific sites and times of sampling. The stoichiometry of this reaction also remains unclear. Other than the methane that is consumed through chemical reactions, other physical processes such as bubble-stripping, a process that replaces methane with oxygen and nitrogen during the

bubble ascending in the water column, is another essential sink prevent methane from leaking to the atmosphere (McGinnis et al., 2006).

1.2 Study methane dynamics in marine sediments using proxies

Proxies or 'proxy variables' are sediment geochemical properties that have a close relationship to environmental parameters. Proxies can deliver useful information for reconstructing environmental parameters. They are measurable descriptors for those desired but unobservable environmental variables (Wefer et al., 1999). To reconstruct a past methane emission history, we must turn to proxies as one can no longer observe methane emission in the past. The figure below illustrated the well-established methane proxies we apply and their relationship with regard to the AOM process.

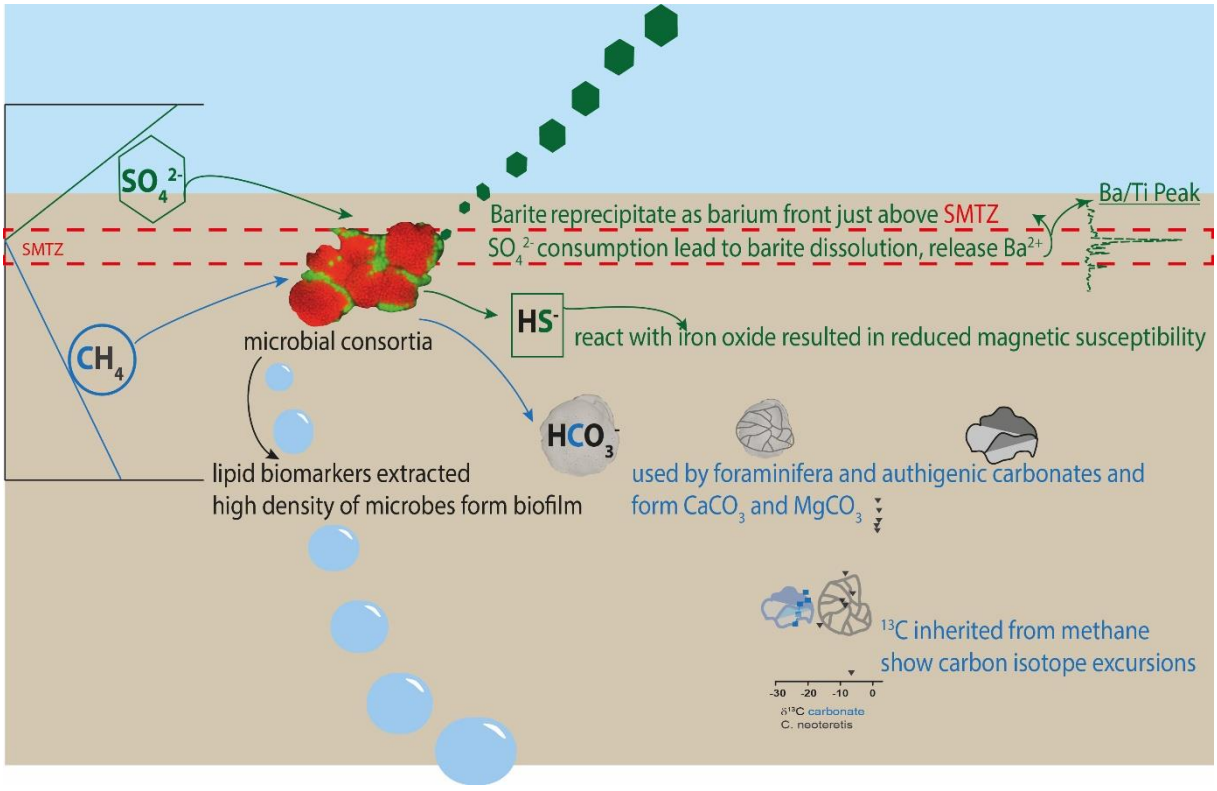

Figure 3. An illustration of proxies related to the AOM process used in my thesis.

1.2.1 Molecular fossils

Previous investigations of lipid biomarkers along with the phylogenetic affiliation of microbial communities revealed that specific biomarker patterns could help identify particular AOM communities (Blumenberg et al., 2004; Elvert et al., 2005; Niemann and Elvert, 2008). The AOM consortia consist of methanotrophic archaea and sulfate-reducing bacteria (SRB). Lipid

biomarkers come from the hydrophobic core of the cell membranes of the microbes. Archaeal cell membranes are mainly comprised of isopranyl glycerol ether lipids, which are contrasting different from the acyl ester lipids found in bacteria (Tornabene et al., 1979). At least three phylogenetically distinct groups of methanotrophic archaea, ANME-1, ANME-2 and ANME-3, have been identified that are qualified for AOM. The corresponding SRB partners of ANME-1 and ANME-2 are two different ecotypes of SRB related to the *Desulfosarcina/Desulfococcus* (DSS) cluster and Seep-1 SRB (Boetius et al., 2000; Knittel et al., 2005). The controlling factors for these different phylogenetic groups include varying sulfate and methane concentrations. It has been observed that at high flux seep sites with significantly higher cell-specific AOM rates are dominated by ANME-2 communities, whereas ANME-1 communities seem to be better adapted to low seepage fluxes and grow within a broader range of temperatures (Blumenberg et al., 2004; Elvert et al., 2005; Nauhaus et al., 2007; Stadnitskaia et al., 2008a; Rossel et al., 2011). Substantial isotopic fractionation occurs during the production of methanotrophic biomass, thus the biomass of methanotrophic archaea involved in AOM is strongly depleted in ^{13}C. In comparison, the corresponding SRB lipids are usually less depleted. It is believed that SRB assimilates methane derived CO_2 autotrophically, whereas archaea utilize methane and assimilate carbon directly from the ^{13}C-depleted source (Wegener et al., 2008). The exact mechanism of the AOM consortia is still in debate (Kellermann et al., 2012; Milucka et al., 2012; Wegener et al., 2015; Scheller et al., 2016).

Among the specific methanotrophic archaeal related lipid biomarkers, higher contents of *sn2*-hydroxyarchaeol relative to archaeol have been reported in most modern ANME-2 dominated seep sites, as well as investigation of lipid biomarkers on carbonates (Blumenberg et al., 2004; Elvert et al., 2005; Niemann and Elvert, 2008; Birgel et al., 2011; Himmler et al., 2015). Abundant strongly ^{13}C-depleted crocetane was also featured in most of the above-mentioned ANME-2 dominated habitats as well. Nearly no crocetane was found in the ancient ANME-1 dominated systems (Niemann and Elvert, 2008; Peckmann et al., 2009; Haas et al., 2010). Therefore, the *sn2*-hydroxyarchaeol/archaeol ratio together with the occurrence of crocetane have been used to contradistinguish the types of archaeal phylogenetic groups mediating AOM (Blumenberg et al., 2004; Niemann and Elvert, 2008). High contents of C16:1ω5 fatty acid and the presence of cyC17:0ω5 fatty acid along with a low ratio of *ai*C15:0 fatty acid relative to *i*-C15:0 fatty acid is attributed to the Seep-1 SRB partner associated with ANME-2

(Niemann and Elvert, 2008). Compound-specific isotopes of the specific archaeal lipid biomarkers can provide more information on the phylogenetical group, as ANME-1 shows less fractionation between the source methane and their lipid biomarkers' carbon isotope (Niemann and Elvert, 2008).

Therefore, the lipid biomarkers of the AOM microbial community can provide useful insight into both modern and paleo methane seepage. Lipid contents, distribution patterns, and compound-specific carbon isotopes of these archaeal and SRB molecular fossils, in combination with other proxies, can be used to differentiate engaged microbial communities and to constrain seepage intensity (Haas et al., 2010; Birgel et al., 2011).

1.2.2 Methane derived authigenic carbonates (MDAC)

AOM is also closely related to carbonate formation at shallow depths beneath the seafloor, as one product of the AOM process is bicarbonate. Bicarbonate can increase alkalinity and form authigenic carbonates as aragonite, calcite, and dolomite depending on the cation (i.e. Mg^{2+}, Ca^{2+}) concentrations. These three are the main carbonate phases associated with methane seeps; the mineralogy correlated to the predominant pore water cation composition at the depth of formation(Burton, 1993; Ferrell and Aharon, 1994; Bohrmann et al., 1998) and can also provide some insight into the precipitating environment. For example, the aragonites are believed to be formed at high sulfate concentrations while the high sulfate would inhibit calcite formation (Bohrmann et al., 1998; Aloisi et al., 2000). Seep carbonates serve as a good chemical archive for methane seepage. They are characterized by negative $\delta^{13}C$ values often below -30 ‰ (Peckmann and Thiel, 2004), which are inherited from ^{13}C-depleted methane, reflecting their light carbon sources (Claypool and Kaplan, 1974; Whiticar, 1999). The $\delta^{18}O$ of the seep carbonates can also reveal information about the precipitating environment. In the sediments containing gas hydrate, hydrate dissociation would produce an elevated $\delta^{18}O$ signature in the seep carbonate (Bohrmann et al., 1998; Aloisi et al., 2000; Bohrmann et al., 2002). Seep carbonate serves as suitable housing for the AOM microbial communities, lipid biomarkers extracted from the carbonates along with other biogeochemical information can shed some light on the methane seepage at the time of carbonate precipitation.

1.2.3 Foraminifera

Foraminifera are single-cell protists with calcified shells or tests. They have pseudopods, fine strands of cytoplasm, and live in the marine domain (Sen Gupta, 2003). Foraminifera are abundant as fossils for the last 540 Ma. Foraminifera can be found in all marine settings, from the cold seeps to hot vent. Some of them live in the water column floating freely, these are known as planktonic foraminifera. The others live on the seafloor (epibenthic) or in the sediments pore space (infaunal), these are known as benthic foraminifera. Their species assemblages, especially the benthic ones, can be very particular and provide information about the environment they live in (Horton, 1999; Todo et al., 2005). Depending on the species, foraminifera develop different chambers of their calcified shells (tests) when they grow. The shell can consist of calcite or aragonite and/or organic compounds (Bentov and Erez, 2006; de Nooijer et al., 2014). Because foraminifera are everywhere in the marine realm, they are one of the most essential biological proxies to study the paleoenvironment (Armstrong and Brasier, 2005).

Foraminifera have been used as geochemical proxies to reconstruct the paleo seepage at different locations such as Cascadian margin Pacific Ocean (Rathburn, 2000; Rathburn et al., 2003; Hill et al., 2003; Hill et al., 2004; Bernhard et al., 2010), Blake ridge Atlantic Ocean (Panieri and Sen Gupta, 2008), the Mediterranean (Panieri, 2006) and Vestnesa Ridge (Schneider et al., 2018). Foraminifera have also been studied in modern seep settings to explore their biological response to methane (Bernhard et al., 2010; Bernhard and Panieri, 2018), as well as the origination of changes in stable isotope composition of their tests (Rathburn et al., 2003; Torres et al., 2003b; Panieri et al., 2009).

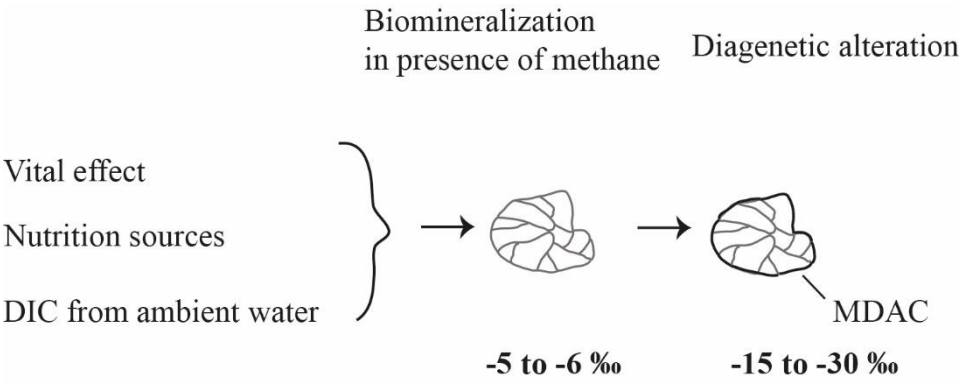

Figure 4. Modified from Schneider et al., 2019

The $\delta^{13}C$ of planktonic foraminifera in a standard marine setting without methane discharge range between -0.5 to 0.5 ‰ in the Barents sea (Knies and Stein, 1998). The $\delta^{13}C$ of benthic foraminifera, such as *C. neoteretis,* in a typical marine environment absent of methane seepage range between 0 to -1.15 ‰ (Wollenburg et al., 2001). More depleted carbon isotopic excursions in modern and fossil foraminiferal tests have been interpreted as a result of methane influence, and have been used to imply the strong ^{13}C-depletions in the tests are associated with ^{13}C-depleted methane. (Kennett, 2000; Hill et al., 2003; Panieri et al., 2009; Martin et al., 2010; Panieri et al., 2014).

The variations and extent of negative excursion in $\delta^{13}C$ of foraminiferal tests at the seep sites are likely the combined outcome of four aspects (Figure 4). Species-specific vital effects, nutrition sources as the ingestion of ^{13}C-depleted AOM microbes (archaea or bacteria) the foraminifera may feed on (Rathburn, 2000; Panieri, 2006; Bernhard and Panieri, 2018), calcification using a ^{13}C-depleted DIC (primary), and diagenetic alteration of the foraminiferal tests.

Vital effect based on the species differences can account for 1-2 ‰ of the carbon isotopic values of the foraminiferal shells (Urey et al., 1951; McCorkle et al., 1990; Mackensen et al., 2006). Foraminifera are attracted to rich organic and microbial food, and some foraminifera were found to prefer the seep-associated microbes (Panieri et al., 2009; Martin et al., 2010). Nonetheless, the nutrition sources can contribute only up to 5-6 ‰ of the negative $\delta^{13}C$ values (Hill et al., 2003).

Primary biomineralization, foraminifera developing their shells with the depleted DIC produced by AOM is suggested to be another factor that may contribute to the negative values of foraminiferal tests. Some research show that living *Cibicides wullerstorffi*'s test become depleted in a culturing experiment with methane-derived DIC, implying the test biomineralization takes place in the presence of methane-derived DIC (Wollenburg et al., 2015). Others have doubts that biomineralization can not occur during seepage as the equilibrium between foraminifera and porewater DIC is not reached (Rathburn et al., 2003; Torres et al., 2003b; Herguera et al., 2014).

The most substantial influence on the negative carbon excursion of foraminiferal test is the diagenetic alteration of the tests under the methane influence (Rathburn, 2000; Rathburn et

al., 2003; Hill et al., 2003; Torres et al., 2003b; Panieri, 2006; Panieri et al., 2009; Panieri et al., 2014; Panieri et al., 2017b; Schneider et al., 2017; Schneider et al., 2018). The ^{13}C-depleted bicarbonate produced during AOM can precipitate not only as authigenic carbonates concretions (Aloisi et al., 2002; Reitner et al., 2005) but also on the foraminiferal shells. Once dead, both benthic and planktonic species can record the ^{13}C signature from the AOM process by acting as a 'template' for authigenic carbonate to precipitate coating layers on (Panieri et al., 2016; Panieri et al., 2017b; Schneider et al., 2017). Such coating carbonate precipitation at the SMTZ cumulatively added a second or third layer of ^{13}C-depleted carbon to the foraminiferal tests is termed as diagenetic alteration (Schneider et al., 2017). These coating layers usually exhibit different states of shell preservation and very depleted $\delta^{13}C$ values up to -20 ‰ (Panieri et al., 2016; Panieri et al., 2017b; Schneider et al., 2017). Both *C. neoteretis* and *N. pachyderma* are excellent templates for the authigenic carbonate formation (Panieri et al., 2017). As a result of multiple coating layers, the diagenetic alteration of foraminiferal tests can cause a much more profound depleted $\delta^{13}C$ signal (Torres et al., 2003b; Hill et al., 2004; Panieri et al., 2009; Martin et al., 2010; Schneider et al., 2017).

1.2.4 Sediment properties

The sediments experienced active methane seepage collect diagenetic overprints as a result of the AOM process. The products of AOM, bicarbonate (HCO_3^-) is consumed in ambient DIC, carbonate precipitation, and foraminifera shell. The other product of AOM is hydrogen sulfide (HS^-), which also increase alkalinity, and can react with iron (II) in the pore water and yield paramagnetic pyrite (FeS_2) (Canfield and Berner, 1987; Peckmann et al., 2001; Riedinger et al., 2006; Dewangan et al., 2013). At the same time, metastable greigite (Fe_3S_4) can form during the pyritization process as a precursor to pyrite (Hunger and Benning, 2007). Both the paramagnetic authigenic pyrite and ferromagnetic greigite can then reduce the magnetic susceptibility of the original sediment magnetic properties.

1.2.5 Others

Other common proxies such as barite formation at the base of SMTZ, dense benthic macrofaunal communities, and AOM biofilm appearance are also used for tracing the methane seepage in combination with the previously discussed proxies.

Briefly, in the sulfate depletion zone below the SMTZ, barite is destabilized and dissolved. Barite can re-precipitate above the SMTZ as sulfate become available again, as the fluid migrates upwards, the barite formation at the base of SMTZ is known as 'barite front' (Torres et al., 1996; Dickens, 2001; Torres et al., 2003a; Solomon and Kastner, 2012). The barite front can be detected with geochemical analysis of barium concentration in both sediment and pore water (Kasten et al., 2012), a simplified way of identifying barite front is from the Ba/Ti ratio or Ba counts of XRF scan of the sediment cores (Sauer et al., 2016). Discovery of a discrete shell bed dominated by Vesicomydae (Phreagena, Isorropodon) at Vestnesa Ridge was interpreted as a high flux seepage episode (Ambrose et al., 2015; Schneider et al., 2018). The seepage not only supports elevated macrofauna biomass, but high methane flux can also support elevated AOM microbial biomass (Yao et al., 2019). In unusual cases, the biomass accumulated so much that form biofilm, which is rarely observed (Briggs et al., 2011; Gründger et al., 2019), but the presence of biofilm is very reliable and serve as a direct piece of evidence for AOM and thus methane seepage.

1.3 Study areas

1.3.1 Vestnesa Ridge

Vestnesa Ridge (79 °N, 5-7 °E, Figure 5), northwest of Svalbard, is one of the northernmost hydrate reservoirs. The water depth is 1200 to 1300 meters, and the ridge is a 100 km long sediment drift on the eastern Fram Strait. Fram Strait was the only deep-water gate to the Arctic Ocean, and it was opened during the late Oligocene to Miocene. The final opening of Fram Strait during the late Miocene (Jakobsson et al., 2007; Knies et al., 2014) led to the development of over 2 km thick sediment accumulation at the eastern segment of the ridge. Moreover, the shallow stratigraphy consist of contourite, turbidite and hemipelagic sediments have been worked by the ocean bottom currents (Howe et al., 2008).

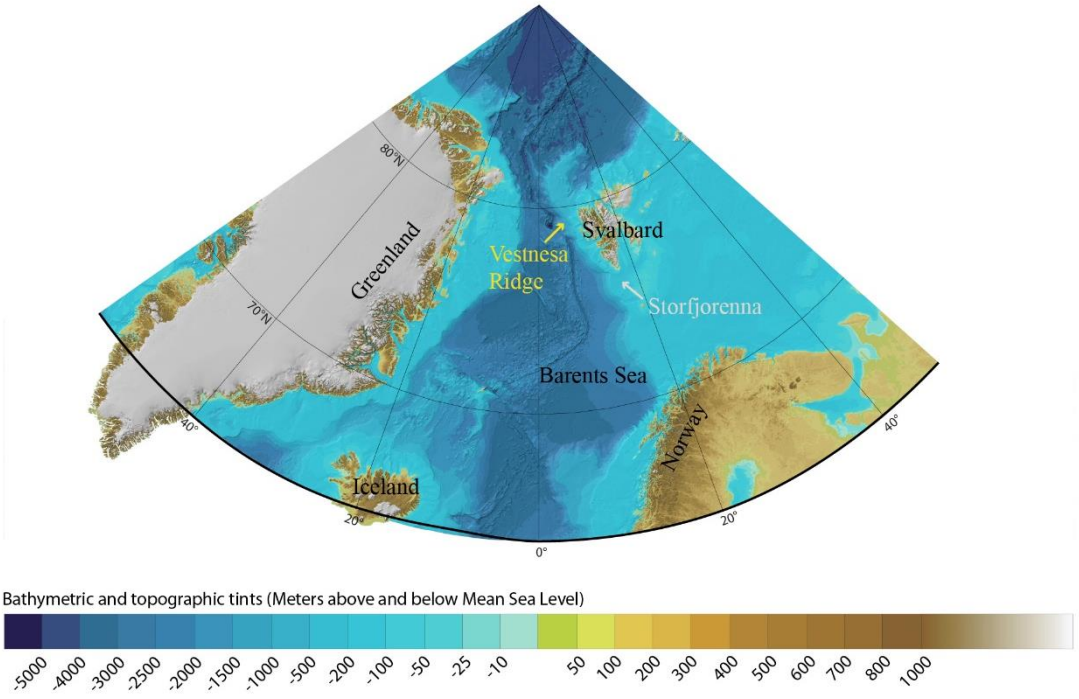

Figure 5. An overview map of the Arctic Ocean with the location of two study areas: Vestnesa Ridge and Storfjordrenna, image section from IBCAO3.0 (Jakobsson et al., 2012).

Since the discovery of pockmarks, the semi-circular seafloor depressions, by Vogt et al. (1994, 1999) in Vestnesa Ridge, the area was mapped thoroughly and well-studied by variously geophysical approaches. Pockmarks are formed under vigorous gas and fluid seepage in unconsolidated sediments (Judd and Hovland, 2007). In addition to the pockmarks as morphological evidence, the eastern segment of Vestnesa Ridge is also characterized by up to 900 m high gas bubble streams (or termed as hydroacoustic flares) in the water column (Smith et al., 2014; Panieri et al., 2017a) (Figure 6) and acoustic chimneys in the sediments from the seismic data as gas migration pathways. It is suggested the methane seepage in Vestnesa was driven by a rare bottom-up mechanism, where heat from the nearby mid-ocean ridge system perturbs the gas hydrate stability after the investigation of the local seismic (Bünz et al., 2012). The fluid and gas migration from deep hydrocarbon reservoirs toward the seafloor has occurred since the early Pleistocene (Knies et al., 2018).

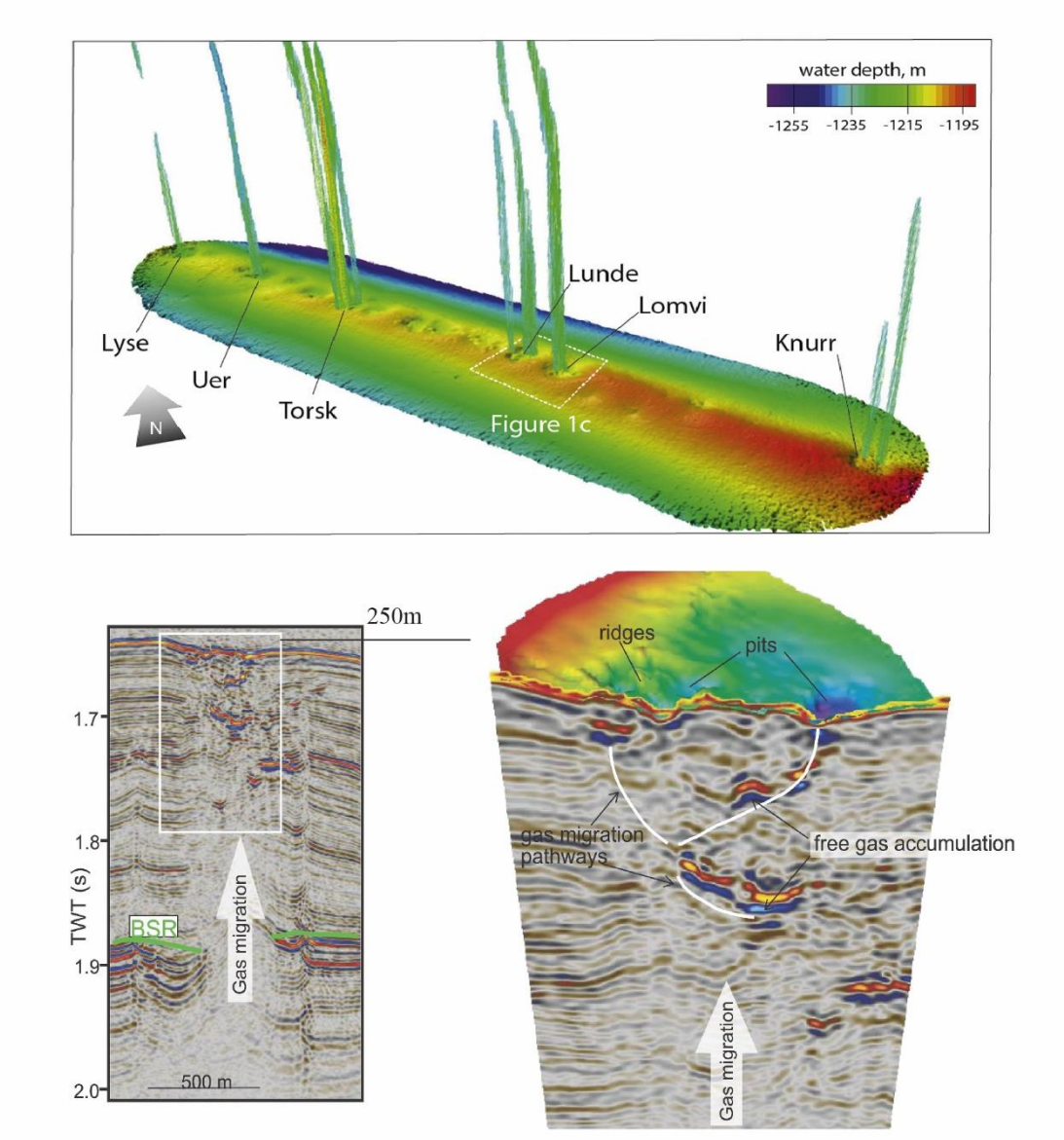

Figure 6. Seafloor bathymetry of the eastern section of Vestnesa Ridge, with gas flares emitting to the water column(above); gas migration pathway and BSR in the seismic data (left below); Seismic profile outlining vertical gas migration pathway and acoustic anomalies beneath Lomvi pockmark (right below). Figures from Panieri et al., 2017a.

Vestnesa Ridge hosts a very complex fluid system from the deep hydrocarbon reservoirs (Petersen et al., 2010; Bünz et al., 2012; Plaza-Faverola et al., 2015; Panieri et al., 2017a). The ridge actively releases methane from seafloor only along the eastern segment of the ridge (Bünz et al., 2012; Plaza-Faverola et al., 2015; Panieri et al., 2017a). It has also been suggested that tectonic stress field controls subsurface faulting and rifting which results in the observed seafloor methane seepage (Plaza-Faverola et al., 2015). Modeling indicated that the onset of the hydrocarbon discharge was the result of the rapid burial of hydrocarbon source after the

onset of Northern Hemisphere glaciations which lead to an increased sediment deposition (Knies et al., 2018). It is this hydrocarbon system from 2.7 Ma ago, that predominantly controls the deep thermogenic methane fluxes and seepage dynamics in Vestnesa Ridge over geological times (Knies et al., 2018).

Recent studies in the area on the $\delta^{13}C$ of foraminifera and methane derived authigenic carbonates correlated the past and ongoing methane seepage and subseafloor methane cycling to the glacio-isostatic adjustment (Schneider et al., 2018; Himmler et al., 2019). New evidence from U-Th dating of methane derived authigenic carbonates also shown that the seepage timing is linked with the wax and wane of the ice sheet (Himmler et al., 2019). Glacio-isostatic adjustments may have triggered the re-activation of tectonic faulting at Vestnesa Ridge and induced the fluid migration pathway for methane transport.

1.3.2 Storfjordrenna Gas hydrate mounds

Storfjordrenna or Storfjorden Trough (76 °N, 15- 16 °E), is located ~50 km south of Svalbard (Figure 5), and the water depth of around 380-400 m (Serov et al., 2017). Storfjorden trough is the second-largest trough in the western Barents Sea and is strongly affected by the ice sheet dynamics. The trough was developed by a dynamic ice stream draining substantial portions of the Barents Sea Ice sheet (BSIS) during the glaciation. Very different from Vestnesa Ridge, Storfjordrenna represents a shallow-water gas hydrate system, which can be directly affected by the bottom water warming and pressure changes induced by ice sheet retreatment (Serov et al., 2017). Indeed, ice sheet modeling suggests that Storfjordrenna was covered by grounded ice up to 2 km in thickness from 33 Ka to 19 Ka BP (Patton et al., 2017) After the deglaciation, relaxation of the underlying lithosphere leads to the glacio-isostatic adjustments which are still happening today (Auriac et al., 2016).

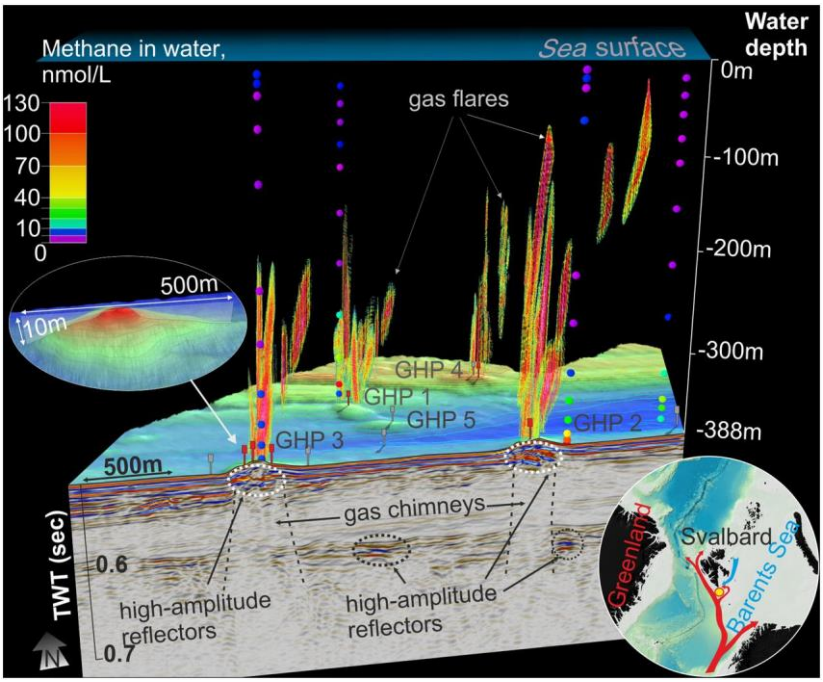

Figure 7. Seafloor morphology, gas chimneys in the seismic, and gas flares emitting to the water column in the Storfjordrenna gas hydrate mounds or gas hydrate pingo (GHP) as denoted in the figure. Figure from Serov et al. (2017).

Several mounds in Storfjordrenna were discovered during 2015 research cruises. These mounds with gas hydrate underneath were named gas hydrate mounds (GHMs) or gas hydrate pingos (GHP, Figure 7) were around 10 m in height and 500 m in width. They feature gas flares above the mounds, and hydrates were recovered from several of them (Hong et al., 2017; Serov et al., 2017). Earlier investigations and modeling suggest that the methane seepage in Storfjordrenna was linked with the ice sheet dynamic as the area was in the glaciated area, and the shallow water depth could be changed due to glacial isostatic adjustment. The gas hydrate stability zone (GHSZ) thickness change as the ice sheet advanced and retreated (Serov

et al., 2017, Figure 8 below).

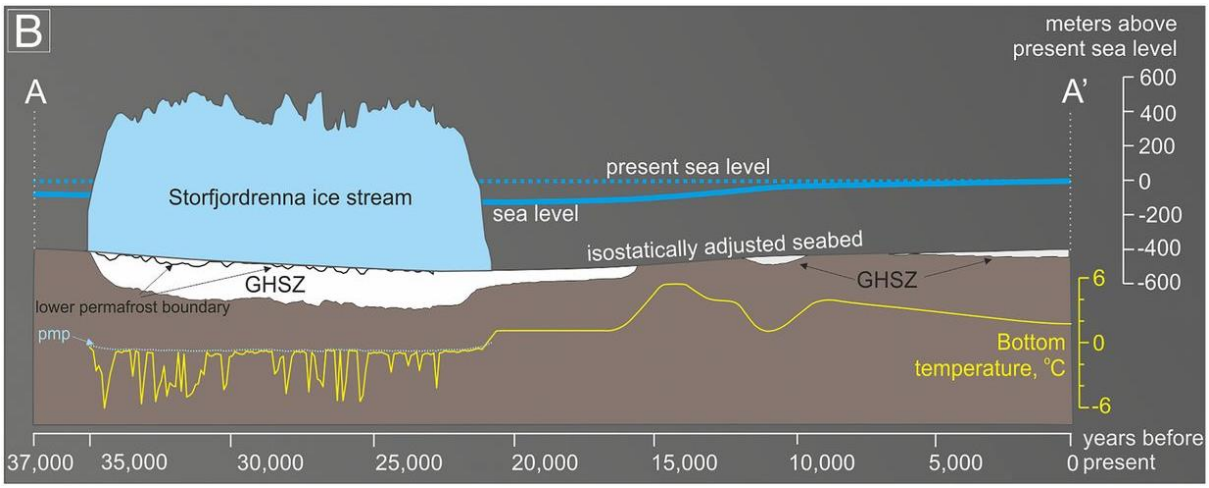

Figure 8. modeling of the relationship between the gas hydrate stability zone and ice sheet coverage in 37,000 year time frame. Figure from Serov et al. (2017).

Seismic data revealed sub-vertical amplitude masking zones beneath the GHMs as the fluid migration pathways (Waage et al., 2019). The upper Paleocene-Eocene and Pliocene-Pleistocene sedimentary rocks offer high-permeability zones for the gas and fluid migration. Waage et al (2019) observed a clear relationship between the thermogenic methane system in Storfjordrenna GHMs and the regional fault system, which could potentially establish a typical scenario of fault-controlled methane migration across the whole Svalbard- Barents Sea margin.

1.4 Methodology

1.4.1 Core collection and sediment properties

In this thesis, the sediment cores were collected from three CAGE cruises CAGE 15-2, CAGE 15-6, CAGE 16-5 (all cruise reports are accessible from the CAGE website)and an NGU cruise P1606. The gravity cores were collected in Storfjordrenna gas hydrate mounds 3 (active) and 5(inactive). Upon recovery of the cores, they were cut into 1m sections, split longitudinally into working and archive halves. Subsamples for stable isotope analyses of foraminifera and authigenic carbonates, lipid biomarker and radiocarbon dating were sampled onboard in the working half. The archive half was stored at 4 °C for sedimentary XRF and MSCL scanning onshore at UiT Geolab. The multi-cores from Vestnesa Ridge were collected by the multicorer system. The system was equipped with a MISO (Multidisciplinary Instrumentation in Support of Oceanography, Woods Hole Oceanographic Institution) towcam. Each deployment collect six paralleled cores at most (Panieri et al., 2015;Panieri et al., 2017a). Among the six cores, one was assigned for porewater analyses, and the two adjacent cores were subsampled for lipid biomarker and headspace gas analyses, respectively. A push core was collected during cruise P1606 using the remotely operated vehicle (ROV) Ægir with a video survey (Yao et al., 2019).

Sedimentary property measurements such as magnetic susceptibility, XRF, and X-ray scanning were done at UiT Geolab on the archive half. Magnetic susceptibility was acquired in 1 cm interval using a GeoTek Multi-Sensor Core Logger (MSCL) on all the gravity cores (except 1520GC). X-ray fluorescence (XRF) element-geochemical data were attained with an Avaatech XRF Core Scanner at 1 cm resolution. All the archived halves of the sediment cores and archiving multicores were scanned with a GEOTEK X-ray core imaging system (MSCL-XCT 3.0), using an X-ray intensity of 120 kV and a measuring resolution of 1 cm.

1.4.2 Stable isotope of foraminifera tests and carbonates

Foraminiferal and carbonates $\delta^{13}C$ and $\delta^{18}O$ analysis were done at the stable isotope laboratory at UiT using a Thermo Scientific MAT253 Isotope Ratio Mass Spectrometer (IRMS) coupled to a Gasbench II. Studies in this thesis were done on two benthic: *Cassidulina neoteretis* (Seidenkrants 1995), *Melonis barleeanu*s (Williamson 1858), and one planktonic (*Neogloboquadrina pachyderma* (Ehrenberg 1861)) foraminiferal species. These species were

picked due to their high abundance in the study areas after an overview survey of all the foraminiferal samples. Carbonate nodules/crusts were sieved out, grounded into homogeneous powder using a quartz mortar. Foraminiferal tests or carbonate powder were placed in specific vials and flushed with helium gas before five drops of water-free H_3PO_4 were added manually. After equilibration (>3 hours at 50°C), the samples were analyzed on the IRMS. Normalization to the Vienna Pee Dee Belemnite (VPDB) for carbon and oxygen isotopes were done using in-house standards. Analytical precision was better than 0.07 ‰ for $\delta^{13}C$ and 0.08 ‰ for $\delta^{18}O$ by measuring the certified standard NBS-19 repeatedly in the sequence queue.

Carbonate nodules/crusts were grounded and analyzed on a Bruker D8 Advanced diffractometer (Cu Ka radiation in 3-75 ° 2θ range) at NGU (Sauer et al., 2017) for mineralogy. The quantification of the carbonate mineralogical composition phases was modeled using the Rietveld algorithm-based code Topas-4 by Bruker. The correction of the spectrum was made on the main quartz peak, and the displacement of calcite d104 was used to estimate the amount of $MgCO_3$ mole percentage (Goldsmith et al., 1958).

1.4.3 Lipid biomarkers of sediment and carbonates

Sediment lipid biomarkers were extracted and analyzed according to previously reported protocols (Elvert et al., 2003). Briefly, a total lipid extract (TLE) was attained by ultrasonication of ~ 20 g wet sediment samples in four steps using solvents with decreasing polarity: dichloromethane (DCM) / methanol (MeOH) 1 : 2; DCM/MeOH 2 : 1; and only DCM for the last two steps. Carbonate lipid biomarkers were extracted similarly but were washed and acidified by 37% HCl before the TLE extraction.

The TLE was saponified with NaOH, the resulting neutral fraction was extracted with hexane prior to methylation to produce fatty acid methyl esters (FAMEs) for chromatographic analysis. The positions of the double bonds in FAMEs were determined by analyzing the corresponding dimethyl–disulfide adducts (DMDS) (Nichols et al., 1986; Moss and Lambert-Fair, 1989). With pipette column chromatography, the neutral fraction was further separated by solvents with increasing polarity into hydrocarbons, ketones, and alcohols. The alcohol fraction was derivatized to form trimethylsilyl (TMS) adducts for analysis.

The individual lipid compound was analyzed using gas chromatography (GC) (Thermo Scientific TRACE™ Ultra), equipped with a capillary column (Rxi-5ms, 50 m, 0.2mmID, 0.33 µm df), helium gas was used as a carrier gas at a constant flow rate of 1mL min^{-1}. The initial oven

temperature was set to be 50 °C, held for 2 min. Increased to 140 °C at a rate of 10 °C min^{-1}, and held for 1 min. Further increased to 300 °C at 4 °Cmin^{-1}. The final hold time was 63 min to analyze FAMEs and 160 min for the neutral hydrocarbon and alcohol fractions to analyze higher boiling points lipids. Concentrations of the lipids were determined by flame-ionization detection (FID) against internal standards. Unknown compounds were identified with a quadrupole mass spectrometry (QMS) unit (Thermo Scientific DSQ II) at the chromatography periphery. Using the same temperature program, compound-specific stable carbon isotope ratios were determined using a magnetic sector isotope ratio mass spectrometry (Thermo Scientific Delta V Advantage) coupled to a GC setup the same as the above-mentioned specification. $\delta^{13}C$ values are reported with an analytical error of ±1‰.

2 List of scientific contributions

- List of first author scientific paper and manuscripts:

Paper 1:

Yao, H., Hong, W. L., Panieri, G., Sauer, S., Torres, M. E., Lehmann, M. F., Gründger, F., and Niemann, H.: Fracture-controlled fluid transport supports microbial methane-oxidizing communities at Vestnesa Ridge, Biogeosciences, 16, 2221-2232, 10.5194/bg-16-2221-2019, 2019

Paper 2:

Yao, H., Niemann, H., and Panieri, G.: Multi-proxy approach to unravel methane emission history of an Arctic cold seep (submitted to Quaternary Science Reviews)

Paper 3:

Yao, H., Panieri, G., Lehmann, M., Himmer, T., and Niemann, H.: Biomarker and isotopic composition of seep carbonates record environmental conditions in two Arctic methane seeps (to be submitted to Deep Sea Research)

- List of co-authored papers:

Paper 4:

Hong, W. L., Torres, M. E., Carroll, J., Cremiere, A., Panieri, G., Yao, H., and Serov, P.: Seepage from an arctic shallow marine gas hydrate reservoir is insensitive to momentary ocean warming, Nat Commun, 8, 15745, 10.1038/ncomms15745, 2017.

Paper 5:

Köseoğlu, D., Belt, S. T., Smik, L., Yao, H., Panieri, G., and Knies, J.: Complementary biomarker-based methods for characterising Arctic sea ice conditions: A case study comparison between multivariate analysis and the PIP25 index, Geochimica et Cosmochimica Acta, 222, 406-420, 10.1016/j.gca.2017.11.001, 2018.

Paper 6:

Su, G., Zopfi, J., Yao, H., Steinle, L., Niemann, H., and Lehmann, M.F.: Manganese/iron-supported sulfate-dependent anaerobic oxidation of methane by archaea in lake sediments, Limnology and Oceanography, n/a, 10.1002/lno.11354,

Paper 7:

Pape, T., Bünz, S., Hong, W.-L., Torres, M. E., Riedel, M., Panieri, G., Lepland, A., Hsu, C.-W., Wintersteller, P., Wallmann, K., Schmidt, C., Yao, H., and Bohrmann, G.: Origin and Transformation of Light Hydrocarbons Ascending at an Active Pockmark on Vestnesa Ridge, Arctic Ocean, Journal of Geophysical Research: Solid Earth, 125, e2018JB016679, 10.1029/2018jb016679, 2020.

Paper 8:

Dessandier, P.-A., Borrelli, C., Yao, H., Sauer, S., Hong, W.-L., and Panieri, G.: Foraminiferal $\delta^{18}O$ reveals gas hydrate dissociation in Arctic and North Atlantic ocean sediments, Geo-Marine Letters, 10.1007/s00367-019-00635-6, 2020.

Paper 1 deals with the modern setting of the methane seep in Vestnesa Ridge. Three short sediment cores were compared for their methane concentrations, porewater geochemistry, and lipid biomarkers. The X-ray image revealed the presence of a mini-fracture in one of the cores. Our investigation revealed this fracture occurred rather recently and served as the methane gas migration pathway in the sediment.

Paper 2 reports the use of a multi-proxy approach to unravel the methane seepage history in another Arctic gas hydrate reservoir- Storfjordrenna gas hydrate mounds. We used the sedimentary Ba/Ti ratio, the carbon isotope of authigenic carbonates, foraminiferal test, and lipid biomarkers to reconstruct the methane history in Storfjordrenna in relation to the glacial-interglacial cycles. In addition to methane history, we also evaluate the use, the pros and cons of these various methane proxies.

Paper 3 is about the lipid biomarkers in methane derived authigenic carbonates. Herein, we studied the carbonates from both Vestnesa Ridge and Storfjordrenna. The studied carbonate samples were collected both from the seafloor and in the subsurface from drill cores. The mineralogy, stable carbon and oxygen isotopes, lipid biomarkers were investigated on these carbonates to reveal their dominant microbial community and the precipitating environment.

All three papers featured the use of lipid biomarkers from the AOM microbial communities in both modern and fossil settings in the Arctic Ocean. The usage of lipid biomarkers in sediments to refer to the methane seepage in non-Arctic marine sediment has a long history over about 20 years (Hinrichs et al., 1999). The lipid biomarker records in the Arctic are rare, mostly in Haakon Mosby mud volcano (Niemann et al., 2006;Chevalier et al., 2010) compare to other

known methane seep sites such as Gulf of Mexico (Zhang, 2002;Zhang et al., 2003;Pancost et al., 2005;Zhang et al., 2011;Kellermann et al., 2012), Black Sea (Peckmann et al., 2001;Blumenberg et al., 2005;Stadnitskaia et al., 2007;Sollai et al., 2019); and Hydrate Ridge (Birgel et al., 2006;Lipp and Hinrichs, 2009;Kaneko et al., 2013;Elvert et al., 2013).

Lipid biomarkers are a useful molecular tool to study methane seepage. They are stable over geological time scales and reflect the size and carbon source from the concentration and their isotopic signatures. Through these characteristics, they can trace the paleo methane seepage in combination with other methane proxies such as foraminifera and authigenic carbonates, as used in paper 2. It can indicate the transport modes of methane when used in combination with other geochemical data, as used in paper 1. The lipid biomarker pattern can provide information on the responsible AOM microbes as used in all three papers.

In comparison to other molecular tools used to investigate the microbes, lipid biomarkers are more stable than RNA and can indicate the recent lived or living microorganisms through intact polar lipid (Zink et al., 2003;Rossel et al., 2008;Lipp and Hinrichs, 2009)or some signature short-lived lipid biomarkers (Blumenberg et al., 2004;Stadnitskaia et al., 2008b). Lipid biomarkers have advantages such as less prone to degradation and contamination, higher detection limits, and the possibility of automating the whole extraction procedure. It is an excellent way to complement DNA detection in recognizing microbial communities.

The extent of the $\delta^{13}C$ of lipid biomarkers is the result of the carbon source and isotope fractionation (Wegener et al., 2008;Kellermann et al., 2012). That identification of specific lipid biomarkers provide means to identify not only the microbial communities, but also the $\delta^{13}C$ of the compound-specific isotope can indicate potential carbon source, and the process methane involved (methanogenic vs. methanotrophic).

Furthermore, the lipid biomarkers have applications beyond the methane seeps. In the co-authored paper list, paper 5 utilized the lipid biomarkers from diatoms living in the sea ice to reconstruct the sea ice coverage history.

3 Research papers

3.1 Fracture-controlled fluid transport supports microbial methane-oxidizing communities at Vestnesa Ridge (full text in the appendix)

3.2 Multi-proxy approach to unravel methane emission history of an Arctic cold seep (full text in the appendix)

3.3 Biomarker and isotopic composition of seep carbonates record environmental conditions in two Arctic methane seeps (full text in the appendix)

4 Summary and conclusion

The overall objective of this Ph.D. project was to investigate the Arctic Ocean sediment methane seepage history, timing, duration, and possible drivers using lipid biomarkers and foraminifera along with other geochemical data. With this goal, we set out to apply the methodology in two gas hydrate provinces in the Arctic: Vestnesa Ridge, one of the northernmost known active methane seep sites, and Storfjordrenna gas hydrate mounds, a shallow-water gas hydrate site. The main conclusions that draw from this Ph.D. project investigations are as follows:

Using lipid biomarkers and porewater data in the active pockmark at Vestnesa Ridge, we demonstrated a recently opened mini-fracture in the sediment that provides a pathway for methane gas transport in advective mode, and therefore facilitating the development of an active AOM community. Mini-fractures are rarely recognized because the detection is mostly incidental. We highlighted the importance of the mini-fracture network in sediment, their relevance for benthic methane dynamic, and benthic carbon cycling.

Reconstruction of methane seepage history in Storfjordrenna allows us to compare and evaluate the use of different proxies, such as sediment properties: magnetic susceptibility, Ba/Ti ratio from sediment XRF scan; $\delta^{13}C$ of foraminifera, $\delta^{13}C$ of authigenic carbonates, mineralogy of carbonates and $\delta^{13}C$ of lipid biomarkers, etc. The signals from these proxies indicate a relationship between the methane seepage and the glacial-interglacial cycles, as our study site is a shallow-water site where the gas hydrate stability zone can be sensitive to isostatic rebound.

The lipid biomarkers in the authigenic carbonates from both study sites further revealed a high methane flux period in the past as the carbonate formation close to the seafloor. The lipid biomarker patterns and the mineralogy of the carbonates are in agreement with the location where the carbonates were found (in core vs. on the seafloor). Lipid biomarkers for aerobic oxidation of methane were also found in these carbonates revealed the close distance between AOM and aerobic oxidation of methane indicate high methane discharge at the study site may release methane bubbles to the water column.

5 Outlook

Other than our main objectives achieved in the Ph.D. project, challenges in the research of methane seep remained. To identify the exact timing of a seepage event, U-Th dating of carbonate is one possible way. The accumulated diagenetic alterations on foraminiferal tests made the dating difficult, incubation of foraminifera (with methane and microbes) and modeling of the authigenic carbonate growth (by weighing the weight differences) from the incubation result could shed some light into the time frame of the diagenetic alteration, and degree of the diagenetic alteration.

In the lipid biomarkers line, as recently discovered, more electron acceptors such as nitrate/nitrite, manganese/iron oxides were able to couple to methane independently from sulfate, some of these microbes were identified by DNA analysis, yet the signature/specific lipid biomarkers have not been identified in these novel methane oxidation modes.

Furthermore, the main goal of methane seep research in the Arctic was to answer questions like, will the methane hydrate dissociation have positive feedback on climate- warming? Will the methane seepage far beneath the seafloor cause Ocean acidification? When will the Arctic methane hydrate dissociate? These questions require a more quantitative rather than qualitative investigation on the carbon storage and carbon cycling in the benthic system.

Reference

Climate Change 2013: The Physical Science Basis. Contribution of Working Group I to the Fifth Assessment Report of the Intergovernmental Panel on Climate Change, Cambridge, United Kingdom and New York, NY, USA, 2018.

Aloisi, G., Pierre, C., Rouchy, J.-M., Foucher, J.-P., and Woodside, J.: Methane-related authigenic carbonates of eastern Mediterranean Sea mud volcanoes and their possible relation to gas hydrate destabilisation, Earth and Planetary Science Letters, 184, 321-338, , 2000.

Aloisi, G., Bouloubassi, I., Heijis, S. K., Pancost, R. D., Pierre, C., Sinninghe Damsté, J. S., Gottschal, J. C., Forney, L. J., and Rouchy, J.-M.: CH4-consuming microorganisms and the formation of carbonate crusts at cold seeps, Earth and Planetary Science Letters, 203, 195-203, 2002.

Ambrose, W. G., Panieri, G., Schneider, A., Plaza-Faverola, A., Carroll, M. L., Åström, E. K. L., Locke, W. L., and Carroll, J.: Bivalve shell horizons in seafloor pockmarks of the last glacial-interglacial transition: a thousand years of methane emissions in the Arctic Ocean, Geochemistry, Geophysics, Geosystems, 16, 4108-4129, 10.1002/2015gc005980, 2015.

Auriac, A., Whitehouse, P. L., Bentley, M. J., Patton, H., Lloyd, J. M., and Hubbard, A.: Glacial isostatic adjustment associated with the Barents Sea ice sheet: A modelling inter-comparison, Quaternary Science Reviews, 147, 122-135, 10.1016/j.quascirev.2016.02.011, 2016.

Badr, O., Probert, S. D., and O'Callaghan, P. W.: Origins of atmospheric methane, Applied Energy, 40, 189-231, https://doi.org/10.1016/0306-2619(91)90057-5, 1991.

Barnes, R. O., and Goldberg, E. D.: Methane production and consumption in anoxic marine sediments, Geology, 279-300, 1976.

Beal, E. J., House, C. H., and Orphan, V. J.: Manganese- and Iron-Dependent Marine Methane Oxidation, Science, 325, 184-187, 2009.

Bentov, S., and Erez, J.: Impact of biomineralization processes on the Mg content of foraminiferal shells: A biological perspective, Geochemistry, Geophysics, Geosystems, 7, 10.1029/2005gc001015, 2006.

Bernhard, J. M., Martin, J. B., and Rathburn, A. E.: Combined carbonate carbon isotopic and cellular ultrastructural studies of individual benthic foraminifera: 2. Toward an understanding of apparent disequilibrium in hydrocarbon seeps, Paleoceanography, 25, n/a-n/a, 10.1029/2010pa001930, 2010.

Bernhard, J. M., and Panieri, G.: Keystone Arctic paleoceanographic proxy association with putative methanotrophic bacteria, Sci Rep, 8, 10610, 10.1038/s41598-018-28871-3, 2018.

Birgel, D., Thiel, V., Hinrichs, K. U., Elvert, M., Campbell, K. A., Reitner, J., Farmer, J. D., and Peckmann, J.: Lipid biomarker patterns of methane-seep microbialites from the Mesozoic convergent margin of California, Organic Geochemistry, 37, 1289-1302, 10.1016/j.orggeochem.2006.02.004, 2006.

Birgel, D., Feng, D., Roberts, H. H., and Peckmann, J.: Changing redox conditions at cold seeps as revealed by authigenic carbonates from Alaminos Canyon, northern Gulf of Mexico, Chemical Geology, 285, 82-96, https://doi.org/10.1016/j.chemgeo.2011.03.004, 2011.

Blees, J., Niemann, H., Wenk, C. B., Zopfi, J., Schubert, C. J., Jenzer, J. S., Veronesi, M., and Lehman, M. F.: Bacterial methanotrophs drive the formation of a seasonal anoxic benthic nepheloid layer in an alpine lake, Limnology and Oceanography, 59, 1410-1420, 10.4319/lo.2014.59.4.141E, 2014.

Blumenberg, M., Seifert, R., Reitner, J., Pape, T., and Michaelis, W.: Membrane lipid patterns typify distinct anaerobic methanotrophic consortia, PNAS, 101, 11111–11116, 2004.

Blumenberg, M., Seifert, R., Nauhaus, K., Pape, T., and Michaelis, W.: In vitro study of lipid biosynthesis in an anaerobically methane-oxidizing microbial mat, Applied and Environmental Microbiology, 71, 4345-4351, 10.1128/AEM.71.8.4345-4351.2005, 2005.

Boetius, A., Ravenschlag, K., Schubert, C. J., Rickert, D., Widdel, F., Gieseke, A., Amann, R., Jørgensen, B., Witte, U., and Pfannkuche, O.: A marine microbial consortium apparentlymediating anaerobic oxidation of methane, Nature, 407, 623-626, 2000.

Boetius, A., and Wenzhöfer, F.: Seafloor oxygen consumption fuelled by methane from cold seeps, Nature Geoscience, 6, 725-734, 10.1038/ngeo1926, 2013.
Bohrmann, G., Greinert, J., Suess, E., and Torres, M.: Authigenic carbonates from the Cascadia subduction zone and their relation to gas hydrate stability, Geology, 26, 647-650, 10.1130/0091-7613(1998)026<0647:ACFTCS>2.3.CO;2 %J Geology, 1998.
Bohrmann, G., Suess, E., Greinert, J., Teichert, B., and Naehr, T.: Gas hydrate carbonates from Hydrate Ridge, Cascadia convergent margin: Indicators of near-seafloor clathrate deposits, Fourth Intern. Conf. Gas Hydrates, 102-107, 2002.
Borowski, W. S., Paull, C. K., and Ussler, W.: Marine pore-water sulfate profiles indicate in situ methane flux from underlying gas hydrate, Geology, 24, 655-658, 1996.
Briggs, B. R., Pohlman, J. W., Torres, M., Riedel, M., Brodie, E. L., and Colwell, F. S.: Macroscopic biofilms in fracture-dominated sediment that anaerobically oxidize methane, Appl Environ Microbiol, 77, 6780-6787, 10.1128/AEM.00288-11, 2011.
Bünz, S., Polyanov, S., Vadakkepuliyambatta, S., Consolaro, C., and Mienert, J.: Active gas venting through hydrate-bearing sediments on the Vestnesa Ridge, offshore W-Svalbard, Marine Geology, 332-334, 189-197, 10.1016/j.margeo.2012.09.012, 2012.
Burton, E. A.: Controls on marine carbonate cement mineralogy: review and reassessment, Chemical Geology, 105, 163-179, https://doi.org/10.1016/0009-2541(93)90124-2, 1993.
Canfield, D. E., and Berner, R. A.: Dissolution and pyritization of magnetite in anoxie marine sediments, Geochimica et Cosmochimica Acta, 51, 645-659, https://doi.org/10.1016/0016-7037(87)90076-7, 1987.
Chevalier, N., Bouloubassi, I., Stadnitskaia, A., Taphanel, M.-H., Lorre, A., Damsté, J. S., and Pierre, C.: Distributions and carbon isotopic compositions of lipid biomarkers in authigenic carbonate crusts from the Nordic margin (Norwegian Sea), Organic Geochemistry, 41, 885-890, 10.1016/j.orggeochem.2010.03.012, 2010.
Claypool, G. E., and Kaplan, I. R.: The Origin and Distribution of Methane in Marine Sediments, in: Natural Gases in Marine Sediments, edited by: Kaplan, I. R., Springer US, Boston, MA, 99-139, 1974.
Clayton, C.: Carbon isotope fractionation during natural gas generation from kerogen, Marine and Petroleum Geology, 8, 232-240, https://doi.org/10.1016/0264-8172(91)90010-X, 1991.
Cohen, J., Screen, J. A., Furtado, J. C., Barlow, M., Whittleston, D., Coumou, D., Francis, J., Dethloff, K., Entekhabi, D., Overland, J., and Jones, J.: Recent Arctic amplification and extreme mid-latitude weather, Nature Geoscience, 7, 627, 10.1038/ngeo2234

https://www.nature.com/articles/ngeo2234#supplementary-information, 2014.
Crémière, A., Lepland, A., Chand, S., Sahy, D., Condon, D. J., Noble, S. R., Martma, T., Thorsnes, T., Sauer, S., and Brunstad, H.: Timescales of methane seepage on the Norwegian margin following collapse of the Scandinavian Ice Sheet, Nat Commun, 7, 11509, 10.1038/ncomms11509, 2016a.
Crémière, A., Lepland, A., Chand, S., Sahy, D., Kirsimäe, K., Bau, M., Whitehouse, M. J., Noble, S. R., Martma, T., Thorsnes, T., and Brunstad, H.: Fluid source and methane-related diagenetic processes recorded in cold seep carbonates from the Alvheim channel, central North Sea, Chemical Geology, 432, 16-33, https://doi.org/10.1016/j.chemgeo.2016.03.019, 2016b.
D'Hondt, S., Rutherford, S., and Spivack, A. J.: Metabolic Activity of Subsurface Life in Deep-Sea Sediments, Science, 295, 2067-2070, 10.1126/science.1064878, 2002.
de Nooijer, L. J., Spero, H. J., Erez, J., Bijma, J., and Reichart, G. J.: Biomineralization in perforate foraminifera, Earth-Science Reviews, 135, 48-58, https://doi.org/10.1016/j.earscirev.2014.03.013, 2014.
Dewangan, P., Basavaiah, N., Badesab, F. K., Usapkar, A., Mazumdar, A., Joshi, R., and Ramprasad, T.: Diagenesis of magnetic minerals in a gas hydrate/cold seep environment off the Krishna–Godavari basin, Bay of Bengal, Marine Geology, 340, 57-70, https://doi.org/10.1016/j.margeo.2013.04.016, 2013.

Dickens, G. R.: Sulfate profiles and barium fronts in sediment on the Blake Ridge: present and past methane fluxes through a large gas hydrate reservoir, Geochimica et Cosmochimica Acta, 65, 529-543, https://doi.org/10.1016/S0016-7037(00)00556-1, 2001.
Dlugokencky, E. J., Nisbet, E. G., Fisher, R., and Lowry, D.: Global atmospheric methane: budget, changes and dangers, Philosophical Transactions of the Royal Society A: Mathematical, Physical and Engineering Sciences, 369, 2058-2072, doi:10.1098/rsta.2010.0341, 2011.
Elvert, M., Boetius, A., Knittel, K., and Jørgensen, B. B.: Characterization of Specific Membrane Fatty Acids as Chemotaxonomic Markers for Sulfate-Reducing Bacteria Involved in Anaerobic Oxidation of Methane, Geomicrobiology Journal, 20, 403-419, 10.1080/01490450303894, 2003.
Elvert, M., Hopmans, E. C., Treude, T., Boetius, A., and Suess, E.: Spatial variations of methanotrophic consortia at cold methane seeps: implications from a high-resolution molecular and isotopic approach, Geobiology, 3, 195-209, 2005.

Elvert, M., Greinert, J., Suess, E., and Whiticar, M. J.: Carbon Isotopes of Biomarkers Derived from Methane-Oxidizing Microbes at Hydrate Ridge, Cascadia Convergent Margin, in: Natural Gas Hydrates, Geophysical Monograph Series, 115-129, 2013.
Etiope, G., and Sherwood Lollar, B.: ABIOTIC METHANE ON EARTH, Reviews of Geophysics, 51, 276-299, 10.1002/rog.20011, 2013.
Ettwig, K. F., Butler, M. K., Le Paslier, D., Pelletier, E., Mangenot, S., Kuypers, M. M. M., Schreiber, F., Dutilh, B. E., Zedelius, J., de Beer, D., Gloerich, J., Wessels, H. J. C. T., van Alen, T., Luesken, F., Wu, M. L., van de Pas-Schoonen, K. T., Op den Camp, H. J. M., Janssen-Megens, E. M., Francoijs, K.-J., Stunnenberg, H., Weissenbach, J., Jetten, M. S. M., and Strous, M.: Nitrite-driven anaerobic methane oxidation by oxygenic bacteria, Nature, 464, 543-548, 10.1038/nature08883, 2010.
Ferrell, R. E., and Aharon, P. J. G.-M. L.: Mineral assemblages occurring around hydrocarbon vents in the northern Gulf of Mexico, 14, 74-80, 10.1007/bf01203717, 1994.
Ferry, J. G., and Lessner, D. J.: Methanogenesis in Marine Sediments, Annals of the New York Academy of Sciences, 1125, 147-157, 10.1196/annals.1419.007, 2008.
Fischer, D., Sahling, H., Nöthen, K., Bohrmann, G., Zabel, M., and Kasten, S.: Interaction between hydrocarbon seepage, chemosynthetic communities, and bottom water redox at cold seeps of the Makran accretionary prism: insights from habitat-specific pore water sampling and modeling, Biogeosciences, 9, 2013-2031, 10.5194/bg-9-2013-2012, 2012.
Floodgate, G. D., and Judd, A. G.: The origins of shallow gas, Continental Shelf Research, 12, 1145-1156, https://doi.org/10.1016/0278-4343(92)90075-U, 1992.
Gautier, D. L., Bird, K. J., Charpentier, R. R., Grantz, A., Houseknecht, D. W., Klett, T. R., Moore, T. E., Pitman, J. K., Schenk, C. J., Schuenemeyer, J. H., Sørensen, K., Tennyson, M. E., Valin, Z. C., and Wandrey, C. J.: Assessment of Undiscovered Oil and Gas in the Arctic, Science, 324, 1175-1179, 10.1126/science.1169467, 2009.
Goldsmith, J. R., Graf, D. L., Chodos, A. A., Joensuu, O. I., and Mcvicker, L. D.: Relation between lattice constants and composition of Ca-Mg carbonates, American Mineralogist, 43, 84-101, 1958.
Gründger, F., Carrier, V., Svenning, M. M., Panieri, G., Vonnahme, T. R., Klasek, S., and Niemann, H.: Methane-fuelled biofilms predominantly composed of methanotrophic ANME-1 in Arctic gas hydrate-related sediments, Sci Rep, 9, 9725, 10.1038/s41598-019-46209-5, 2019.
Haas, A., Peckmann, J., Elvert, M., Sahling, H., and Bohrmann, G.: Patterns of carbonate authigenesis at the Kouilou pockmarks on the Congo deep-sea fan, Marine Geology, 268, 129-136, 10.1016/j.margeo.2009.10.027, 2010.
Hanson, R. S., and Hanson, T. E.: Methanotrophic bacteria, Microbiol Rev, 60, 439-471, 1996.
Herguera, J. C., Paull, C. K., Perez, E., Ussler, W., and Peltzer, E.: Limits to the sensitivity of living benthic foraminifera to pore water carbon isotope anomalies in methane vent environments, Paleoceanography, 29, 273-289, 10.1002/2013pa002457, 2014.
Hill, T. M., Kennett, J. P., and Spero, H. J.: Foraminifera as indicators of methane-rich environments: A study of modern methane seeps in Santa Barbara Channel, California, Marine Micropaleontology, 49, 123-138, 10.1016/s0377-8398(03)00032-x, 2003.

Hill, T. M., Kennett, J. P., and Valentine, D. L.: Isotopic evidence for the incorporation of methane-derived carbon into foraminifera from modern methane seeps, Hydrate Ridge, Northeast Pacific, Geochimica et Cosmochimica Acta, 68, 4619-4627, 10.1016/j.gca.2004.07.012, 2004.
Himmler, T., Birgel, D., Bayon, G., Pape, T., Ge, L., Bohrmann, G., and Peckmann, J.: Formation of seep carbonates along the Makran convergent margin, northern Arabian Sea and a molecular and isotopic approach to constrain the carbon isotopic composition of parent methane, Chemical Geology, 415, 102-117, 10.1016/j.chemgeo.2015.09.016, 2015.
Himmler, T., Sahy, D., Martma, T., Bohrmann, G., Plaza-Faverola, A., Bünz, S., Condon, D. J., Knies, J., and Lepland, A.: A 160,000-year-old history of tectonically controlled methane seepage in the Arctic, Science Advances, 5, eaaw1450, 10.1126/sciadv.aaw1450, 2019.
Hinrichs, K.-U., Summons, R. E., Orphan, V., Sylva, S. P., and Hayes, J. M.: Molecular and isotopic analysis of anaerobic methane-oxidizing communities in marine sediments, Organic Geochemistry, 31, 1685-1701, https://doi.org/10.1016/S0146-6380(00)00106-6, 2000.
Hinrichs, K. U., Hayes, J. M., Sylva, S. P., Brewer, P. G., and Delong, E. F.: Methane-consuming archaebacteria in marinesediments, Nature, 398, 802-805, 1999.
Holmes, C. D.: Methane Feedback on Atmospheric Chemistry: Methods, Models, and Mechanisms, Journal of Advances in Modeling Earth Systems, 10, 1087-1099, 10.1002/2017ms001196, 2018.
Hong, W.-L., Sauer, S., Panieri, G., Ambrose, W. G., James, R. H., Plaza-Faverola, A., and Schneider, A.: Removal of methane through hydrological, microbial, and geochemical processes in the shallow sediments of pockmarks along eastern Vestnesa Ridge (Svalbard), Limnology and Oceanography, 61, S324-S343, 10.1002/lno.10299, 2016.
Hong, W. L., Torres, M. E., Carroll, J., Cremiere, A., Panieri, G., Yao, H., and Serov, P.: Seepage from an arctic shallow marine gas hydrate reservoir is insensitive to momentary ocean warming, Nat Commun, 8, 15745, 10.1038/ncomms15745, 2017.
Horton, B. P.: The distribution of contemporary intertidal foraminifera at Cowpen Marsh, Tees Estuary, UK: implications for studies of Holocene sea-level changes, Palaeogeography, Palaeoclimatology, Palaeoecology, 149, 127-149, https://doi.org/10.1016/S0031-0182(98)00197-7, 1999.
Howe, J. A., SHIMMIELD, T. M., HARLAND, R., and Eyles, N.: Late Quaternary contourites and glaciomarine sedimentation in the Fram Strait, Sedimentology, 55, 179-200, 10.1111/j.1365-3091.2007.00897.x, 2008.
Jakobsson, M., Backman, J., Rudels, B., Nycander, J., Frank, M., Mayer, L., Jokat, W., Sangiorgi, F., O'Regan, M., Brinkhuis, H., King, J., and Moran, K.: The early Miocene onset of a ventilated circulation regime in the Arctic Ocean, Nature, 447, 986-990, 10.1038/nature05924, 2007.
Jakobsson, M., Mayer, L., Coakley, B., Dowdeswell, J. A., Forbes, S., Fridman, B., Hodnesdal, H., Noormets, R., Pedersen, R., Rebesco, M., Schenke, H. W., Zarayskaya, Y., Accettella, D., Armstrong, A., Anderson, R. M., Bienhoff, P., Camerlenghi, A., Church, I., Edwards, M., Gardner, J. V., Hall, J. K., Hell, B., Hestvik, O., Kristoffersen, Y., Marcussen, C., Mohammad, R., Mosher, D., Nghiem, S. V., Pedrosa, M. T., Travaglini, P. G., and Weatherall, P.: The International Bathymetric Chart of the Arctic Ocean (IBCAO) Version 3.0, Geophysical Research Letters, 39, n/a-n/a, 10.1029/2012gl052219, 2012.
James, R. H., Bousquet, P., Bussmann, I., Haeckel, M., Kipfer, R., Leifer, I., Niemann, H., Ostrovsky, I., Piskozub, J., Rehder, G., Treude, T., Vielstädte, L., and Greinert, J.: Effects of climate change on methane emissions from seafloor sediments in the Arctic Ocean: A review, Limnology and Oceanography, 61, S283-S299, 10.1002/lno.10307, 2016.
Joye, S. B., Boetius, A., Orcutt, B. N., Montoya, J. P., Schulz, H. N., Erickson, M. J., and Lugo, S. K.: The anaerobic oxidation of methane and sulfate reduction in sediments from Gulf of Mexico cold seeps, Chemical Geology, 205, 219-238, https://doi.org/10.1016/j.chemgeo.2003.12.019, 2004.
Judd, A., and Hovland, M.: Seabed Fluid Flow: The Impact on Geology, Biology and the Marine Environment, Cambridge University Press, Cambridge, 2007.
Judd, A. G.: Geological Sources of Methane, in: Atmospheric Methane: Its Role in the Global Environment, edited by: Khalil, M. A. K., Springer Berlin Heidelberg, Berlin, Heidelberg, 280-303, 2000.

Judd, A. G.: Natural seabed gas seeps as sources of atmospheric methane, Environmental Geology, 46, 988-996, 10.1007/s00254-004-1083-3, 2004.
Kaneko, M., Naraoka, H., Takano, Y., and Ohkouchi, N.: Distribution and isotopic signatures of archaeal lipid biomarkers associated with gas hydrate occurrences on the northern Cascadia Margin, Chemical Geology, 343, 76-84, 10.1016/j.chemgeo.2013.02.003, 2013.
Kasten, S., Nöthen, K., Hensen, C., Spieß, V., Blumenberg, M., and Schneider, R. R. J. G.-M. L.: Gas hydrate decomposition recorded by authigenic barite at pockmark sites of the northern Congo Fan, 32, 515-524, 10.1007/s00367-012-0288-9, 2012.
Kellermann, M. Y., Schubotz, F., Elvert, M., Lipp, J. S., Birgel, D., Prieto-Mollar, X., Dubilier, N., and Hinrichs, K. U.: Symbiont-host relationships in chemosynthetic mussels: A comprehensive lipid biomarker study, Organic Geochemistry, 43, 112-124, 10.1016/j.orggeochem.2011.10.005, 2012.
Kennett, J. P.: Carbon isotopic evidence for methane hydrate instability during quaternary interstadials, Science, 288, 128-133, 10.1126/science.288.5463.128, 2000.
Kessler, J. D., Valentine, D. L., Redmond, M. C., Du, M., Chan, E. W., Mendes, S. D., Quiroz, E. W., Villanueva, C. J., Shusta, S. S., Werra, L. M., Yvon-Lewis, S. A., and Weber, T. C.: A Persistent Oxygen Anomaly Reveals the Fate of Spilled Methane in the Deep Gulf of Mexico, Science, 331, 312-315, 10.1126/science.1199697, 2011.
Kirschke, S., Bousquet, P., Ciais, P., Saunois, M., Canadell, J. G., Dlugokencky, E. J., Bergamaschi, P., Bergmann, D., Blake, D. R., Bruhwiler, L., Cameron-Smith, P., Castaldi, S., Chevallier, F., Feng, L., Fraser, A., Heimann, M., Hodson, E. L., Houweling, S., Josse, B., Fraser, P. J., Krummel, P. B., Lamarque, J.-F., Langenfelds, R. L., Le Quéré, C., Naik, V., O'Doherty, S., Palmer, P. I., Pison, I., Plummer, D., Poulter, B., Prinn, R. G., Rigby, M., Ringeval, B., Santini, M., Schmidt, M., Shindell, D. T., Simpson, I. J., Spahni, R., Steele, L. P., Strode, S. A., Sudo, K., Szopa, S., van der Werf, G. R., Voulgarakis, A., van Weele, M., Weiss, R. F., Williams, J. E., and Zeng, G.: Three decades of global methane sources and sinks, Nature Geoscience, 6, 813, 10.1038/ngeo1955

https://www.nature.com/articles/ngeo1955#supplementary-information, 2013.
Knies, J., and Stein, R.: New aspects of organic carbon deposition and its paleoceanographic implications along the Northern Barents Sea Margin during the last 30,000 years, Paleoceanography, 13, 384-394, 10.1029/98pa01501, 1998.
Knies, J., Mattingsdal, R., Fabian, K., Grøsfjeld, K., Baranwal, S., Husum, K., De Schepper, S., Vogt, C., Andersen, N., Matthiessen, J., Andreassen, K., Jokat, W., Nam, S.-I., and Gaina, C.: Effect of early Pliocene uplift on late Pliocene cooling in the Arctic–Atlantic gateway, Earth and Planetary Science Letters, 387, 132-144, https://doi.org/10.1016/j.epsl.2013.11.007, 2014.
Knies, J., Daszinnies, M., Plaza-Faverola, A., Chand, S., Sylta, Ø., Bünz, S., Johnson, J. E., Mattingsdal, R., and Mienert, J.: Modelling persistent methane seepage offshore western Svalbard since early Pleistocene, Marine and Petroleum Geology, 91, 800-811, 10.1016/j.marpetgeo.2018.01.020, 2018.
Knittel, K., Losekann, T., Boetius, A., Kort, R., and Amann, R.: Diversity and distribution of methanotrophic archaea at cold seeps, Appl Environ Microbiol, 71, 467-479, 10.1128/AEM.71.1.467-479.2005, 2005.
Knittel, K., and Boetius, A.: Anaerobic oxidation of methane: progress with an unknown process, Annu Rev Microbiol, 63, 311-334, 10.1146/annurev.micro.61.080706.093130, 2009.
Kvenvolden, K. A., and Rogers, B. W.: Gaia's breath—global methane exhalations, Marine and Petroleum Geology, 22, 579-590, 10.1016/j.marpetgeo.2004.08.004, 2005.
Lelieveld, J., Crutzen, P. J., and Dentener, F. J.: Changing concentration, lifetime and climate forcing of atmospheric methane, Tellus B: Chemical and Physical Meteorology, 50, 128-150, 10.3402/tellusb.v50i2.16030, 1998.
Lipp, J. S., and Hinrichs, K.-U.: Structural diversity and fate of intact polar lipids in marine sediments, Geochimica et Cosmochimica Acta, 73, 6816-6833, 10.1016/j.gca.2009.08.003, 2009.
Luff, R., and Wallmann, K.: Fluid flow, methane fluxes, carbonate precipitation and biogeochemical turnover in gas hydrate-bearing sediments at Hydrate Ridge, Cascadia Margin: numerical modeling

and mass balances, Geochimica et Cosmochimica Acta, 67, 3403-3421, 10.1016/s0016-7037(03)00127-3, 2003.
Mackensen, A., Wollenburg, J., and Licari, L.: Low δ13C in tests of live epibenthic and endobenthic foraminifera at a site of active methane seepage, Paleoceanography, 21, 10.1029/2005pa001196, 2006.
Martin, R. A., Nesbitt, E. A., and Campbell, K. A.: The effects of anaerobic methane oxidation on benthic foraminiferal assemblages and stable isotopes on the Hikurangi Margin of eastern New Zealand, Marine Geology, 272, 270-284, 10.1016/j.margeo.2009.03.024, 2010.
Mau, S., Blees, J., Helmke, E., Niemann, H., and Damm, E.: Vertical distribution of methane oxidation and methanotrophic response to elevated methane concentrations in stratified waters of the Arctic fjord Storfjorden (Svalbard, Norway), Biogeosciences, 10, 6267-6278, 10.5194/bg-10-6267-2013, 2013.
McCorkle, D. C., Keigwin, L. D., Corliss, B. H., and Emerson, S. R.: The influence of microhabitats on the carbon isotopic composition of deep-sea benthic foraminifera, Paleoceanography, 5, 161-185, 10.1029/PA005i002p00161, 1990.
McGinnis, D. F., Greinert, J., Artemov, Y., Beaubien, S. E., and Wüest, A.: Fate of rising methane bubbles in stratified waters: How much methane reaches the atmosphere?, Journal of Geophysical Research, 111, 10.1029/2005jc003183, 2006.
Milucka, J., Ferdelman, T. G., Polerecky, L., Franzke, D., Wegener, G., Schmid, M., Lieberwirth, I., Wagner, M., Widdel, F., and Kuypers, M. M.: Zero-valent sulphur is a key intermediate in marine methane oxidation, Nature, 491, 541-546, 10.1038/nature11656, 2012.
Nauhaus, K., Albrecht, M., Elvert, M., Boetius, A., and Widdel, F.: In vitro cell growth of marine archaeal-bacterial consortia during anaerobic oxidation of methane with sulfate, Environ Microbiol, 9, 187-196, 10.1111/j.1462-2920.2006.01127.x, 2007.
Niemann, H., Elvert, M., Hovland, M., Orcutt, B., Judd, A., Suck, I., Gutt, J., Joye, S., Damm, E., Finster, K., and Boetius, A.: Methane emission and consumption at a North Sea gas seep (Tommeliten area), Biogeosciences, 2, 335-351, 2005.
Niemann, H., Losekann, T., de Beer, D., Elvert, M., Nadalig, T., Knittel, K., Amann, R., Sauter, E. J., Schluter, M., Klages, M., Foucher, J. P., and Boetius, A.: Novel microbial communities of the Haakon Mosby mud volcano and their role as a methane sink, Nature, 443, 854-858, 10.1038/nature05227, 2006.
Niemann, H., and Elvert, M.: Diagnostic lipid biomarker and stable carbon isotope signatures of microbial communities mediating the anaerobic oxidation of methane with sulphate, Organic Geochemistry, 39, 1668-1677, 10.1016/j.orggeochem.2007.11.003, 2008.
Pancost, R. D., Zhang, C. L., Tavacoli, J., Talbot, H. M., Farrimond, P., Schouten, S., Sinninghe Damsté, J. S., and Sassen, R.: Lipid biomarkers preserved in hydrate-associated authigenic carbonate rocks of the Gulf of Mexico, Palaeogeography, Palaeoclimatology, Palaeoecology, 227, 48-66, 10.1016/j.palaeo.2005.04.035, 2005.
Panieri, G.: Foraminiferal response to an active methane seep environment: A case study from the Adriatic Sea, Marine Micropaleontology, 61, 116-130, 10.1016/j.marmicro.2006.05.008, 2006.
Panieri, G., and Sen Gupta, B. K.: Benthic Foraminifera of the Blake Ridge hydrate mound, Western North Atlantic Ocean, Marine Micropaleontology, 66, 91-102, https://doi.org/10.1016/j.marmicro.2007.08.002, 2008.
Panieri, G., Camerlenghi, A., Conti, S., Pini, G. A., and Cacho, I.: Methane seepages recorded in benthic foraminifera from Miocene seep carbonates, Northern Apennines (Italy), Palaeogeography, Palaeoclimatology, Palaeoecology, 284, 271-282, https://doi.org/10.1016/j.palaeo.2009.10.006, 2009.
Panieri, G., James, R. H., Camerlenghi, A., Westbrook, G. K., Consolaro, C., Cacho, I., Cesari, V., and Cervera, C. S.: Record of methane emissions from the West Svalbard continental margin during the last 23.500yrs revealed by δ13C of benthic foraminifera, Global and Planetary Change, 122, 151-160, 10.1016/j.gloplacha.2014.08.014, 2014.

Panieri, G., Fornari, D. J., Serov, P., Astrom, E. K. L., Plaza-Faverola, A., Mienert, J., and Torres, M.: Gas hydrate, carbonate cruists, and chemosynthetic organisms on Vestnesa Ridge Pockmark- Preliminary findings., Fire in the ice, 15, 14-17, 2015.
Panieri, G., Graves, C. A., and James, R. H.: Paleo-methane emissions recorded in foraminifera near the landward limit of the gas hydrate stability zone offshore western Svalbard, Geochemistry, Geophysics, Geosystems, 17, 521-537, 10.1002/, 2016.
Panieri, G., Bünz, S., Fornari, D. J., Escartin, J., Serov, P., Jansson, P., Torres, M. E., Johnson, J. E., Hong, W., Sauer, S., Garcia, R., and Gracias, N.: An integrated view of the methane system in the pockmarks at Vestnesa Ridge, 79°N, Marine Geology, 390, 282-300, 10.1016/j.margeo.2017.06.006, 2017a.
Panieri, G., Lepland, A., Whitehouse, M. J., Wirth, R., Raanes, M. P., James, R. H., Graves, C. A., Crémière, A., and Schneider, A.: Diagenetic Mg-calcite overgrowths on foraminiferal tests in the vicinity of methane seeps, Earth and Planetary Science Letters, 458, 203-212, 10.1016/j.epsl.2016.10.024, 2017b.
Patton, H., Hubbard, A., Andreassen, K., Auriac, A., Whitehouse, P. L., Stroeven, A. P., Shackleton, C., Winsborrow, M., Heyman, J., and Hall, A. M.: Deglaciation of the Eurasian ice sheet complex, Quaternary Science Reviews, 169, 148-172, 10.1016/j.quascirev.2017.05.019, 2017.
Peckmann, J., Reimer, A., Luth, U., Luth, C., Hansen, B. T., Heinicke, C., Hoefs, J., and Reitner, J.: Methane-derived carbonates and authigenic pyrite from the northwestern Black Sea, Marine Geology, 177, 129-150, https://doi.org/10.1016/S0025-3227(01)00128-1, 2001.
Peckmann, J., and Thiel, V.: Carbon cycling at ancient methane-seeps, Chemical Geology, 205, 443-467, 10.1016/j.chemgeo.2003.12.025, 2004.
Peckmann, J., Birgel, D., and Kiel, S.: Molecular fossils reveal fluid composition and flow intensity at a Cretaceous seep, Geology, 37, 847-850, 10.1130/G25658A.1, 2009.
Petersen, C. J., Bünz, S., Hustoft, S., Mienert, J., and Klaeschen, D.: High-resolution P-Cable 3D seismic imaging of gas chimney structures in gas hydrated sediments of an Arctic sediment drift, Marine and Petroleum Geology, 27, 1981-1994, 10.1016/j.marpetgeo.2010.06.006, 2010.
Plaza-Faverola, A., Bünz, S., Johnson, J. E., Chand, S., Knies, J., Mienert, J., and Franek, P.: Role of tectonic stress in seepage evolution along the gas hydrate-charged Vestnesa Ridge, Fram Strait, Geophysical Research Letters, 42, 733-742, 10.1002/2014gl062474, 2015.
Rathburn, A. E.: Benthic foraminifera associated with cold methane seeps on the northern California margin: Ecology and stable isotopic composition, Marine Micropaleontology 38, 247–266, 2000.
Rathburn, A. E., Pérez, M. E., Martin, J. B., Day, S. A., Mahn, C., Gieskes, J., Ziebis, W., Williams, D., and Bahls, A.: Relationships between the distribution and stable isotopic composition of living benthic foraminifera and cold methane seep biogeochemistry in Monterey Bay, California, Geochemistry, Geophysics, Geosystems, 4, 10.1029/2003gc000595, 2003.
Reeburgh, W. S.: Oceanic Methane Biogeochemistry, Chem. Rev, 107, 486-513, 2007.
Reitner, J., Peckmann, J., Blumenberg, M., Michaelis, W., Reimer, A., and Thiel, V.: Concretionary methane-seep carbonates and associated microbial communities in Black Sea sediments, Palaeogeography, Palaeoclimatology, Palaeoecology, 227, 18-30, 10.1016/j.palaeo.2005.04.033, 2005.
Riedinger, N., Kasten, S., Gröger, J., Franke, C., and Pfeifer, K.: Active and buried authigenic barite fronts in sediments from the Eastern Cape Basin, Earth and Planetary Science Letters, 241, 876-887, 10.1016/j.epsl.2005.10.032, 2006.
Rossel, P. E., Lipp, J. S., Fredricks, H. F., Arnds, J., Boetius, A., Elvert, M., and Hinrichs, K.-U.: Intact polar lipids of anaerobic methanotrophic archaea and associated bacteria, Organic Geochemistry, 39, 992-999, 10.1016/j.orggeochem.2008.02.021, 2008.
Rossel, P. E., Elvert, M., Ramette, A., Boetius, A., and Hinrichs, K.-U.: Factors controlling the distribution of anaerobic methanotrophic communities in marine environments: Evidence from intact polar membrane lipids, Geochimica et Cosmochimica Acta, 75, 164-184, 10.1016/j.gca.2010.09.031, 2011.

Sauer, S., Hong, W.-L., Knies, J., Lepland, A., Forwick, M., Klug, M., Eichinger, F., Baranwal, S., Crémière, A., Chand, S., and Schubert, C. J.: Sources and turnover of organic carbon and methane in fjord and shelf sediments off northern Norway, Geochemistry, Geophysics, Geosystems, 17, 4011-4031, 10.1002/2016gc006296, 2016.
Sauer, S., Crémière, A., Knies, J., Lepland, A., Sahy, D., Martma, T., Noble, S. R., Schönenberger, J., Klug, M., and Schubert, C. J.: U-Th chronology and formation controls of methane-derived authigenic carbonates from the Hola trough seep area, northern Norway, Chemical Geology, 470, 164-179, 10.1016/j.chemgeo.2017.09.004, 2017.
Scheller, S., Yu, H., Chadwick, G. L., McGlynn, S. E., and Orphan, V. J.: Artificial electron acceptors decouple archaeal methane oxidation from sulfate reduction, Science, 351, 703-707, 2016.
Schneider, A., Crémière, A., Panieri, G., Lepland, A., and Knies, J.: Diagenetic alteration of benthic foraminifera from a methane seep site on Vestnesa Ridge (NW Svalbard), Deep Sea Research Part I: Oceanographic Research Papers, 123, 22-34, https://doi.org/10.1016/j.dsr.2017.03.001, 2017.
Schneider, A., Panieri, G., Lepland, A., Consolaro, C., Crémière, A., Forwick, M., Johnson, J. E., Plaza-Faverola, A., Sauer, S., and Knies, J.: Methane seepage at Vestnesa Ridge (NW Svalbard) since the Last Glacial Maximum, Quaternary Science Reviews, 193, 98-117, 10.1016/j.quascirev.2018.06.006, 2018.
Scranton, M. I., and Brewer, P. G.: Consumption of dissolved methane in the deep ocean 1, Limnology and Oceanography, 23, 1207-1213, 10.4319/lo.1978.23.6.1207, 1978.
Sen Gupta, B. K.: Introduction to modern Foraminifera, in: Modern Foraminifera, edited by: Sen Gupta, B. K., Springer Netherlands, Dordrecht, 3-6, 2003.
Serov, P., Vadakkepuliyambatta, S., Mienert, J., Patton, H., Portnov, A., Silyakova, A., Panieri, G., Carroll, M. L., Carroll, J., Andreassen, K., and Hubbard, A.: Postglacial response of Arctic Ocean gas hydrates to climatic amelioration, Proc Natl Acad Sci U S A, 10.1073/pnas.1619288114, 2017.
Sivan, O., Antler, G., Turchyn, A. V., Marlow, J. J., and Orphan, V. J.: Iron oxides stimulate sulfate-driven anaerobic methane oxidation in seeps, Proc Natl Acad Sci U S A, 111, E4139-4147, 10.1073/pnas.1412269111, 2014.
Smith, A. J., Mienert, J., Bunz, S., and Greinert, J.: Thermogenic methane injection via bubble transport into the upper Arctic Ocean from the hydrate-charged Vestnesa Ridge, Svalbard, Geochemistry, Geophysics, Geosystems, 15, 1945–1959, 10.1002/, 2014.
Sollai, M., Villanueva, L., Hopmans, E. C., Reichart, G. J., and Sinninghe Damste, J. S.: A combined lipidomic and 16S rRNA gene amplicon sequencing approach reveals archaeal sources of intact polar lipids in the stratified Black Sea water column, Geobiology, 17, 91-109, 10.1111/gbi.12316, 2019.
Solomon, E. A., and Kastner, M.: Progressive barite dissolution in the Costa Rica forearc – Implications for global fluxes of Ba to the volcanic arc and mantle, Geochimica et Cosmochimica Acta, 83, 110-124, 10.1016/j.gca.2011.12.021, 2012.
Stadnitskaia, A., Blinova, V., Ivanov, M. K., Baas, M., Hopmans, E., van Weering, T. C. E., and Sinninghe Damsté, J. S.: Lipid biomarkers in sediments of mud volcanoes from the Sorokin Trough, NE Black Sea: Probable source strata for the erupted material, Organic Geochemistry, 38, 67-83, 10.1016/j.orggeochem.2006.08.012, 2007.
Stadnitskaia, A., Bouloubassi, I., Elvert, M., Hinrichs, K. U., and Sinninghe Damsté, J. S.: Extended hydroxyarchaeol, a novel lipid biomarker for anaerobic methanotrophy in cold seepage habitats, Organic Geochemistry, 39, 1007-1014, 10.1016/j.orggeochem.2008.04.019, 2008a.
Stadnitskaia, A., Nadezhkin, D., Abbas, B., Blinova, V., Ivanov, M. K., and Sinninghe Damsté, J. S.: Carbonate formation by anaerobic oxidation of methane: Evidence from lipid biomarker and fossil 16S rDNA, Geochimica et Cosmochimica Acta, 72, 1824-1836, 10.1016/j.gca.2008.01.020, 2008b.
Todo, Y., Kitazato, H., Hashimoto, J., and Gooday, A.: Simple Foraminifera Flourish at the Ocean's Deepest Point, Science (New York, N.Y.), 307, 689, 10.1126/science.1105407, 2005.
Tornabene, T. G., Langworthy, T. A., Holzer, G., and Oró, J.: Squalenes, phytanes and other isoprenoids as major neutral lipids of methanogenic and thermoacidophilic “archaebacteria”, Journal of Molecular Evolution, 13, 73-83, 10.1007/BF01732755, 1979.

Torres, M. E., Brumsack, H. J., Bohrmann, G., and Emeis, K. C.: Barite fronts in continental margin sediments: a new look at barium remobilization in the zone of sulfate reduction and formation of heavy barites in diagenetic fronts, Chemical Geology, 127, 125-139, https://doi.org/10.1016/0009-2541(95)00090-9, 1996.
Torres, M. E., Bohrmann, G., Dubé, T. E., and Poole, F. G.: Formation of modern and Paleozoic stratiform barite at cold methane seeps on continental margins, Geology, 31, 897-900, 10.1130/G19652.1 %J Geology, 2003a.
Torres, M. E., Mix, A. C., Kinports, K., Haley, B., Klinkhammer, G. P., McManus, J., and de Angelis, M. A.: Is methane venting at the seafloor recorded by δ13C of benthic foraminifera shells?, Paleoceanography, 18, n/a-n/a, 10.1029/2002pa000824, 2003b.
Trenberth, K. E., and Fasullo, J.: Water and energy budgets of hurricanes and implications for climate change, Journal of Geophysical Research: Atmospheres, 112, 10.1029/2006jd008304, 2007.
Treude, T., Boetius, A., Knittel, K., Wallmann, K., and Jørgensen, B.: Anaerobic oxidation of methane above gas hydrates at Hydrate Ridge, NE Pacific Ocean, Marine Ecology Progress Series, 264, 1-14, 2003.
UREY, H. C., LOWENSTAM, H. A., EPSTEIN, S., and McKINNEY, C. R.: MEASUREMENT OF PALEOTEMPERATURES AND TEMPERATURES OF THE UPPER CRETACEOUS OF ENGLAND, DENMARK, AND THE SOUTHEASTERN UNITED STATES, GSA Bulletin, 62, 399-416, 10.1130/0016-7606(1951)62[399:Mopato]2.0.Co;2, 1951.
Valentine, D. L., and Reeburgh, W. S.: New perspectives on anaerobic methane oxidation, Environmental Microbiology, 2, 477-484, 2000.
Wefer, G., Berger, W. H., Bijma, J., and Fischer, G.: Clues to Ocean History: a Brief Overview of Proxies, in: Use of Proxies in Paleoceanography: Examples from the South Atlantic, edited by: Fischer, G., and Wefer, G., Springer Berlin Heidelberg, Berlin, Heidelberg, 1-68, 1999.
Wegener, G., Niemann, H., Elvert, M., Hinrichs, K. U., and Boetius, A.: Assimilation of methane and inorganic carbon by microbial communities mediating the anaerobic oxidation of methane, Environmental Microbiology, 10, 2287–2298, 2008.
Wegener, G., Krukenberg, V., Riedel, D., Tegetmeyer, H. E., and Boetius, A.: Intercellular wiring enables electron transfer between methanotrophic archaea and bacteria, Nature, 526, 587-590, 10.1038/nature15733, 2015.
Whiticar, M.: Carbon and hydrogen isotope systematics of bacterial formation and oxidation of methane, Chemical Geology 161, 291-314, 1999.
Wollenburg, J. E., Kuhnt, W., and Mackensen, A.: Changes in Arctic Ocean paleoproductivity and hydrography during the last 145 kyr: The benthic foraminiferal record, Paleoceanography, 16, 65-77, 10.1029/1999pa000454, 2001.
Wollenburg, J. E., Raitzsch, M., and Tiedemann, R.: Novel high-pressure culture experiments on deep-sea benthic foraminifera — Evidence for methane seepage-related δ13C of Cibicides wuellerstorfi, Marine Micropaleontology, 117, 47-64, 10.1016/j.marmicro.2015.04.003, 2015.
Yao, H., Hong, W. L., Panieri, G., Sauer, S., Torres, M. E., Lehmann, M. F., Gründger, F., and Niemann, H.: Fracture-controlled fluid transport supports microbial methane-oxidizing communities at Vestnesa Ridge, Biogeosciences, 16, 2221-2232, 10.5194/bg-16-2221-2019, 2019.
Zhang, C. L.: Lipid and carbon isotopic evidence of methane-oxidizing and sulfate-reducing bacteria in association with gas hydrates from the Gulf of Mexico, Geology, 30, 239–242, 2002.
Zhang, C. L., Pancost, R. D., Sassen, R., Qian, Y., and Macko, S. A.: Archaeal lipid biomarkers and isotopic evidence of anaerobic methane oxidation associated with gas hydrates in the Gulf of Mexico, Organic Geochemistry, 34, 827-836, 10.1016/s0146-6380(03)00003-2, 2003.
Zhang, Y., Maignien, L., Zhao, X., Wang, F., and Boon, N.: Enrichment of a microbial community performing anaerobic oxidation of methane in a continuous high-pressure bioreactor, BMC Microbiology, 11, 137, 10.1186/1471-2180-11-137, 2011.
Zink, K.-G., Wilkes, H., Disko, U., Elvert, M., and Horsfield, B.: Intact phospholipids—microbial “life markers” in marine deep subsurface sediments, Organic Geochemistry, 34, 755-769, 10.1016/s0146-6380(03)00041-x, 2003.

Paper I

Fracture-controlled fluid transport supports microbial methane-oxidizing communities at Vestnesa Ridge

Haoyi Yao, Wei-Li Hong, Giuliana Panieri, Simone Sauer Marta E. Torres, Moritz F. Lehmann, Friederike Gründger, and Helge Niemann

Biogeosciences, 16, 2221-2232, 10.5194/bg-16-2221-2019, 2019.

Biogeosciences, 16, 2221–2232, 2019
https://doi.org/10.5194/bg-16-2221-2019

Biogeosciences Open Access EGU

Fracture-controlled fluid transport supports microbial methane-oxidizing communities at Vestnesa Ridge

Haoyi Yao[1], Wei-Li Hong[1,2], Giuliana Panieri[1], Simone Sauer[1,2], Marta E. Torres[3], Moritz F. Lehmann[4], Friederike Gründger[1], and Helge Niemann[1,4,5,6]

[1]Centre for Arctic Gas Hydrate (CAGE), Environment and Climate, Department of Geosciences, UiT The Arctic University of Norway in Tromsø, Tromsø, Norway
[2]Geological Survey of Norway (NGU), Trondheim, Norway
[3]College of Earth, Ocean, and Atmospheric Sciences (CEOAS), Oregon State University, Corvallis, USA
[4]Department of Environmental Sciences, University of Basel, Basel, Switzerland
[5]Royal Netherlands Institute for Sea Research (NIOZ), Department of Marine Microbiology and Biogeochemistry, and Utrecht University, den Burg, the Netherlands
[6]Department of Earth Sciences, Faculty of Geosciences, Utrecht University, Utrecht, the Netherlands

Correspondence: Haoyi Yao (haoyi.yao@uit.no)

Received: 2 July 2018 – Discussion started: 13 August 2018
Revised: 8 March 2019 – Accepted: 9 May 2019 – Published: 29 May 2019

Abstract. We report a rare observation of a mini-fracture in near-surface sediments (30 cm below the seafloor) visualized using a rotational scanning X-ray of a core recovered from the Lomvi pockmark, Vestnesa Ridge, west of Svalbard (1200 m water depth). Porewater geochemistry and lipid biomarker signatures revealed clear differences in the geochemical and biogeochemical regimes of this core compared with two additional unfractured cores recovered from pockmark sites at Vestnesa Ridge, which we attribute to differential methane transport mechanisms. In the sediment core featuring the shallow mini-fracture at pockmark Lomvi, we observed high concentrations of both methane and sulfate throughout the core in tandem with moderately elevated values for total alkalinity, ^{13}C-depleted dissolved inorganic carbon (DIC), and ^{13}C-depleted lipid biomarkers (diagnostic for the slow-growing microbial communities mediating the anaerobic oxidation of methane with sulfate – AOM). In a separate unfractured core, recovered from the same pockmark about 80 m away from the fractured core, we observed complete sulfate depletion in the top centimeters of the sediment and much more pronounced signatures of AOM than in the fractured core. Our data indicate a gas advection-dominated transport mode in both cores, facilitating methane migration into sulfate-rich surface sediments. However, the moderate expression of AOM signals suggest a rather recent onset of gas migration at the site of the fractured core, while the geochemical evidence for a well-established AOM community at the second coring site suggest that gas migration has been going on for a longer period of time. A third core recovered from another pockmark along the Vestnesa Ridge Lunde pockmark was dominated by diffusive transport with only weak geochemical and biogeochemical evidence for AOM. Our study highlights that advective fluid and gas transport supported by mini-fractures can be important in modulating methane dynamics in surface sediments.

1 Introduction

Large-scale fractures are commonly observed on seismic profiles (Tobin et al., 2001; Weinberger and Brown, 2006; Plaza-Faverola et al., 2015) and can provide increased sediment permeability and conduits for fluid and gas transport. Macro-fractures were often observed in association with cold seep systems, where methane-rich fluids from greater sediment depth reach shallow sediments and may even be transported across the sediment–water interface (Berndt et al., 2014; Sahling et al., 2014). Prominent examples of fracture-controlled fluid migration at cold seep systems include locations such as Hydrate Ridge (Torres et al., 2002; Weinberger

and Brown, 2006; Briggs et al., 2011), Blake Ridge (Egeberg and Dickens, 1999), and the recently documented Storfjordrenna gas hydrate mounds in the Barents Sea (Hong et al., 2017b, 2018; Waage et al., 2019). Seepage at these locations can sustain high biomass levels of chemosynthetic communities that either directly oxidize methane or metabolize products of methane oxidation, such as sulfide (Boetius and Suess, 2004; Niemann et al., 2013). Fractures visible on seismic profiles often exceed 10 m in length (Gabrielsen et al., 1998). However, surface sediments may also feature smaller-scale, branched fracture networks (hereafter referred to as mini-fractures) which propagate from macro-fractures as the fluid pressure increases (Friedman, 1975; Briggs et al., 2011; Anders et al., 2014).

The role of small-scale fracture networks in routing methane upwards into the near-surface sediments is not well understood. In particular, the biogeochemical effects of mini-fractures in sediments with methane-dependent microbial communities is poorly constrained but is important for our understanding of how fracture networks influence microbial dynamics. Geochemically, fractures facilitate migration of deep fluids that are laden with electron donors from deeper sediments, which can then be used by sedimentary microbes as metabolic or bioenergetics substrates. To date, such mini-fractures have either been detected by X-ray images of cores under pressure (Riedel et al., 2006), or by the presence of macroscopic biofilms lining subseafloor fractures (Briggs et al., 2011). These biofilms were usually present at the sulfate–methane transition zone (SMTZ), where methane is oxidized by a consortium of anaerobic methanotrophic archaea (ANME) and sulfate-reducing bacteria (SRB) mediating the anaerobic oxidation of methane (AOM) with sulfate as the terminal electron acceptor (Knittel and Boetius, 2009):

$$CH_4 + SO_4^{2-} \rightarrow HCO_3^- + HS^- + H_2O. \quad \text{(R1)}$$

In contrast to large-scale transport pathways, mini-fractures are difficult to detect as they cannot be resolved with seismic tools (Emery and Myers, 1996; Gabrielsen et al., 1998) and may thus play an underappreciated but potentially important role in sediment methane dynamics, and the efficiency of the benthic microbial methane filter.

In this study, we report on the presence of a mini-fracture in the near-surface sediments of the active pockmark Lomvi, located on Vestnesa Ridge (79° N, 6° E), west of the Svalbard archipelago. Using an interdisciplinary approach that combines geochemical and organic geochemical methods, we investigate the effects that such mini-fractures may impose on benthic methane dynamics and associated microbial communities. Our data show that mini-fractures can provide conduits for advective gas migration fostering AOM, but the moderate expression of AOM-associated biogeochemical signals along the mini-fracture at the Lomvi pockmark suggest a rather recent opening of this particular fracture.

2 Material and methods

2.1 Study sites

Vestnesa Ridge is NW–SE trending, ∼ 100 km long, and covered with ∼ 1 km thick contourite drifted sediments. Vestnesa Ridge features numerous pockmark structures (see a more detailed description of the geological setting in Plaza-Faverola et al., 2015, and Panieri et al., 2017). This ridge is part of a submarine gas-hydrate system on the west Svalbard margin (1200 m water depth), where fluid and gas migration from deep hydrocarbon reservoirs towards the seafloor has potentially been ongoing since the early Pleistocene (Knies et al., 2018). Past investigations have shown that the ridge actively releases methane gas from the seafloor along the eastern segment of the structure (Bünz et al., 2012; Smith et al., 2014; Plaza-Faverola et al., 2015; Panieri et al., 2017), and seismic data suggest that seepage is related to intensive seabed faulting and rifting (Plaza-Faverola et al., 2015). The eastern part of Vestnesa Ridge features the pockmarks Lunde and Lomvi (Fig. 1), both belonging to the most active structures known in the area (Bünz et al., 2012; Panieri et al., 2017). Pockmarks are morphological expressions of fluid and/or gas eruptions from sediments, and are commonly observed in active hydrocarbon systems (Hovland et al., 2002). Pockmarks can be prominent in the seafloor bathymetry, ranging in shape from circular, crater-like edifices to "push-down" sediment features (Hovland et al., 2002). Enhanced reflections and "push-down" features observed in the seismic transects of Lunde and Lomvi were interpreted as chimney structures containing free gas, which originate from beneath the bottom of the gas-hydrate stability zone (Bünz et al., 2012; Smith et al., 2014). Excessive pore pressure at the summit of this gas column fractured the sediments and led to the presence of free gas in the hydrate stability zone (Weinberger and Brown, 2006; Bünz et al., 2012).

2.2 Sample collection

We investigated three sediment cores from Vestnesa Ridge: two were collected by a multicorer (MC) during cruise CAGE15-2 with R/V *Helmer Hanssen* in 2015 (core Lomvi 893MC and core Lunde 886MC), and an additional push core (core Lomvi 008PC) was recovered with the remotely operated vehicle (ROV) Ægir about 80 m away from core Lomvi 893MC during the P1606 cruise with R/V *G.O. Sars* in 2016 (Table 1). The MC system used during cruise CAGE15-2 can collect up to six parallel cores during every deployment, and a MISO (Multidisciplinary Instrumentation in Support of Oceanography, Woods Hole Oceanographic Institution) towcam was attached to the MC frame, allowing targeted video-controlled sampling (Panieri et al., 2015, 2017). Among the six cores, one was subsampled for porewater analyses, and two adjacent cores were used for lipid biomarker and headspace gas analyses, respectively. The cores for porewater

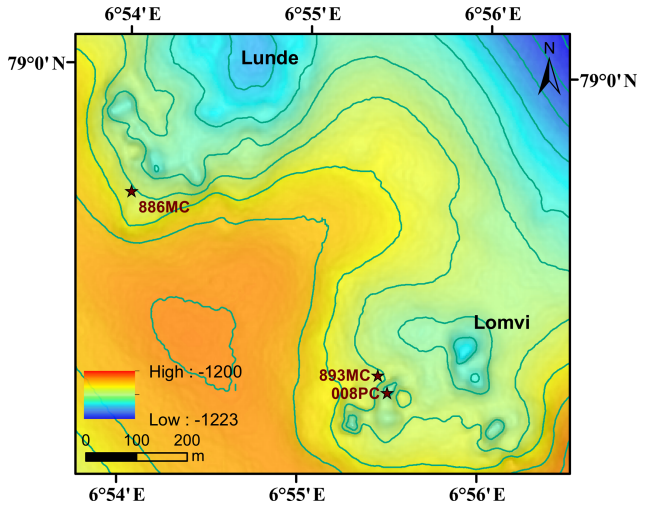

Figure 1. Regional multibeam bathymetric map of Vestnesa Ridge showing the Lunde and Lomvi pockmarks and sampling locations. Locations of multicores and push cores used in this paper are denoted as stars.

extraction were used for X-ray analysis. Core Lomvi 893MC was collected at a site with bacterial mats around outcropping carbonate crusts at the Lomvi pockmark, whereas core Lunde 886MC was collected at a soft sediment site with patchy bacterial mats and tubeworms at the Lunde pockmark (Figs. 1 and 2). The push core Lomvi 008PC was recovered from a large patch of bacterial mat at the Lomvi pockmark. This core was only sampled for the analysis of porewater and lipid biomarkers (limited sample material impeded the analysis of the gas composition from Lomvi 008PC).

Immediately upon recovery, we subsampled the cores for subsequent gas, porewater, and biomarker analyses. Details on headspace sampling and gas analysis in the multicores were described in Panieri et al. (2017) and references therein. Briefly, 5 mL of bulk sediments were sampled into a 20 mL headspace glass vial, containing 5 mL of 1M NaOH and two glass beads. The gas analysis was performed with a ThermoScientific Trace 1310 gas chromatograph (GC) equipped with a TG-BOND alumnia (Na_2SO_4) column (30 m × 0.53 mm × 10 µm). The methane headspace samples were obtained on a parallel core as the fractured core in the same set of the multicorer frame. Porewater was extracted at ambient temperature (ca. −1 °C), at a resolution of 2 cm, with either 10 cm (Lomvi 893MC and Lunde 886MC) or 5 cm rhizon samplers (Lomvi 008PC) attached to acid-cleaned syringes (Seeberg-Elverfeldt et al., 2005). Rhizon membranes were soaked in Milli-Q water before use. The first 0.5 mL of the recovered porewater was discarded to avoid dilution or contamination with residual Milli-Q water in the rhizons. Sediment samples for biomarker analyses were collected on board with a methanol pre-cleaned spatula at a resolution of 2 cm, wrapped in aluminum foil and subsequently stored frozen at −20 °C until analysis. Intact sediment cores were kept at 4 °C for further X-ray analysis in onshore laboratories using a Geotek MSCL-XCT at UiT.

2.3 Porewater analyses

Total alkalinity (TA) was measured on board using the Gran titration method (Grasshoff et al., 1999) within a few hours after the syringes were disconnected from the rhizon samplers. The HCl titrant (0.012 M) was checked daily on board with local surface seawater and 10 mM of borax to verify the acid concentration. The pH meter of the titrator was calibrated with pH standard solutions (pH of 4, 7, and 11) both before and during the cruise. Porewater aliquots (2 mL) for sulfate analysis were preserved with 3 mL zinc acetate solution (23 mM) to precipitate the dissolved sulfide (Gieske et al., 1991; Grasshoff et al., 1999) for CAGE 15-2 samples. All sulfate analyses were performed using a Dionex ICS-1100 Ion Chromatograph equipped with a Dionex IonPac AS23 column at the Geological Survey of Norway (NGU) (Sauer et al., 2016). For sulfide concentration measurements, the precipitated zinc sulfide was quantified in the onshore geology laboratory at UiT with a spectrophotometric method (Cline, 1969) using a UV-1280 UV–vis Spectrophotometer (Shimadzu). The amount of zinc acetate added to samples from core 008PC was too low to precipitate all dissolved sulfide; thus the measured sulfide concentrations are minimum values. For the subsequent measurement of $\delta^{13}C$ of dissolved inorganic carbon (DIC), 2 mL aliquots of porewater were fixed on board with saturated $HgCl_2$ (27 mM final concentration) (Grasshoff et al., 1999). The $\delta^{13}C$ DIC of CAGE 15-2 samples (Bernhard and Panieri, 2018) were analyzed using a Finnigan DELTA-Plus mass spectrometer coupled to a GasBench II as described in Torres et al. (2005). The $\delta^{13}C$ DIC in pore waters of core Lomvi 008PC was determined from the CO_2 liberated from the water after acidification with phosphoric acid. Measurements were carried out at EAWAG (The Swiss Federal Institute of Aquatic Science and Technology) using an IRMS (Isotope Ratio Mass Spectrometer, Isoprime) equipped with a Gilson 222XL Liquid Handler and a Multiflow unit (Isoprime). The standard deviation of the $\delta^{13}C$ DIC measurements from repeated measurements of standards was ±0.1 ‰ (1σ, $n = 27$). The stable carbon isotope values for DIC are reported in the conventional δ notation in per mill (‰) relative to V-PDB (Vienna Pee Dee Belemnite).

2.4 Lipid extraction, quantification, identification, and determination of compound-specific stable carbon isotope composition

Lipid biomarkers were extracted and analyzed according to previously reported protocols (Elvert et al., 2003) with modification for alcohol derivatization (Niemann et al., 2005) and instrument setup (Blees et al., 2014; Steinle et al., 2018). Briefly, a total lipid extract (TLE) was obtained by ultrasonication of ∼ 20 g wet sediment samples in four extraction

Table 1. Information on coring stations, coring coordinates, seafloor habitat information, and analyses performed at each site. DIC: dissolved inorganic carbon; TA: total alkalinity; conc.: concentration; NA – not available.

Pockmark (cruise)	Lomvi (CAGE15-2)	Lomvi (P1606)	Lunde (CAGE15-2)
Core	Lomvi 893MC	Lomvi 008PC	Lunde 886MC
Coordinates	79°0.180′ N	79°0.162′ N	79°0.366′ N
	6°55.434′ E	6°55.488′ E	6°54.030′ E
Habitat	bacterial mats and carbonate crusts	bacterial mats	tubeworms
Methane	methane headspace	NA	methane headspace
Porewater analyses	sulfate, sulfide, TA, δ^{13}C DIC	sulfate, sulfide, TA, δ^{13}C DIC	sulfate, sulfide, TA, δ^{13}C DIC
Lipid biomarkers	conc. and δ^{13}C	conc. and δ^{13}C	conc. and δ^{13}C

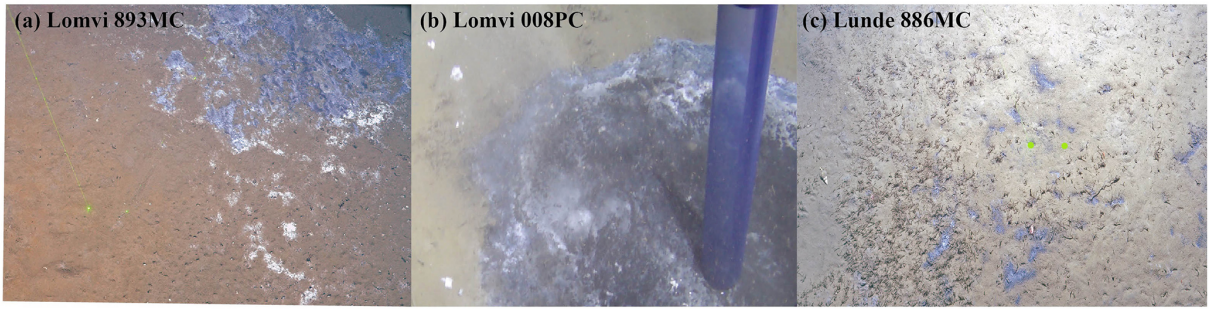

Figure 2. Still images of the seafloor before launching of the multicorer at coring site Lomvi 893MC **(a)** and coring site Lunde 886MC **(c)**, as well as during ROV guided push coring at coring site Lomvi 008PC **(b)**. Coring site Lomvi 893MC **(a)** and 008PC feature bacterial mats and reduced, black sediments, while the coring site Lunde 886MC **(c)** is characterized by soft sediments with tubeworms and small patchy bacterial mats. Green laser points **(a, c)** are 20 cm apart and the diameter of the push core **(b)** is 8.5 cm.

steps with solvents of decreasing polarity: dichloromethane (DCM) / methanol (MeOH) 1 : 2; DCM/MeOH 2 : 1; and DCM for the last two extraction steps. The TLE was then saponified, and a neutral lipid fraction was extracted prior to methylation of the remaining polar fraction (comprising free fatty acids) to yield fatty acid methyl esters (FAMEs) for chromatographic analysis. Double bond positions of FAMEs were determined by analyzing dimethyl–disulfide adducts (Nichols et al., 1986; Moss and Lambert-Fair, 1989). The neutral fraction was further separated into hydrocarbons, ketones, and alcohols, the latter of which was derivatized to form trimethylsilyl adducts for analysis.

Individual lipid compounds were analyzed using a GC (Thermo Scientific TRACE™ Ultra), equipped with a capillary column (Rxi-5ms, 50 m, 0.2 mm ID, 0.33 µm d_f), using helium gas as a carrier gas at a constant flow rate of 1 mL min^{-1}. The initial oven temperature was set to 50 °C, held for 2 min and then increased to 140 °C at a rate of 10 °C min^{-1}, held for 1 min, then further increased to 300 °C at 4 °C min^{-1}. The final hold time was 63 min to analyze FAMEs or 160 min to analyze larger (i.e., high boiling point) lipids in the hydrocarbon and alcohol fractions. Concentrations were determined by flame-ionization detection (FID) against internal standards. Unknown compounds were identified with a quadrupole mass spectrometry unit (Thermo Scientific DSQ II) at the chromatography periphery. Similarly, compound-specific stable carbon isotope ratios were determined using a magnetic sector isotope ratio mass spectrometry unit (Thermo Scientific Delta V Advantage) coupled to a gas chromatography setup with the above-outlined specification. δ^{13}C values are reported with an analytical error of ±1 ‰.

3 Results and discussion

3.1 Sediment X-ray imaging and porewater geochemistry

Our detailed X-ray imaging of cores retrieved from locations of known methane seepage in Vestnesa Ridge revealed a mini-fracture in the core Lomvi 893MC in the top 30 cm (Fig. 3) but not in any other core. However, it is important to note that X-ray imaging can only confirm the presence of a fracture while the size or expansion of the original fracture cannot be resolved. Upon recovery, core Lomvi 893MC showed extensive gas ebullition. Thus it is possible that the fracture expanded during core retrieval because of pressure-induced volume changes in sedimentary gases. Nevertheless, our analyses revealed a substantial increase in methane concentrations in the upper section of the core (Fig. 4), which is

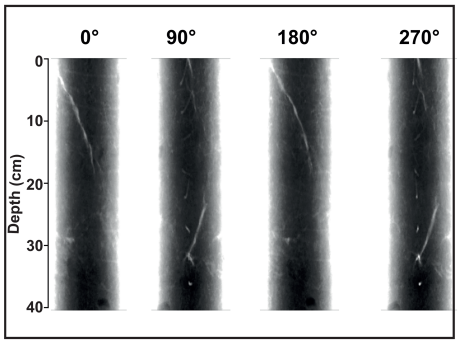

Figure 3. X-ray images of core Lomvi 893MC. The different rotational planes show a whitish X-ray transparency extending throughout the core. This zone is interpreted as a zone of weakness facilitating fluid and gas migration in situ. The void probably became gas filled after core recovery. A rotational video of this core is available in the Supplement.

an uncommon observation in marine settings where methane originates at greater sediment depth (i.e., methane concentrations typically increase downcore). We argue that the higher concentration at the surface of the core directly indicates an advective (fracture controlled) influx of methane into the top sediment section at the coring side of the core Lomvi 893MC. Typically, high methane concentrations in marine sediments lead to elevated rates of AOM, which in return lead to sulfate depletion and sulfide production, and thus the development of a sulfate methane transition zone (SMTZ). Furthermore, excess production of DIC during AOM leads to elevated sediment TA and low δ^{13}C DIC values. The marked methane increase at coring site Lomvi 893MC was not paralleled by changes in other parameters, which are commonly associated with AOM (Fig. 4a). Rather, the smooth porewater profiles of sulfate, sulfide, TA, and δ^{13}C of DIC in this core seem typical for locations with low methane input, as often found in settings characterized by diffusive transport regimes (Treude et al., 2003; Egger et al., 2018; Niemann et al., 2009). We attribute this apparently contradictory observation of enhanced methane concentrations on the one hand and the rather "inconspicuous" signals for AOM activity on the other to a recent genesis of the fracture (see additional discussion below). To further investigate the changes associated with the highly heterogeneous nature of the methane dynamics in this region, we compared this first core with two additional cores from contrasting settings at Vestnesa Ridge.

The push core Lomvi 008PC retrieved from an active venting site (ca. 80 m to the SE of core Lomvi 893MC) at the Lomvi pockmark showed sulfate depletion within the first 5 cm b.s.f. (below the sea floor) (Fig. 4b), indicating a high methane flux and a shallow SMTZ (Reeburgh, 2007). This shallow SMTZ is comparable to those typically observed at locations of high methane flux, such as the *Beggiatoa* fields at Hydrate Ridge (Treude et al., 2003), the Gulf of Mexico (Ussler and Paull, 2008), or Haakon Mosby Mud Volcano (Niemann et al., 2006a, b). At these high-flux sites, AOM rates have been estimated to be on the order of several millimoles per square meter per day. A third core (core Lunde 886MC) was retrieved from a soft-sediment site characterized by the extensive occurrence of tubeworms and bacterial mats (Fig. 2) at the adjacent active Lunde Pockmark. Sulfate concentrations in this core showed only a moderate decrease with sediment depth and traces of methane were detected in the upper 20 cm of the core (Fig. 4c). These data are consistent with observations of low sulfide concentrations and TA. Together, our results indicate a substantially lower methane flux and efficient methane retention through AOM in sediments at this coring site, similar to previous findings from seep sites characterized by macrofauna-inducing bioventilation (e.g., Niemann et al., 2006a, b; Levin et al., 2016). Although core Lunde 886MC is located in a diffusive system, the convex shape of the sulfate concentration profile along with increasing methane concentration at the bottom suggest non-steady-state conditions. The convex shape of the sulfate profile can be related to an ongoing increase in methane flux (Fischer et al., 2013; Hong et al., 2017b). It may also be related to the intrusion of seawater into the shallower sediments, which can be induced by bioventilation, and/or ascending methane bubbles from the sub-seafloor (Haeckel et al., 2007; Hong et al., 2016). Our visual investigations of the seafloor revealed the presence of tubeworms but there are a few bivalves; therefore bioventilation would be moderate. Methane concentration in the upper sediment section was very low, and we did not observe methane bubbles emanating from the seafloor at the coring site. We thus assume that moderate bio-irrigation and a recent increase in the diffusive methane flux at the coring site (Lunde 886MC) can explain the non-steady-state sulfate and methane profiles in the Lunde pockmark core.

3.2 Methanotrophic community development

To further investigate the role of the detected mini-fracture in core Lomvi 893MC on the biogeochemistry and microbial community, we investigated archaeal and bacterial lipid biomarkers and their associated stable carbon isotope signatures that are diagnostic for AOM communities (Niemann and Elvert, 2008, and references therein). ANMEs typically produce a suite of glycerol ether lipids comprising isoprenoidal alkyl moieties that may also occur as free hydrocarbons in environmental samples. We found the isoprenoidal dialkyl glycerol diethers archaeol and *sn2*-hydroxyarchaeol in all three cores (Fig. 4a–c). Furthermore, the ^{13}C-depleted signatures of these compounds provide evidence that their source organisms mediate sulfate-dependent AOM. Indeed, ANME biomass is characterized by a strongly ^{13}C-depleted isotope composition because the metabolized methane is typically ^{13}C-depleted, and AOM is associated with a strong kinetic isotope effect (Whiticar, 1999). The sulfate-reducing

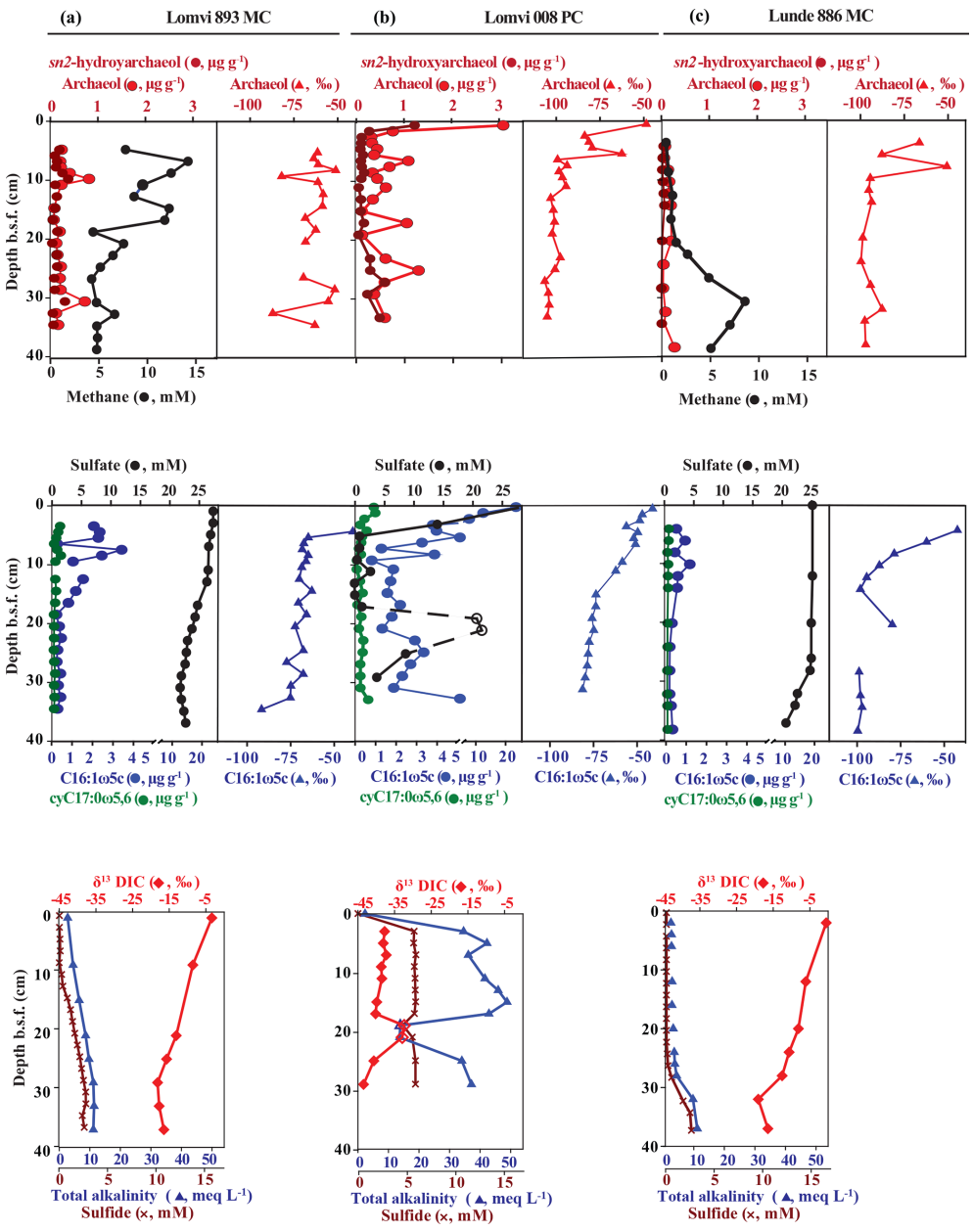

Figure 4. Biogeochemical profiles of archaeal (*sn2*-hydroxyarchaeol, archaeol) and bacterial lipid biomarkers (fatty acids C16 : 1ω5c, cyC17 : 0ω5, 6), methane, and pore water constituents (sulfate, sulfide, DIC, and total alkalinity) in the three cores: Lomvi 893MC **(a)**, Lomvi 008PC **(b)** and Lunde 886MC **(c)**.

partner bacteria involved in AOM produce characteristic fatty acids (C16 : 1ω5c, and cyC17 : 0ω5, 6) which we observed at relatively high concentrations (Fig. 4a–c). As these bacteria incorporate ^{13}C-depleted DIC produced by the anaerobic methanotrophs (Wegener et al., 2008), their stable carbon isotope signature was also depleted in ^{13}C. The biomarker data are consistent with an active AOM microbial population at all Vestnesa Ridge sites.

Our data also show, however, clear differences in the abundance of AOM-derived lipids at the three investigated coring sites (Fig. 4a–c). To highlight these differences, we calculated average concentrations and the isotopic depletion of archaeol and fatty acid C16 : 1ω5c (i.e., typical ANME and associated SRB lipids) relative to source methane ($\Delta\delta^{13}$C values) and compared these values to a non-seeping reference site south of Svalbard (Yao et al., 2017) and a known high methane flux site at Hydrate Ridge (Elvert et al., 2005) (Fig. 5). We chose Hydrate Ridge as the high flux comparison site because the only other observation of a mini-fracture was documented from that location (Briggs et al., 2011). We

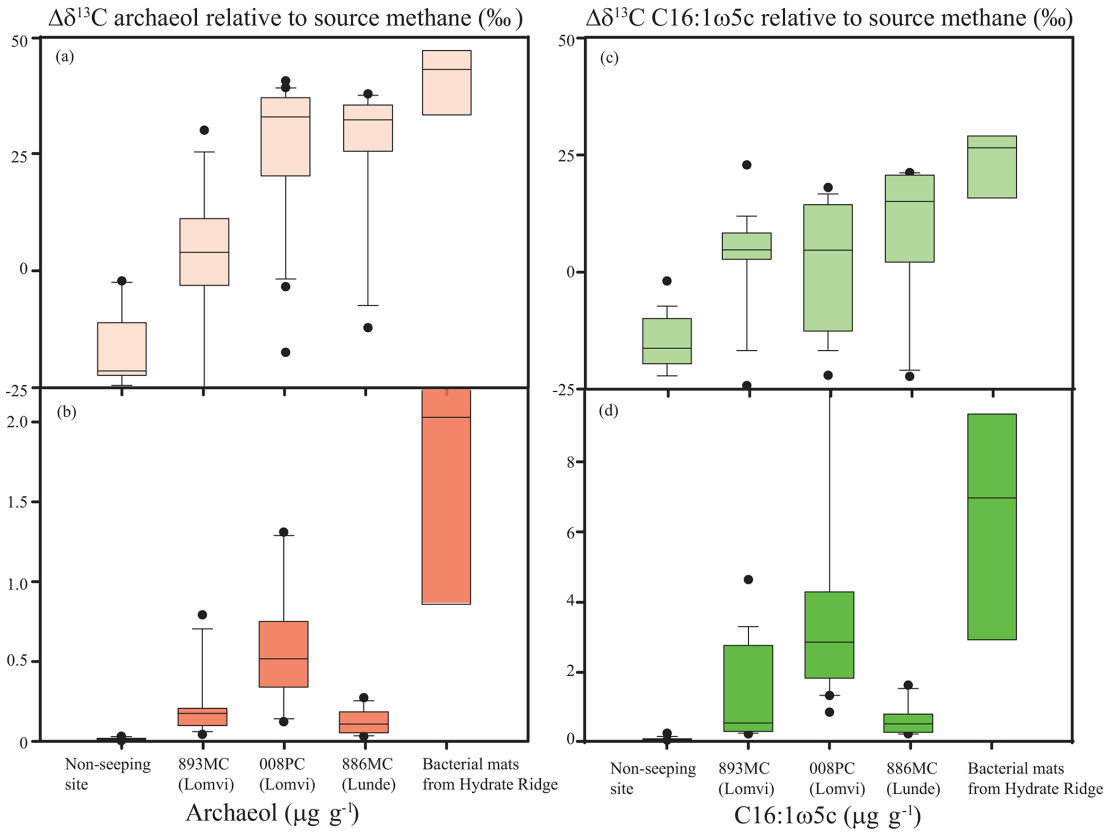

Figure 5. Average lipid biomarker concentrations and isotopic differences to source methane of the archaeal lipid archaeol ($\Delta\delta^{13}$C) **(a, b)** and the bacterial fatty acid C16 : 1ω5c **(c, d)**. Cores Lomvi 893MC (averaged from 0–35 cm), Lomvi 008PC (averaged from 0–33 cm), and Lunde 886MC (averaged from 0–38 cm) are compared to a high flux site at Hydrate Ridge (Elvert et al., 2005) and a core from a non-seeping site south of Svalbard (1522GC, 76.107° N, 15.957° E, averaged from 0–350 cm; Yao et al., 2017).

found the lowest concentrations of the diagnostic lipids at the non-seeping reference site, followed by the core Lunde 886MC, the core Lomvi 893MC, the core Lomvi 008PC, and finally the Hydrate Ridge core. The substantially higher concentration of AOM-derived lipids at the Lomvi (particular in core Lomvi 008PC) compared to the Lunde site (core Lunde 886MC) is consistent with the geochemical signals of AOM (e.g., sulfate, sulfide, δ^{13}C of DIC) in the respective cores. The differences in concentrations of diagnostic lipids suggest a high standing stock of AOM communities in core Lomvi 008PC, and a much lower one in the other two cores. AOM communities grow very slowly, with doubling times of several months (Nauhaus et al., 2007; Zhang et al., 2011; Timmers et al., 2015). A sudden increase in methane flux and methane concentrations in the sulfate-rich sediments, which comprise only a small initial standing stock of AOM microorganisms, may eventually lead to elevated AOM activity, but with a significant lag time of several months to years. Our biomarker data suggest that the methanotrophic community at coring site Lomvi 893MC was not well developed, indicating that the increase in methane concentrations at that site occurred rather recently, probably less than a few years prior to our sampling campaign. We found a more mature AOM community at the site Lomvi 008PC. Similarly, the previous findings of biofilms associated with the mini-fracture at Hydrate Ridge (Briggs et al., 2011) indicate a more mature AOM community at this site. This suggests that the methane flux was higher at these sites for a longer period of time, allowing for the establishment of the slow-growing AOM community.

Because of the spatial dynamics of venting at the Lomvi pockmark in Vestnesa Ridge (Bohrmann et al., 2017; Hong et al., 2017a, b; Panieri et al., 2017), it is likely that the biomarker results reflect the cumulative history of microbial AOM activity, rather than solely the most recent situation. Nonetheless, we observed a general decrease in δ^{13}C of both bacterial and archaeal lipids in horizons of present-day sulfate depletion, indicating a higher contribution of AOM-derived compounds to the lipid pool. Such a decrease in δ^{13}C was apparent at $\sim$ 10 cm b.s.f. in Lomvi 893MC where sulfide started to accumulate, at $\sim$ 5 cm b.s.f. in core Lomvi 008PC where sulfate was depleted, and at 10–15 cm b.s.f. in Lunde 886MC where methane began to increase downcore (Fig. 4). At these depths, the ratios of *sn2*-hydroxyarchaeol

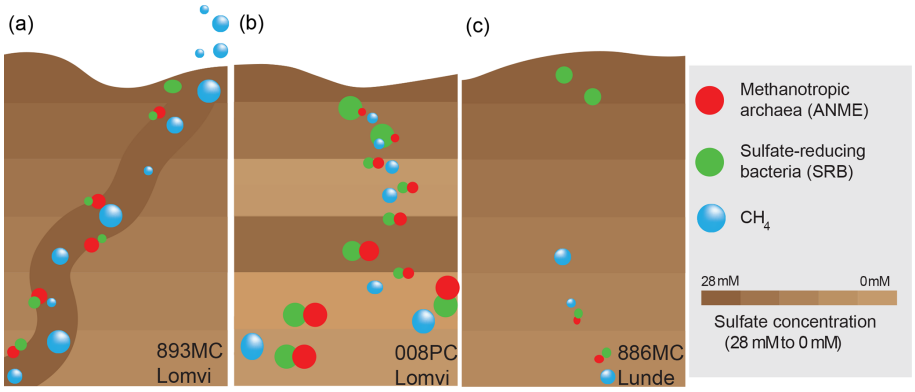

Figure 6. Schematic illustration of different methane transport modes in the study area (big bubble and circle sizes highlight high methane concentrations and the approximate size of the standing stocks of AOM communities, respectively). Low amounts of methane in a diffusion-dominated setting sustain a weakly defined AOM microbial community **(c)**. Mini-fracturing enhances the methane availability and fosters AOM community growth **(a)**. The AOM community is fully developed after advective methane transport has continued for a longer period of time **(b)**.

to archaeol were 0.98 (core Lomvi 893MC), 0.37 (core Lomvi 008PC), and 0.26 (core Lunde 886MC), indicating that ANME-1 is likely to be a key AOM organism at all the investigated coring sites (Niemann and Elvert, 2008). The known SRB types associated with ANME-1 and ANME-2 belong to the *Deltaproteobacteria, Desulfosarcina/Desulfococcus* clade Seep-SRB1, which typically display distinct ratios of the fatty acids C16 : 1ω5c relative to isoC15 : 0. In systems dominated by Seep-SRB1 associated with ANME-1 this value is commonly < 2, while it is $\gg 2$ in systems where Seep-SRB-1 is associated with ANME-2 (Niemann and Elvert, 2008). At all coring locations, this biomarker ratio was > 2 (3.2, core Lomvi 893MC; 5.4, core Lomvi 008PC; 7.9, core Lunde 886MC), which is indicative of an SRB eco-type associated with ANME-2 rather than ANME-1. At this point, we can only speculate about these contradicting lipid patterns, and additional DNA-based tools would be needed to further identify the key AOM microbes at the investigated sites.

The ^{13}C values of lipids from AOM communities are mainly influenced by isotope fractionation during AOM and the δ^{13}C value of the carbon sourced from methane (Summons et al., 1994; Riou et al., 2010), though other environmental parameters such as substrate availability and temperature are also known to influence lipid δ^{13}C signals. δ^{13}C CH_4 values are typically low and the additional isotope fractionation during AOM results in AOM-derived lipid, with δ^{13}C values $\ll -50$ ‰. Our reference site showed δ^{13}C values of archaeal and bacterial lipids that were not conspicuously depleted. This indicates a low or negligible standing stock of AOM microbes at this site. Here, archaeal and bacterial lipids likely originated from processes other than AOM (e.g., organic matter degradation by heterotrophs). At site Lomvi 893MC, the δ^{13}C values of archaeal and bacterial lipids were not as negative as at the other three sites. The differences in the δ^{13}C signature of archaeol with respect to the source methane (δ^{13}C $CH_4 = -57.8$ ‰ in core Lomvi 893MC and -62.9 ‰ in core Lunde 886MC; Panieri et al., 2017), were slightly lower in core Lomvi 893MC than in core Lunde 886MC (Fig. 5a). This may reflect an overprint by lipids that are not related to AOM, which supports our assumption that the mini-fracture in core Lomvi 893MC and the associated AOM community developed rather recently. We do not know the source methane δ^{13}C value for core Lomvi 008PC, but, assuming a uniform source methane value of -55 ‰ for the whole Lomvi pockmark area, the highest $\Delta\delta^{13}$C values were observed at Lomvi 008PC (Fig. 5). Together with the biomarker evidence for a significant AOM community and the rapid depletion of sulfate in this core, this indicates that AOM biomass (and probably AOM activity) is more dominant at the Lomvi 008PC coring site than at the other two investigated sites. Although the AOM community seemed lower at Lunde 886MC, the $\Delta\delta^{13}$C values were similar to the ones observed at Lomvi 008PC. This suggests that here, despite the lower methane flux, AOM communities also dominated the overall microbial community.

4 Summary and conclusion

At the Lomvi pockmark, we found evidence for advective methane transport, with an indication for different onsets of gas seepage at the different coring sites, while at the coring site at the Lunde pockmark, methane transport is dominated by diffusion (Fig. 6). Together with the porewater geochemical constraints, the distribution of ^{13}C-depleted lipid biomarkers underscores that the pockmark methane biogeochemistry is differentially affected by the advective vs. diffusive transport regimes. Our data show that high standing stocks of AOM communities thrive in surface sediments where methane concentrations are high, while in sediments

where methane availability is limited, only a comparably low AOM biomass developed. The co-occurrence of a well-developed AOM standing stock and high CH_4 concentrations, however, cannot be considered a universal rule. Despite high methane concentrations in sediments featuring a mini-fracture, sediments contained a comparably low standing stock of AOM communities, and geochemical signals for AOM activity were rather subtle. Methane transport through mini-fractures is advective and fractures thus represent important conduits for methane, facilitating the development of an active AOM community. Yet a high biomass of the slow-growing AOM communities require that advective transport has proceeded for an extended period of time after the onset of sediment fracturing (i.e., the development of AOM communities temporally lags behind). Our data suggest that the mini-fracture detected here opened rather recently, whereas methane transport at the other coring sites probably started much earlier. Mini-fractures are rarely recognized because they are below the resolution of seismic imaging tools and their detection is mostly incidental. Our study clearly highlights their relevance for benthic methane dynamics and adds to the very limited knowledge on the potential contribution of fracture networks to benthic carbon cycling.

Data availability. All the data in the paper can be found in the Supplement.

Supplement. The supplement related to this article is available online at: https://doi.org/10.5194/bg-16-2221-2019-supplement.

Author contributions. HY and GP collected biomarker samples. WLH, MET, and SS contributed to porewater sampling and analyses. HN and MFL supported lipid biomarker analyses. HY wrote the majority of the paper. GP and HN supervised the research. All authors contributed to the discussion of data and the writing of the paper at different stages.

Competing interests. The authors declare that they have no conflict of interest.

Acknowledgements. We would like to acknowledge the captains, crews and all scientists on board R/V *Helmer Hanssen* cruise CAGE 15-2 and R/V *G.O. Sars* cruise P1606. We are especially thankful for Towcam operation by the team from Woods Hole Oceanographic Institution (WHOI) MISO (Multidisciplinary Instrumentation in Support of Oceanography) as well as ROV operation by the Ægir pilots. We would further like to thank Carsten J. Schubert and Serge Robert from EAWAG for the support during carbon isotopic analyses. This work was supported by the Research Council of Norway through its Centres of Excellence funding scheme (project number 223259). The publication charges for this article have been funded by a grant from the publication fund of UiT The Arctic University of Norway in Tromsø.

Financial support. This research has been supported by the Research Council of Norway (grant no. 223259).

Review statement. This paper was edited by Aninda Mazumdar and reviewed by Wriddhiman Ghosh and one anonymous referee.

References

Anders, M. H., Laubach, S. E., and Scholz, C. H.: Microfractures: A review, J. Struct. Geol., 69, 377–394, https://doi.org/10.1016/j.jsg.2014.05.011, 2014.

Berndt, C., Feseker, T., Treude, T., Krastel, S., Liebetrau, V., Niemann, H., Bertics, V. J., Dumke, I., Dunnbier, K., Ferre, B., Graves, C., Gross, F., Hissmann, K., Huhnerbach, V., Krause, S., Lieser, K., Schauer, J., and Steinle, L.: Temporal constraints on hydrate-controlled methane seepage off Svalbard, Science, 343, 284–287, https://doi.org/10.1126/science.1246298, 2014.

Bernhard, J. M. and Panieri, G.: Keystone Arctic paleoceanographic proxy association with putative methanotrophic bacteria, Sci. Rep.-UK, 8, 10610, https://doi.org/10.1038/s41598-018-28871-3, 2018.

Blees, J., Niemann, H., Wenk, C. B., Zopfi, J., Schubert, C. J., Jenzer, J. S., Veronesi, M., and Lehman, M. F.: Bacterial methanotrophs drive the formation of a seasonal anoxic benthic nepheloid layer in an alpine lake, Limnol. Oceanogr., 59, 1410–1420, https://doi.org/10.4319/lo.2014.59.4.1410, 2014.

Boetius, A. and Suess, E.: Hydrate Ridge: a natural laboratory for the study of microbial life fueled by methane from near-surface gas hydrates, Chem. Geol., 205, 291–310, https://doi.org/10.1016/j.chemgeo.2003.12.034, 2004.

Bohrmann, G., Ahrlich, F., Bergenthal, M., Bünz, S., Düßmann, R., Ferreira, C., Freudenthal, T., Fröhlich, S., Hamann, K., Hong, W.-L., Hsu, C., Johnson, J. E., Kaszemeik, K., Kausche, A., Klein, T., Lange, M., Lepland, A., Malnati, J., Meckel, S., Meyer-Schack, B., Noorlander, K., Panieri, G., Pape, T., Reuter, M., Riedel, M., Rosiak, U., Schmitdt, C., Schmidt, W., Seiter, C., Spagnoli, G., Stachowski, A., Stange, N., Wallmann, K., Wintersteller, P., Wunsch, D., and Yao, H.: R/V *MARIA S. MERIAN* Cruise Report MSM57, Gas Hydrate Dynamics at the Continental Margin of Svalbard, Reykjavik – Longyearbyen – Reykjavik, 29 July–07 September 2016, MARUM – Zentrum für Marine Umweltwissenschaften, Fachbereich Geowissenschaften, Universität Bremen, 1–204, 2017.

Briggs, B. R., Pohlman, J. W., Torres, M., Riedel, M., Brodie, E. L., and Colwell, F. S.: Macroscopic biofilms in fracture-dominated sediment that anaerobically oxidize methane, Appl. Environ. Microb., 77, 6780–6787, https://doi.org/10.1128/AEM.00288-11, 2011.

Bünz, S., Polyanov, S., Vadakkepuliyambatta, S., Consolaro, C., and Mienert, J.: Active gas venting through hydrate-bearing sediments on the Vestnesa Ridge, offshore W-Svalbard, Mar. Geol., 332–334, 189–197, https://doi.org/10.1016/j.margeo.2012.09.012, 2012.

Cline, J. D.: Spectrophotometric Determination of Hydrogen Sulfide in Natural Waters, Anal. Chem., 21, 1005–1009, 1969.

Egeberg, P. K. and Dickens, G. R.: Thermodynamic and pore water halogen constraints on gas hydrate distribution at ODP Site 997 Blake Ridge, Chem. Geol., 153, 53–79, 1999.

Egger, M., Riedinger, N., Mogollón, J. M., and Jørgensen, B. B.: Global diffusive fluxes of methane in marine sediments, Nat. Geosci., 11, 421–425, https://doi.org/10.1038/s41561-018-0122-8, 2018.

Elvert, M., Boetius, A., Knittel, K., and Jørgensen, B. B.: Characterization of Specific Membrane Fatty Acids as Chemotaxonomic Markers for Sulfate-Reducing Bacteria Involved in Anaerobic Oxidation of Methane, Geomicrobiol. J., 20, 403–419, https://doi.org/10.1080/01490450303894, 2003.

Elvert, M., Hopmans, E. C., Treude, T., Boetius, A., and Suess, E.: Spatial variations of methanotrophic consortia at cold methane seeps: implications from a high-resolution molecular and isotopic approach, Geobiology, 3, 195–209, 2005.

Emery, D. and Myers, K. J.: Sequence Stratigraphy, Blackwell Science, Oxford, 1996.

Fischer, D., Mogollón, J. M., Strasser, M., Pape, T., Bohrmann, G., Fekete, N., Spiess, V., and Kasten, S.: Subduction zone earthquake as potential trigger of submarine hydrocarbon seepage, Nat. Geosci., 6, 647–651, https://doi.org/10.1038/ngeo1886, 2013.

Friedman, M.: Fractur in Rock, Rev. Geophys. Space Phys., 13, 352–358, 1975.

Gabrielsen, R. H., Aarland, R.-K., and Alsaker, E.: Identification and spatial distribution of fractures in porous, siliclastic sediments, in: Structrual Geology in Reservoir Characterization, edited by: Coward, M. P., Daltaban, T. S., and Johnson, H., Geological Society, London, 49–64, 1998.

Gieske, J., Gamo, T., and Brumsack, H.: Chemical methods for interstitial water analysis aboard joides resolution ocean drilling program, Texas A&M University Technical Note 15, 1991.

Grasshoff, K., Kremling, K., and Ehrhardt, M.: Methods of Seawater Analysis, Wiley-VCH, Weinheim/Deerfield Beach, Florida, 1999.

Haeckel, M., Boudreau, B. P., and Wallmann, K.: Bubble-induced porewater mixing: A 3-D model for deep porewater irrigation, Geochim. Cosmochim. Ac., 71, 5135–5154, https://doi.org/10.1016/j.gca.2007.08.011, 2007.

Hong, W.-L., Sauer, S., Panieri, G., Ambrose, W. G., James, R. H., Plaza-Faverola, A., and Schneider, A.: Removal of methane through hydrological, microbial, and geochemical processes in the shallow sediments of pockmarks along eastern Vestnesa Ridge (Svalbard), Limnol. Oceanogr., 61, S324–S343, https://doi.org/10.1002/lno.10299, 2016.

Hong, W.-L., Schmidt, C., Yao, H., Wallmann, K., Rae, J., Lepland, A., Torres, M., Plaza-Faverola, A., Latour, P., Bunz, S., and Bohrmann, G.: Fracture-Induced Fluid Migration in an Arctic Deep Water Pockmark: Porewater Geochemistry from the MEBO Drilling (MSM57) in Vestnesa Ridge (Svalbard), Goldschmidt Abstract, Paris, 2017a.

Hong, W. L., Torres, M. E., Carroll, J., Cremiere, A., Panieri, G., Yao, H., and Serov, P.: Seepage from an arctic shallow marine gas hydrate reservoir is insensitive to momentary ocean warming, Nat. Commun., 8, 15745, https://doi.org/10.1038/ncomms15745, 2017b.

Hong, W. L., Torres, M. E., Portnov, A., Waage, M., Haley, B., and Lepland, A.: Variations in Gas and Water Pulses at an Arctic Seep: Fluid Sources and Methane Transport, Geophys. Res. Lett., 45, 4153–4162, https://doi.org/10.1029/2018gl077309, 2018.

Hovland, M., Gardner, J. V., and Judd, A. G.: The significance of pockmarks to understanding fluid flow processes and geohazards, Geofluids, 2, 127–136, https://doi.org/10.1046/j.1468-8123.2002.00028.x, 2002.

Knies, J., Daszinnies, M., Plaza-Faverola, A., Chand, S., Sylta, Ø., Bünz, S., Johnson, J. E., Mattingsdal, R., and Mienert, J.: Modelling persistent methane seepage offshore western Svalbard since early Pleistocene, Mar. Petrol. Geol., 91, 800–811, https://doi.org/10.1016/j.marpetgeo.2018.01.020, 2018.

Knittel, K. and Boetius, A.: Anaerobic oxidation of methane: progress with an unknown process, Annu. Rev. Microbiol., 63, 311–334, https://doi.org/10.1146/annurev.micro.61.080706.093130, 2009.

Levin, L. A., Baco, A. R., Bowden, D. A., Colaco, A., Cordes, E. E., Cunha, M. R., Demopoulos, A. W. J., Gobin, J., Grupe, B. M., Le, J., Metaxas, A., Netburn, A. N., Rouse, G. W., Thurber, A. R., Tunnicliffe, V., Van Dover, C. L., Vanreusel, A., and Watling, L.: Hydrothermal Vents and Methane Seeps: Rethinking the Sphere of Influence, Front. Mar. Sci., 3, https://doi.org/10.3389/fmars.2016.00072, 2016.

Moss, C. W. and Lambert-Fair, M. A.: Location of Double Bonds in Monounsaturated Fatty Acids of Campylobacter cryaerophila with Dimethyl Disulfide Derivatives and Combined Gas Chromatography-Mass Spectrometry, J. Clin. Microbiol., 27, 1467–1470, 1989.

Nauhaus, K., Albrecht, M., Elvert, M., Boetius, A., and Widdel, F.: In vitro cell growth of marine archaeal-bacterial consortia during anaerobic oxidation of methane with sulfate, Environ. Microbiol., 9, 187–196, https://doi.org/10.1111/j.1462-2920.2006.01127.x, 2007.

Nichols, P. D., Guckert, J. B., and White, D. C.: Determination of monounsaturated fatty acid double-bond position and geometry for microbial monocultures and complex consortia by capillary GC-MS of their dimethyl disulphide adducts, J. Microbiol. Meth., 5, 49–55, 1986.

Niemann, H. and Elvert, M.: Diagnostic lipid biomarker and stable carbon isotope signatures of microbial communities mediating the anaerobic oxidation of methane with sulphate, Org. Geochem., 39, 1668–1677, https://doi.org/10.1016/j.orggeochem.2007.11.003, 2008.

Niemann, H., Elvert, M., Hovland, M., Orcutt, B., Judd, A., Suck, I., Gutt, J., Joye, S., Damm, E., Finster, K., and Boetius, A.: Methane emission and consumption at a North Sea gas seep (Tommeliten area), Biogeosciences, 2, 335–351, https://doi.org/10.5194/bg-2-335-2005, 2005.

Niemann, H., Duarte, J., Hensen, C., Omoregie, E., Magalhães, V. H., Elvert, M., Pinheiro, L. M., Kopf, A., and Boetius, A.: Microbial methane turnover at mud volcanoes of the Gulf of Cadiz, Geochim. Cosmochim. Ac., 70, 5336–5355, https://doi.org/10.1016/j.gca.2006.08.010, 2006a.

Niemann, H., Losekann, T., de Beer, D., Elvert, M., Nadalig, T., Knittel, K., Amann, R., Sauter, E. J., Schluter, M., Klages, M., Foucher, J. P., and Boetius, A.: Novel microbial communities of the Haakon Mosby mud volcano

and their role as a methane sink, Nature, 443, 854–858, https://doi.org/10.1038/nature05227, 2006b.

Niemann, H., Fischer, D., Graffe, D., Knittel, K., Montiel, A., Heilmayer, O., Nöthen, K., Pape, T., Kasten, S., Bohrmann, G., Boetius, A., and Gutt, J.: Biogeochemistry of a low-activity cold seep in the Larsen B area, western Weddell Sea, Antarctica, Biogeosciences, 6, 2383–2395, https://doi.org/10.5194/bg-6-2383-2009, 2009.

Niemann, H., Linke, P., Knittel, K., MacPherson, E., Boetius, A., Bruckmann, W., Larvik, G., Wallmann, K., Schacht, U., Omoregie, E., Hilton, D., Brown, K., and Rehder, G.: Methane-carbon flow into the benthic food web at cold seeps – a case study from the Costa Rica subduction zone, PLoS One, 8, e74894, https://doi.org/10.1371/journal.pone.0074894, 2013.

Panieri, G., Fornari, D. J., Serov, P., Astrom, E. K. L., Plaza-Faverola, A., Mienert, J., and Torres, M.: Gas hydrate, carbonate cruists, and chemosynthetic organisms on Vestnesa Ridge Pockmark – Preliminary findings, Fire in the Ice, 15, 14–17, 2015.

Panieri, G., Bünz, S., Fornari, D. J., Escartin, J., Serov, P., Jansson, P., Torres, M. E., Johnson, J. E., Hong, W., Sauer, S., Garcia, R., and Gracias, N.: An integrated view of the methane system in the pockmarks at Vestnesa Ridge, 79° N, Mar. Geol., 390, 282–300, https://doi.org/10.1016/j.margeo.2017.06.006, 2017.

Plaza-Faverola, A., Bünz, S., Johnson, J. E., Chand, S., Knies, J., Mienert, J., and Franek, P.: Role of tectonic stress in seepage evolution along the gas hydrate-charged Vestnesa Ridge, Fram Strait, Geophys. Res. Lett., 42, 733–742, https://doi.org/10.1002/2014gl062474, 2015.

Reeburgh, W. S.: Oceanic Methane Biogeochemistry, Chem. Rev., 107, 486–513, 2007.

Riedel, M., Collett, T. S., Malone, M. J., and the Expedition 311 Scientists: Proc. IODP, 311: Washington, DC (Integrated Ocean Drilling Program Management International, Inc.), https://doi.org/10.2204/iodp.proc.311.2006, 2006.

Riou, V., Bouillon, S., Serrão Santos, R., Dehairs, F., and Colaço, A.: Tracing carbon assimilation in endosymbiotic deep-sea hydrothermal vent Mytilid fatty acids by ^{13}C-fingerprinting, Biogeosciences, 7, 2591–2600, https://doi.org/10.5194/bg-7-2591-2010, 2010.

Sahling, H., Römer, M., Pape, T., Bergès, B., dos Santos Fereirra, C., Boelmann, J., Geprägs, P., Tomczyk, M., Nowald, N., Dimmler, W., Schroedter, L., Glockzin, M., and Bohrmann, G.: Gas emissions at the continental margin west of Svalbard: mapping, sampling, and quantification, Biogeosciences, 11, 6029–6046, https://doi.org/10.5194/bg-11-6029-2014, 2014.

Sauer, S., Hong, W.-L., Knies, J., Lepland, A., Forwick, M., Klug, M., Eichinger, F., Baranwal, S., Crémière, A., Chand, S., and Schubert, C. J.: Sources and turnover of organic carbon and methane in fjord and shelf sediments off northern Norway, Geochem. Geophy. Geosy., 17, 4011–4031, https://doi.org/10.1002/2016gc006296, 2016.

Seeberg-Elverfeldt, J., Schluter, M., Feseker, T., and Kolling, M.: Rhizon sampling of porewaters near the sediment-water interface of aquatic systems, Limnol. Oceanogr., 3, 361–371, 2005.

Smith, A. J., Mienert, J., Bunz, S., and Greinert, J.: Thermogenic methane injection via bubble transport into the upper Arctic Ocean from the hydrate-charged Vestnesa Ridge, Svalbard, Geochem. Geophy. Geosy., 15, 1945–1959, 2014.

Steinle, L., Knittel, K., Felber, N., Casalino, C., de Lange, G., Tessarolo, C., Stadnitskaia, A., Sinninghe Damsté, J. S., Zopfi, J., Lehmann, M. F., Treude, T., and Niemann, H.: Life on the edge: active microbial communities in the Kryos $MgCl_2$-brine basin at very low water activity, ISME J., 12, 1414–1426, https://doi.org/10.1038/s41396-018-0107-z, 2018.

Summons, R. E., Jahnke, L. L., and Roksandic, Z.: Carbon isotopic fractionation in lipids from methanotrophic bacteria: Relevance for interpretation of the geochemical record of biomarkers, Geochim. Cosmochim. Ac., 58, 2853–2863, https://doi.org/10.1016/0016-7037(94)90119-8, 1994.

Timmers, P. H., Gieteling, J., Widjaja-Greefkes, H. C., Plugge, C. M., Stams, A. J., Lens, P. N., and Meulepas, R. J.: Growth of anaerobic methane-oxidizing archaea and sulfate-reducing bacteria in a high-pressure membrane capsule bioreactor, Appl. Environ. Microb., 81, 1286–1296, https://doi.org/10.1128/AEM.03255-14, 2015.

Tobin, H., Vannucchi, P., and Meschede, M.: Structure, inferred mechanical properties, and implications for fluid transport in the décollement zone, Costa Rica convergent margin, Geology, 29, 907–910, https://doi.org/10.1130/0091-7613(2001)029<0907:SIMPAI>2.0.CO;2, 2001.

Torres, M. E., McManus, J., Hammond, D. E., De Angelis, M. A., Heeschen, K. U., Colbert, S. L., Tryon, M. D., Brown, K. M., and Suess, E.: Fluid and chemical fluxes in and out of sediments hosting methane hydrate deposits on Hydrate Ridge, OR, I: Hydrological provinces, Earth Planet. Sc. Lett., 201, 525–540, 2002.

Torres, M. E., Mix, A. C., and Rugh, W. D.: Precise δ^{13}C analysis of dissolved inorganic carbon in natural waters using automated headspace sampling and continuous-flow mass spectrometry, Limnol. Oceanogr.-Meth., 3, 349–360, https://doi.org/10.4319/lom.2005.3.349, 2005.

Treude, T., Boetius, A., Knittel, K., Wallmann, K., and Jørgensen, B.: Anaerobic oxidation of methane above gas hydrates at Hydrate Ridge, NE Pacific Ocean, Mar. Ecol.-Prog. Ser., 264, 1–14, 2003.

Ussler, W. and Paull, C. K.: Rates of anaerobic oxidation of methane and authigenic carbonate mineralization in methane-rich deep-sea sediments inferred from models and geochemical profiles, Earth Planetary Sc. Lett., 266, 271–287, https://doi.org/10.1016/j.epsl.2007.10.056, 2008.

Waage, M., Portnov, A., Serov, P., Bünz, S., Waghorn, K. A., Vadakkepuliyambatta, S., Mienert, J., and Andreassen, K.: Geological Controls on Fluid Flow and Gas Hydrate Pingo Development on the Barents Sea Margin, Geochem. Geophy. Geosy., 20, 630–650, https://doi.org/10.1029/2018GC007930, 2019.

Wegener, G., Niemann, H., Elvert, M., Hinrichs, K. U., and Boetius, A.: Assimilation of methane and inorganic carbon by microbial communities mediating the anaerobic oxidation of methane, Environ. Microbiol., 10, 2287–2298, 2008.

Weinberger, J. and Brown, K.: Fracture networks and hydrate distribution at Hydrate Ridge, Oregon, Earth Planet. Sc. Lett., 245, 123–136, https://doi.org/10.1016/j.epsl.2006.03.012, 2006.

Whiticar, M.: Carbon and hydrogen isotope systematics of bacterial formation and oxidation of methane, Chem. Geol., 161, 291–314, 1999.

Yao, H., Panieri, G., Knies, J., Belt, S. T., Koseoglu, D., and Niemann, H.: Past Methane Emissions in the Storfjordrenna Gas Hydrate-Bearing Mounds, Goldschmidt Abstract, Paris, 2017.

Zhang, Y., Maignien, L., Zhao, X., Wang, F., and Boon, N.: Enrichment of a microbial community performing anaerobic oxidation of methane in a continuous high-pressure bioreactor, BMC Microbiol., 11, 137, https://doi.org/10.1186/1471-2180-11-137, 2011.

Paper II

Multi-proxy approach to unravel methane emission history of an Arctic cold seep

Haoyi Yao, Helge Niemann , Giuliana Panieri

submitted to Quaternary Science Reviews

Multi-proxy approach to unravel methane emission history of an Arctic cold seep

Haoyi Yao[1], Helge Niemann [1,2,3], Giuliana Panieri[1],
[1] CAGE - Centre for Arctic Gas Hydrate, Environment and Climate, Department of Geosciences, UiT The Arctic University of Norway in Tromsø, Norway
[2] NIOZ Royal Institute for Sea Research, Department of Marine Microbiology and Biogeochemistry, and Utrecht University, P.O. Box 59, 1790 AB Den Burg, Texel, The Netherlands
[3] Department of Environmental Sciences, University of Basel, Bernoullistrasse 30, CH-4056 Basel, Switzerland

Arctic Ocean sediments contain large amounts of methane in the form of free gas and gas hydrate. This highly dynamic reservoir is susceptible to bottom water warming. The warming may lead to gas hydrate destabilization with elevated methane fluxes. Reconstructing past methane dynamics can be achieved by using proxy indicators left in the geological record, but the fidelity of a single indicator is often poor. To overcome the restrictions of single proxies, we applied a multiple proxy approach for paleo seepage reconstruction from sediment records at gas hydrate mounds (GHMs) in Storfjordrenna (south of the Svalbard archipelago). These shallow water systems are potentially vulnerable to climate forcing. ^{14}C dating of foraminifera shells indicated an onset of deglaciation in the Storfjordrenna region at ~ 20kyr BP and allowed us to establish a stratigraphic context based on sediment Zr/Rb and Fe/Ca ratios. We identified several major (between 15- 17 kyr BP) and smaller venting phases due to gas hydrate stability changes triggered by isostatic adjustment right after the onset of the LGM. The detection of all major phases was only possible by combining data sets of stable carbon isotope compositions of foraminifera, mineralogy of authigenic carbonates, and abundance and stable carbon isotope signatures of lipid biomarkers, while single proxies did not record all events. The most robust single proxy were stable isotope signatures of archaeal biomarkers. In contrast, with sediment Ba/Ti ratios, we could only detected the major events. Our approach highlights the complexity and heterogeneity of the methane dynamic in relatively spatially limited (hundreds of meters) system. Simultaneously, it provides a comprehensive foundation for future investigation offering insights and guidance depending on the available samples and environmental conditions.

Keywords:
Methane reconstruction, proxies, foraminifera, authigenic carbonates, lipid biomarkers, geochemistry

1. General Introduction

Current global warming raises concerns about greenhouse gas emissions. One of the most potent greenhouse gas is methane. In addition to the anthropogenic methane, methane is also released from natural resources on land, from wetlands and permafrost, as well as in the ocean. In the ocean, methane seeps occur on convergent and passive continental margins, in shallow and deep-water settings (Judd and Hovland, 2007). At these seep sites, methane enriched fluids expulse from sediments into the water column at ambient temperature. Because of that, the methane seeps are also called "cold seeps," to be distinguished from "hot vents" characterized by high-temperature fluids. Methane in cold seeps is microbial, when produced in the early diagenesis, thermogenic from later burial of sedimentary organic matter (Whiticar, 1999) or abiotic through magmatic and gas-water-rock reaction. The latter formation is very rarely observed and poorly understood (Etiope and Sherwood Lollar, 2013).

On the seafloor, methane can occur as free gas, dissolved and as methane gas hydrates (MacLeod, 1982; Bohrmann and Torres, 2013). Gas hydrates (GH) are ice-like crystals consisting of methane molecules that are caged by water molecules and stable under high pressure and low temperatures (i.e. conditions that are typically met in Arctic sediments at ~400 m water depth), and where methane availability exceeds the solubility in pore fluids. Globally, gas hydrates constitute a vast and dynamic carbon reservoir in marine sediments and play an essential role in the global carbon cycle (Dickens, 2003; Ruppel and Kessler, 2017).

Especially for high latitudes, concern exists that bottom water temperatures will rise as a result of climate change. In such a scenario, the GH stability limit is shifted to greater depth (i.e., higher pressure), and GH that are stable at present may become unstable and dissociate. When gas hydrate dissociates, methane is liberated in the sediment-ocean system (Bohrmann et al., 1998; Suess et al., 2001). Indeed, already seasonal temperature differences can affect sedimentary shallow gas hydrate systems (Ferre et al., 2020) and it is expected that climate warming in the near future will accelerate the methane release. As it has been shown for the geological past hydrate dissociation induced by warming might release a vast amount of methane (Andreassen et al., 2017; Serov et al., 2017) since 1 m^3 of hydrates comprise 164 m^3 of methane gas at atmospheric pressure.

To estimate the effects of climate change on methane dynamics in the Arctic Ocean, it is useful to reconstruct the geological past of methane systems, because data on past variations of environmental parameters such as temperature and methane seepage can be used for developing model for the prediction of future methane release scenarios (Holmes et al., 2013). To establish a past methane emission history, we cannot observe the critical variable in a methane system

that no longer exists; but instead, we can use proxies. Proxies are measurable descriptors for a desired but unobservable environmental variable (Wefer et al., 1999).

In this paper, we applied a set of the most common (bio)geochemical proxies (multi-proxy approach) to investigate benthic methane dynamics, and we apply these to the case of a shallow-water gas hydrate area, Storfjordrenna, to reconstruct the emission history of this Arctic cold seep.

We investigate the (i) sedimentological parameters; (ii) geochemical evidence of gas/fluid migration; (iii) the isotope systematics of carbonate precipitates and foraminifera as well as (iv) past methanotrophic communities and the isotope signal they leave behind.

Anaerobic oxidation of methane (AOM)

In ocean sediment, most methane is consumed anaerobically within the sediment through anaerobic oxidation of methane (AOM: Eq. 1).

$$CH_4 + SO_4^{2-} \rightarrow HCO_3^- + HS^- + H_2O \qquad \text{Eq. 1.}$$

This process is mediated by a microbial consortium of sulfate-reducing bacteria (SRB) and methanotrophic archaea (ANME) (Boetius et al., 2000). The upward methane migration towards the sediment-water interface reacts with sulfate with the AOM microbial consortia. Uprising methane and sulfate (diffusing from the ocean water column) are typically consumed in a distinct zone, the sulfate-methane transition zone (SMTZ) (Barnes and Goldberg 1976; Iversen and Jørgensen, 1985), where highest AOM reaction rates usually take place.

Sedimentary proxies (Barite front and magnetic susceptibility) indicate migrating SMTZ

In marine settings, barite dissolves in the sulfate depletion zone, and reforms in the sulfate replete sediments, which can be used to infer the SMTZ when pore water data are not available (Kasten et al., 2012; Sauer et al., 2016). In sulfate-depleted sediments below the SMTZ, barite is destabilized and dissolved as barium. As the fluid migrates upwards, the dissolved barium is transported across the SMTZ and once it comes into contact with sulfate above the SMTZ barite precipitates building a 'barite front' (Torres et al., 1996; Torres et al., 2003a; Dickens, 2001; Solomon and Kastner, 2012). Indeed, barite, which can easily be detected by X-ray Fluorescence (XRF) core scanning as Ba/Ti ratio, or Ba counts, is an established proxy for reconstructing the vertical positioning of the SMTZ. Once the flux of methane increases, the SMTZ shifts upward, as does the barite front. The size of the old barite front reduces when the dissolution is slower than the upward flux, a double peak can occur (Kasten et al., 2012), or the

old barite may disappear if the dissolution is faster than the upward flux. When the methane flux decreases, the SMTZ shift downward: if there are still enough barium ions in the ambient water, a new barite front forms at the new SMTZ; if the barium ions are completely consumed, no barite front forms at the new SMTZ. The old barite front should not disappear under decreasing methane conditions. Furthermore, the appearance of the barite front also depends on the equilibrium between SMTZ stabilization and barite dissolution/precipitation.

The reducing conditions at the SMTZ generated the Fe-sulfides (Canfield and Berner, 1987; Peckmann et al., 2001; Riedinger et al., 2006; Dewangan et al., 2013) and the alteration of the initial sediment composition and magnetic properties due to replacement of magnetic Fe-oxides by paramagnetic authigenic Fe-sulfides reduced the magnetic susceptibility.

Methane derived authigenic carbonates as AOM archive

^{13}C-depleted bicarbonate is produced during AOM, which contributes to the pore water dissolved inorganic carbon (DIC), increase in alkalinity pore water, and resulting in the precipitation of methane derived authigenic carbonates (MDACs). Authigenic carbonates are characterized by negative δ^{13}C values, often below -30‰ VPDB (Peckmann and Thiel, 2004). At cold seeps, AOM is typically fueled by already ^{13}C-depleted methane carbon, and experiences strong isotope fractionation during AOM (ε = 12 to 39‰; (Holler et al., 2009)). However, the δ^{13}C values of seep carbonates are isotopically heavier than their parent methane due to admixture of relatively ^{13}C-enriched DIC during precipitation. Authigenic carbonates represent a good geochemical archive to study the history of methane seeps (Bohrmann et al., 1998; Aloisi et al., 2000; Peckmann et al., 2001; Mazzini et al., 2004; Birgel and Peckmann, 2008). Mineralogy of the carbonates can also provide some insight into the conditions of the precipitating environment. For example, the aragonites are believed to be formed close to the seafloor because the high sulfate concentration prohibits the formation of magnesium calcite and high magnesium calcite are formed in deeper sediments (Bohrmann et al., 1998; Aloisi et al., 2000; Aloisi et al., 2002; Han and Aizenberg, 2003).

Foraminifera tests: a template for authigenic carbonates

The ^{13}C-depleted bicarbonate produced during AOM can precipitate not only as authigenic carbonates concretions (Aloisi et al., 2002; Blumenberg, 2010) but also around foraminiferal shells (Panieri et al., 2009). Once dead, both benthic and planktonic species can record the ^{13}C signature from the AOM process by acting as a 'template' for carbonate to precipitate coating layers on (Panieri et al., 2016; Panieri et al., 2017; Schneider et al., 2017). The coating layers

usually exhibiting depleted ^{13}C values up to -20 ‰ and different state of shell preservation (Panieri et al., 2016; Schneider et al., 2017; Panieri et al., 2017). The $\delta^{13}C$ record of planktonic *N. pachyderma* from normal marine conditions in the Barents Sea ranges between -0.5 and 0.5 ‰ (Knies and Stein, 1998). A $\delta^{13}C$ range between 0 and 1 ‰ is considered representative of normal marine conditions in benthic *C. neoteretis* test from the northern Barents Sea (Wollenburg et al., 2001). However, the $\delta^{13}C$ as depleted as to -20 ‰ can only be explained by the diagenetic alteration after death. Both *C. neoteretis* and *N. pachyderma* are good templates for the authigenic carbonate to precipitate on (Schneider et al., 2017; Panieri et al., 2017), such MDAC precipitation at the SMTZ cumulatively added a second or third layer of ^{13}C-depleted carbon to the foraminiferal tests. The diagenetic alteration of foraminiferal test can cause a much more profound depleted ^{13}C signal as much as to -36 ‰ (Torres et al., 2003b; Hill et al., 2004; Panieri et al., 2009; Martin et al., 2010; Panieri et al., 2017; Schneider et al., 2017). Living benthic foraminifera can also incorporate the ^{13}C signature from AOM process in several ways such as using the ^{13}C-depleted bicarbonate to build the test, taking the AOM-microbes as a food source, resulting in a slightly negative $\delta^{13}C$ to the extent of -5.6 ‰ (Panieri, 2006; Panieri and Sen Gupta, 2008). Therefore, the foraminifera represents another good geochemical proxy to trace the past methane history in the marine sediments. No endemic foraminiferal species have been found at methane seeps. Particular species distribution suggests that a high abundance of endobenthic foraminifera may indicate methane seeps (Panieri and Sen Gupta, 2008) and agglutinated foraminifera are less abundant in sediments influenced by methane seepage, suggesting that this group of foraminifera does not tolerate the geochemical conditions at seeps (Dessandier et al., 2019)

Lipid biomarkers of AOM communities

AOM mediating microbes can be traced in the geological record AOM with lipid biomarkers (Niemann and Elvert, 2003, and references therein). Typically, these are constituents of the cellular membranes originating, for the case of AOM, mostly from anaerobic methanotrophic archaea - ANMEs, and sulfate-reducing bacteria – SRB). Major components of archaeal cell membranes are isopranyl glycerol di- or tetraether lipids, which are distinct from the acyl mono or di ester lipids found in bacteria. The different sulfate depends on AOM communities (ANME-1, -2, -3 and SRB of the SeepSRB1 cluster and related to *Desulfobulbus sp*.) in modern and paleoenvironments have indeed been identified through the analysis of lipid biomarkers (Hinnrichs et al., 1999; Niemann and Elvert, 2008; Lee et al., 2018; Yao et al., 2019).

Furthermore, methane of microbial and thermogenic origin, the most common methane sources, is usually ^{13}C-depleted (-100 – -50 ‰, respectively) (Whiticar, 1999), and AOM further discriminates against ^{13}C-CH_4 (ε = 12 to 39 ‰; (Holler et al., 2009)). Consequently, AOM associated lipids often display extremely depleted ^{13}C-signatures (as low as -105 ‰ for example), which allows to distinct lipids of AOM origin from background material (e.g., organic matter (OM) of photosynthetic or methanogenic origin). The SRB (partner) bacteria in AOM also show ^{13}C-depleted lipid signatures, most probably because they incorporate AOM-derived and, thus, ^{13}C-depleted CO_2 (Wegener et al., 2008).

The lipid biomarkers of ANME and SRB can trace past AOM communities and thus to some degree also AOM activity directly (in contrast to the δ^{13}C-values of foraminifera), making lipids a valuable tool for understanding methane cycling in anaerobic sedimentary environments (Hinrichs et al., 1999; Niemann et al., 2006a; Niemann et al., 2006b; Lee et al., 2018; Yao et al., 2019). However, depending on the environmental setting, lipids are also subjected to degradation (microbial and diagenetic), leading, for example, to shifts in the saturation patterns of alkyl chains (Volkman and Smittenberg, 2017) or an overall reduction in concentration. Also, the diagnostic δ^{13}C-signature of AOM lipids may be overprinted by lipids related to processes other than AOM, for example, methanogenesis (Lim et al., 2012; Kaneko et al., 2013).

Living biofilm at the AOM

The most promising evidence (proxy) for AOM would be living biomass, such as the biofilm detected by Gründger et al. (2019). However, to recover such a biofilm depends on serendipity (Gründger et al., 2019). In high seepage areas, such as Gulf of Mexico (Zhang, 2002; Joye et al., 2004), Hydrate Ridge (Borowski et al., 1997; Torres et al., 2002), only once the presence of biofilm was reported (Briggs et al., 2011), and the biofilm from the Storfjordenna GHM5 was the second report (Gründger et al., 2019). The biofilm provides direct evidence for AOM, it is measurable and the microbial community can be identified by genetic markers such as DNA.

2. Study Area

Storfjordrenna is located between the islands of Spitsbergen to the north and Bjørnøya to the south. Storfjorden trough is a broad trough that extends from the mouth of the fjord to the shelf edge. The trough was generated by glacial erosion of former ice streams of the Svalbard-Barents Sea ice sheet (Vorren et al., 1998; Dowdeswell and Elverhoi, 2002).

During a research cruise in May 2015 with R/V Helmer Hansen (CAGE 15-2 cruise), a group of mounds actively seeping methane gas from the seafloor to the water column was discovered in the Storfjordrenna area. These mounds are about 500m in diameter and about 10m in height above the seafloor. Gas hydrates were recovered from these mounds, therefore they are named as gas hydrate-bearing mounds (GHM) (Hong et al., 2017; Hong et al., 2018) or gas hydrate pingos (Serov et al., 2017; Waage et al., 2019). Real-time visually guided observations with the TowCam-Multicore system (TC-MC) (CAGE 15–2 cruise) and ROV dives (CAGE 16-5 cruise) reveal methane bubble streams rising from the mounds. Of the three identified edifices, GHM 3 (left), and 5 (lower right) objectives of this study are shown in Fig 1.

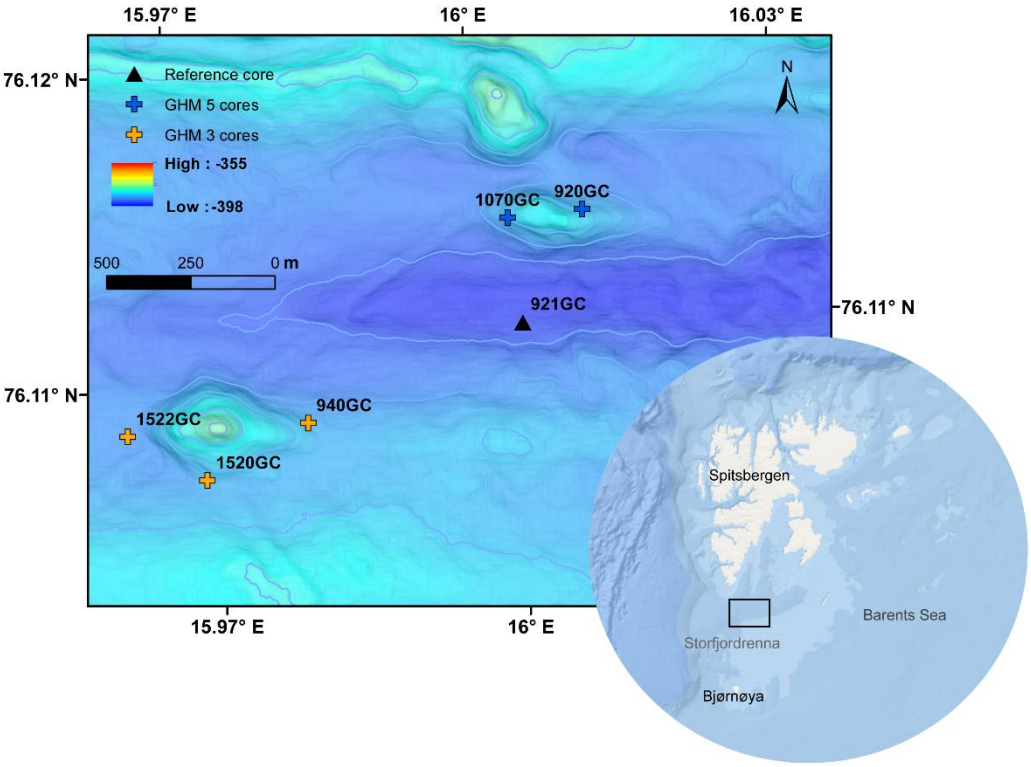

Figure 1. Map of Svalbard margin, the black square indicates the location of the study area, Storfjordrenna. Bathymetry of the study area and the site of investigated cores.

Table 1. Coring coordinates, water depths, cruises, lengths and seafloor settings of the investigated cores.

Core ID	Coordinates	Water depth (m)	Cruise	Recovery(cm)	Gas hydrate mound **(GHM)**
921GC	76.109 °N,16.002 °E	393	CAGE 15-2	365	reference
1522GC	76.107 °N,15.957 °E	388	CAGE 15-6	325	GHM 3
1520GC	76.106 °N,15.966 °E	386	CAGE 15-6	300	GHM 3
940GC	76.107 °N,15.977 °E	386	CAGE 15-2	320	GHM 3
1070GC	76.112 °N,16.002 °E	385	CAGE 16-5	260	GHM 5
920GC	76.112 °N,16.011 °E	386	CAGE 15-2	250	GHM 5

At Storfjordrenna, repeated growth and retreat of grounding glaciers shaped the seafloor bathymetry (Patton et al., 2015). Glacial-isostatic events may also reactivate fractures and faults, imposing a temporal variability on spatially heterogeneous fluid flows (Wallmann et al., 2018; Andreassen et al., 2007)). Fluid flows migrate along faults, fractures, and inclined bedding planes and transferred through unlithified sediments (Chand et al., 2012; Cartwright, 2007). In both the active (GHM 3) and inactive (GHM5) mound we studied, Waage et al., (2019) observed chimneys connected to well-defined fractures and faults within the underlying sedimentary rocks, suggesting that fault-controlled Paleocene hydrocarbon pool is responsible for charging the GHMs with free gas for thousands of years. While glacial cycles control the subsurface pore pressure related to GHSZ and the activity of the fluid flow system (Serov et al., 2017), the influence of ice-retreat in the area plays an essential role of the stability of gas hydrate stability zone (GHSZ).

3. Material and Methods:

3.1 Core collection, and non-destructive analyses (MSCL and XRF)

In this study, we selected six sediment gravity cores collected from three CAGE cruises 15-2, 15-6, and 16-5 on which we have applied the multi-proxy approach. Three cores (CAGE 15-2 940GC, CAGE 15-6 1520GC, and 1522GC) were retrieved from the most acoustically active gas hydrate mound (GHM3), and two (CAGE 15-2 920GC, CAGE 16-5 1070GC) were recovered from the only acoustically inactive mound GHM5. Finally, one reference core (CAGE-15-2 921GC) was retrieved from an area that does not show any indications of seep activity or evidence of gas hydrate presence.

Upon recovery, the cores were cut into 1m sections, split longitudinally into working and archive halves. The working half was sampled onboard for stable isotope analyses of foraminifera and authigenic carbonates, lipid biomarkers, and radiocarbon dating. The archive halves were stored at 4 °C for the non-destructive analyses sedimentary analyses.

Magnetic susceptibility was measured on the archive half in 1cm interval using a GEOTEK X-ray core imaging system (MSCL-XCT 3.0) (1520GC was not measured due to high appearances of carbonate nodules and low surface contact with the sensor). Element-geochemical data for all the cores were acquired with an Avaatech XRF Core Scanner at 1cm steps. Zr and Rb were quantified with 30 kV, 2,000 μA, at 10 s using the Pd filter. For this study, we show here the zirconium (Zr), rubidium (Rb), calcium (Ca), titanium (Ti), iron (Fe) and barium (Ba) counts ratios.

3.2 Stable isotope analyses of foraminifera and authigenic carbonates

Sediment samples were collected with variable spacing (5cm, 10cm and 20cm) throughout the cores for micropaleontological carbon and oxygen stable isotope analyses. Samples were freeze-dried and wet sieved through 63 and 125 μm mesh size sieve, and the sieved residues were oven-dried at 40 °C. The dry residue, or an aliquot obtained with a micro-splitter, was examined under a light microscope to pick out planktonic and benthic foraminifera for stable isotope analyses. Planktonic foraminifera *Neogloboquadrina pachyderma* (Ehrenberg, 1861) and benthonic foraminifera *Cassidulina neoteretis* (Seidenkrantz, 1995), and *Melonis barleeanum* (Williamson, 1858) were picked from the >125 μm size fraction and examined

using light microscopy to determine the state of preservation of foraminifera carbonate tests. Special attention was paid to signs of diagenesis, or post-depositional alteration due to the presence of authigenic carbonates (secondary overgrowth) on the foraminifera tests to be analyzed for stable isotope analyses ($\delta^{13}C$ and $\delta^{18}O$). Approximately 10µg of foraminiferal tests, which corresponds to roughly 10 to 30 individuals, were picked for each analyses.

The carbon and oxygen stable isotope compositions of the *N. pachyderma* from 921GC were measured on a Thermo Finnigan MAT252 mass spectrometer coupled to a CarboKiel-II carbonate preparation device at the stable isotope lab in Oregon State University. Other cores' foraminiferal $\delta^{13}C$ and $\delta^{18}O$ analysis were done at the stable isotope laboratory at UiT using a Thermo Scientific MAT253 Isotope Ratio Mass Spectrometer (IRMS) coupled to a Gasbench II. Foraminiferal shells were placed in 4.5 mL vials and flushed with helium gas. Prior to equilibration (over 3 hours at 50 °C), five drops of anhydrous H_3PO_4 were added manually. The samples were then analysed on the IRMS. Normalization to the VPDB for carbon and oxygen isotopes was done using in-house standards. The analytical precision was estimated to be better than 0.07 ‰ for $\delta^{13}C$ and 0.08 ‰ for $\delta^{18}O$ against the certified standard NBS-19 (Dessandier et al., 2019).

Some core intervals (Figs. 4, 8, and 9) contains carbonate nodules (from 0.5 to 2 cm in diameter) were selected for elemental composition and stable oxygen and carbon analyses. The $\delta^{13}C$ and $\delta^{18}O$ were measured using the same method as the foraminiferal shell described above at UiT.

3.3 Radiocarbon dating

Radiocarbon dating was carried out at the Beta Analytic Radiocarbon Dating facilities in Miami, US. Conventional radiocarbon ages of 17550+/- 50BP and 14680+/- 40BP were obtained from *N. pachyderma* sampled from 921GC (depth interval 325-326cm; laboratory code Beta-492581) and bivalve shell from 1070GC (depth interval 316-317cm; laboratory code Beta-492580). The ages were converted into calendar years using the calibration program Calib 7.1 (Stuiver et al., 1998) considering a marine reservoir age of -400 years that was incorporated within the Marine 13 calibration curve (Reimer et al., 2013). Also, a regional reservoir age correction ΔR of 67+/- 34 was applied (Mangerud et al., 2006). The age model is based on the calibrated ages obtained from the peaks of the probability curves within the 2σ range.

3.4 Lipid biomarker analyses

Samples for biomarker analyses were collected immediately after the retrieve of the sediment

cores onboard with a methanol-cleaned spatula at a resolution of 2 to 10 cm, wrapped in aluminum foil, and stored frozen at -20 °C until further analyses.

Extraction: Lipid biomarkers were extracted and further analyzed according to previous publications (Niemann et al., 2005; Blees et al., 2014). Briefly, a total lipid extract (TLE) was obtained by ultrasonication of ~20g wet sediment samples in four extraction steps. With decreasing polarity solvents: dichloromethane (DCM)/methanol (MeOH) 1: 2, then DCM/ MeOH 2: 1; and only DCM for the last two steps. The TLE was then saponified with NaOH and a neutral lipid fraction was extracted with hexane. The remaining polar fration which contains free fatty acids was methylated to yield fatty acid methyl esters (FAME) for gas chromatographic (GC) analyses. The double bond positions in the FAMEs were determined by analyzing the dimethyl-disulfide (DMDS) adducts. The neutral fraction obtained after saponification was further separated into hydrocarbons, ketones, and alcohols with pipette column. The alcohol fraction was further derivatized to form trimethylsilyl (TMS) adducts for gas chromatographic analyses.

Quantification, identification, and stable carbon isotope composition: Individual lipid molecules were analyzed on Gas Chromatograph (GC; Thermo Scientific TRACE™ Ultra), equipped with a capillary column (Rxi-5ms, 50 m, 0.2 mm id, 0.33 µm df) with helium as carrier gas at a constant flow of 1 mL min^{-1}. The initial oven temperature was 50 °C, held for 2 min and then increased to 140 °C at a rate of 10 °C per min, holding time at 140 °C is 1 min. Then further increased to 300°C at 4 °C per min. Final hold time was 63 min to analyze FAMEs or 160 min to analyze larger / high boiling point lipids (in the hydrocarbon and alcohol fractions), respectively. Concentrations were quantified by flame-ionization detection (FID) against internal standards. Unknown compounds were identified with a quadrupole mass spectrometry unit at the chromatography periphery (Thermo Scientific DSQ II). Similarly, compound-specific stable carbon isotope ratios were determined using a magnetic sector isotope ratio mass spectrometry unit (Thermo Scientific Delta V Advantage) coupled to the GC setup using the same temperature program as mentioned above. $\delta^{13}C$ values reported here have an analytical error of ± 1‰.

3.5 Carbonate mineralogy

We performed X-ray diffraction (XRD) analyses of unoriented carbonate nodules (ca 2-cm in diameter) found in core 1520GC, 920GC, and 940GC. Mineralogy was determined by XRD on homogenized bulk powders from the MDAC sample pieces. Before analysis, all samples were

ground in isopropanol cleaned McCrone mill. Unoriented specimens of the dried powders were prepared by side loading. All samples were measured on a Bruker D8 Advance X-ray diffractometer (Cu Kα radiation in 3-75° 2θ range) (Sauer et al., 2017). Quantitative data were obtained with the Rietveld algorithm-based code, Topas-4, provided by Bruker. Following a displacement correction of the spectrum made on the main quartz peak, the displacement of calcite d104 was used to estimate the amount of $MgCO_3$ mol% (Goldsmith et al., 1958).

4. Result and Discussion

4.1 Chronology of the study site (using reference core 921GC).

To establish the chronology of the study site, we use the 365cm long reference core 921GC collected in-between the gas hydrate mounds (GHMs) where seismic and echo sounder surveys during cruises CAGE 15-2, 15-6 and 16-5 did not find indications of seepage. We used magnetic susceptibility, Zr/Rb and Fe/Ca ratio and foraminiferal $\delta^{18}O$ from 921GC to correlate our sedimentary record with literature data (Lucchi et al., 2013; Jessen et al., 2010; Knies et al., 2018) to establish the chronology of the core. After that, we used sediment Zr/Rb and Fe/Ca ratios to correlate the reference core 921GC with the other investigated cores.

The Zr/Rb ratio is generally used to indicate the particle size, and increases as sediment grain-size increases (Dypvik and Harris, 2001). Here we use it to trace high IRD content in the cores (Lucchi et al., 2013). Importantly, the Zr/Rb ratio is not affected by methane-derived diagenesis (Dypvik and Harris, 2001). The Fe/Ca ratio can differentiate terrestrial sources input vs. marine origin. Because all cores are from a relatively small-scale area, the primary organic matter source is expected to be similar so we use Fe/Ca ratio to reinforce our correlation. We also identified and used three stratigraphic marker horizons as discussed in the next section, from post-LGM to Early Holocene in order to correlate the 921 GC with the other cores.

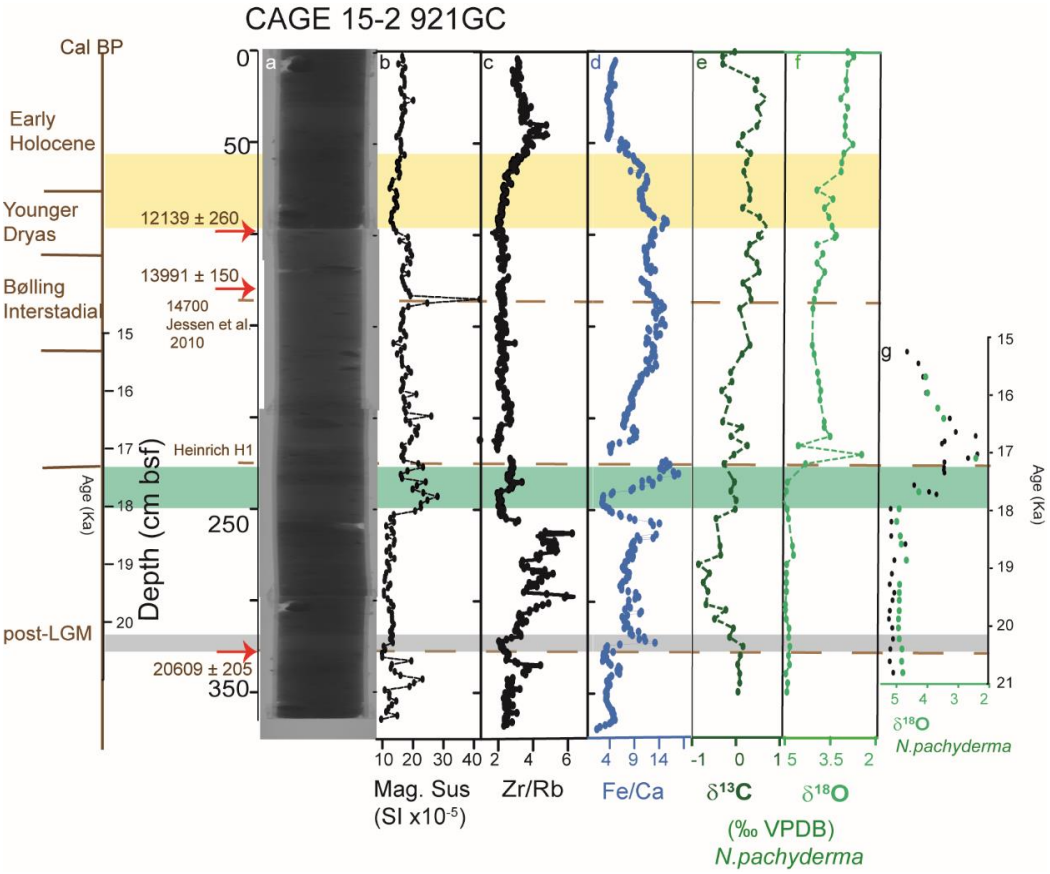

Figure 2. Reference core 921GC, from a to f, X-ray image, Magnetic Susceptibility (Mag.Sus), XRF sediment ratios of Zr/Rb, Fe/Ca, stable carbon and oxygen isotope records from *N. pachyderma*. (g) In green, partial stable oxygen isotope from core 921GC; in black, stable oxygen isotope records from the reference core obtained by Knies et al., 2018. Red arrows show radiocarbon dating from *N.pachyderma*, and dash lines show correlation from Jessen et al., 2010 in the area based on magnetic susceptibility. Yellow, green and grey bars are horizon markers. All isotope data are available in the supplementary file.

The stratigraphic sequence on 921GC is very consistent within the cores and the magnetic susceptibility values in core 921 mostly follow the Storfjordrenna Trough Mouth Fans (TMF) cores curve (Lucchi et al., 2013; Jessen et al., 2010). The three stratigraphic marker horizons for the Storfjordrenna area cover a period from post-LGM to Early Holocene. The stratigraphic marker horizon (i), coincides with a foraminifera rich event (highlighted in gray at 325 cm bsf, Fig.3 and 4), and one direct dating point of the planktonic foraminifera *N. pachyderma* at the base of it (325-326cm) revealed an age of 20609 ± 205 cal BP (highlighted in grey in Fig. 3). The marker horizon (ii) is a foraminifera rich and reddish oxidized event at 220-240 cm, characterized by increasing magnetic susceptibility, Zr/Rb and Fe/Ca ratios (highlighted in green in Fig. 3 and 4). The marker horizon (iii) is characterized by a decreasing Zr/Rb ratio together with increasing Fe/Ca ratio (highlighted in yellow in Fig. 3 and 4).

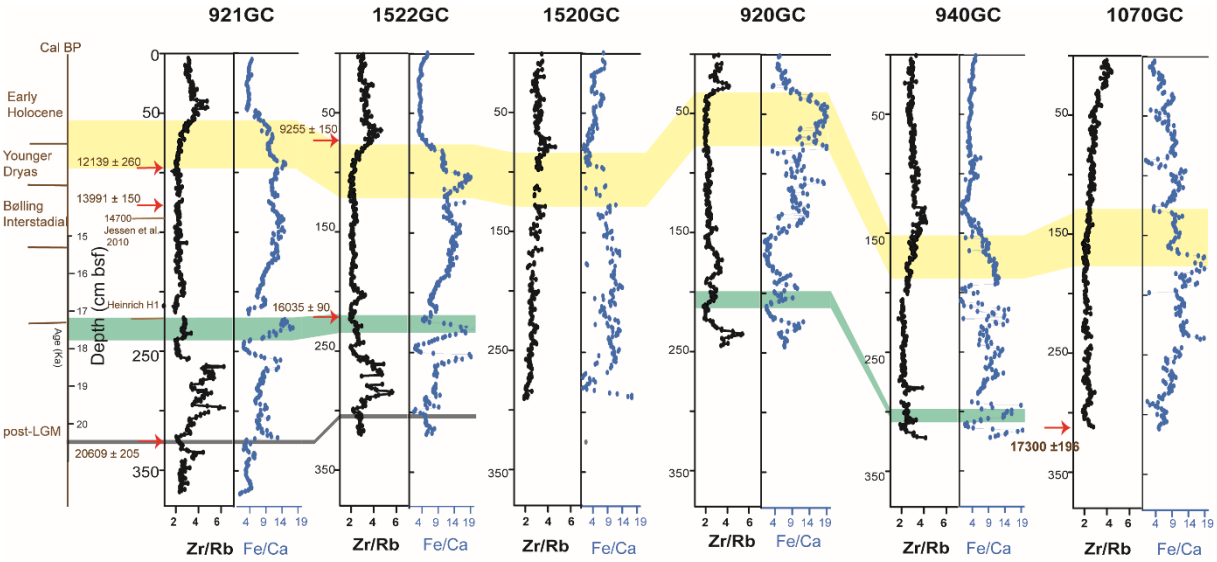

Figure 3. Core correlation with XRF Zr/Rb and Fe/Ca among all the investigated cores. Yellow, green, and grey highlighted the horizon markers; red arrows point to the direct dating point in the core.

Lucchi et al., (2013), suggest the onset of deglaciation on the Storfjorden TMF occurred around 20000 cal. BP and no later than 18000 cal. BP based on the observation of an oxidized event (assigned as OX-2), located at the base of the coarse-massive-IRD facies. The oxidized event (OX-2), believed to derived from near seabed oxidation of detrital Fe under interglacial well-ventilated conditions, marks the inception of deglaciation with the release of fresh oxygenated waters ventilating bottom oceans in the Storfjorden TMF. We found this oxidized event below the marker horizon (i) at 330-340 cm bsf in 921GC. Together with the detected signals of a foraminifera bloom and the high Zr/Rb-ratios, our observations thus support the earlier interpretations of a deglaciation onset in our study area at ~20000 cal. BP, or even earlier. The second booming of planktonic foraminifera follows the start of the deglaciation in the area, suggesting a short, renewed productivity under warmer, oxygen/nutrient-rich environment conditions (Lucchi et al., 2013).

We correlate δ^{18}O-values of *N. pachyderma* from core 921GC to a reference core from the Bjørnoya area (Knies et al., 2018) to constrain the chronology in the bottom part of our core (Fig. 3g data from Knies et al. in black vs. green from 921GC). We established that the foraminifer-rich event observed at 240-260 cm (horizon marker ii) was around 18 Ka cal BP. The decreasing Zr/Rb values (horizon marker iii) together with an increasing Fe/Ca ratio at 60 -100 cm bsf (highlighted in yellow, Fig. 3) and a peak of MS, indicate an increased supply of IRD deposited during the Heinrich H1 (Lucchi et al., 2013; Jessen et al., 2010). The other

dating tie points in the Younger Dryas and Bølling Interstadial were based on IP_{25} concentration peak correlation with another dated reference core in the area (Koseoglu et al., 2019).

Based on the chronology obtained from the reference core 921GC, we continued to use the Zr/Rb and Fe/Ca ratio to establish the chronology for the other investigated cores. We exclude the use of magnetic susceptibility (MS) for correlation purposes because, in methane seeps, iron oxides are exposed to hydrogen sulfide as the end product of AOM and produce paramagnetic pyrite (FeS_2) (Canfield and Berner, 1987). The pyrite can cause a reduction in the MS signal that can interfere with the interpretation of the MS profile. However, we used MS to reconstruct the moving of SMTZ. We also exclude the use of $\delta^{18}O$ of *N. pachyderma* for correlation purpose as well because in our cores we recovered gas hydrate; it has been shown that oxygen isotopes of foraminiferal calcareous shells from gas hydrate settings may be affected by gas hydrate formation/dissociation (Dessandier et al., 2019).

In the five cores recovered from active and inactive GHMs in Storfjordrenna, at least one of the stratigraphic marker horizons can be recognized in all the cores allowing a good core correlation. The first foraminifera rich event horizon marker (i) was also found at core 1522GC from GHM3 at the bottom of the core (305-310 cm). The reddish oxidized event (OX-1) horizon marker (ii) was recognized in core 1522GC at 220 cm (Fig.7), 200cm in 920GC (Fig.4) and 300cm in 940GC (FIG:9) (green marker). The radiocarbon date of 16035 ±90 cal BP obtained from the *N.pachyderma* in 1522GC confirms the upper boundary of the oxidized event. Another radiocarbon date from bivalve shells at the bottom of the core 1070GC confirms the beginning of Heinrich event 1.

From the correlation of all the cores, we also noticed that some of the sites might have experienced more intensive erosions than others; for example, 940GC and 1070GC retained more early Holocene sediment than other cores. The proximity of the cores excludes the possibility of erosion caused by a strong bottom water current that would have affected the entire area. Because in Storfjordrenna TMF early Holocene sediments appeared to be well-preserved (Lucchi et al., 2013), we suggested that the local erosion observed in our cores may be due to trawling activity in the area. Nonetheless, the slightly varied but similar depositional characteristics among the sites exclude the influence of major sedimentation events, such as mass transport deposits (MTDs).

4.1 Multi-proxy approach on inactive GHM5

Previous investigations on gas hydrate mound GHM5 revealed a generally decreasing methane flux (Hong et al., 2018; Sen et al., 2018), confirmed by seismic surveys showing no prominent acoustic blanking or gas chimneys beneath the mound (Waage et al., 2019) and absence of flares in the water column (Serov et al., 2017). Waage et al. (2019) suggested that GHM5 was more active in the past when the gas reservoir beneath the mound was probably better connected to Paleocene sedimentary rock. Porewater geochemistry indicates that today, the GHM5 is in a post active stage where the gas reservoir is exhausted, and only the dissolved methane is delivered to the subsurface (Hong et al., 2018). The absence of chemosynthetic megafauna (e.g., frenulate aggregations) at the seafloor on top of the mound suggests a potential low sulfide flux, which, in return, is indicative of a low AOM activity within the sediments and thus methane flux (Sen et al., 2018).

Applying the multi-proxy approach on sediment core 920GC from the inactive GHM 5 we were able to identify four major seeping events (A to D) occurred in the last 18000 years together with their sequences, the duration, and their relative intensity. In the following text, event A referred to the current/most recent event, and event BCD follows the depth increases in the sediment.

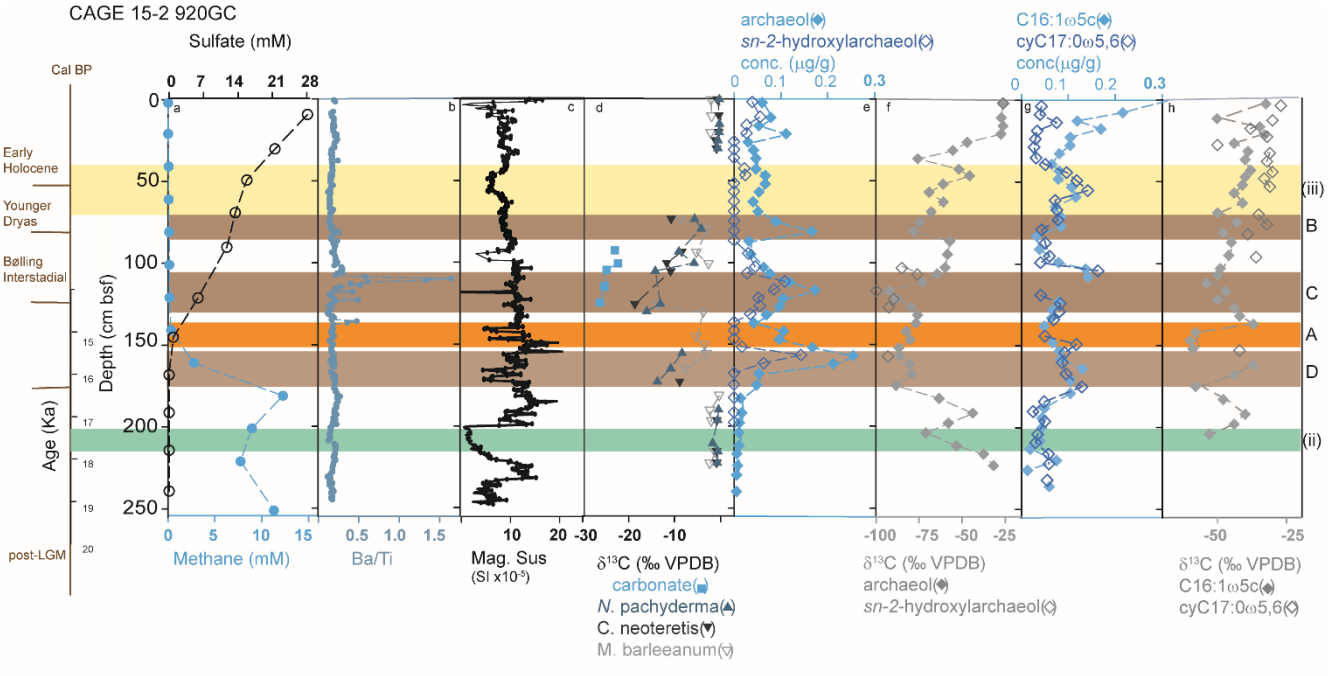

Figure 4. Core 920GC, from a to h, pore water sulfate and methane from Hong et al., 2017, Serov et al., 2017, sediment elemental ratio Ba/Ti, magnetic susceptibility, $\delta^{13}C$ of carbonate nodules, planktonic foraminifera (*N. pachyderma*), and benthic foraminifera; archaeal and bacterial lipid biomarker concentration and $\delta^{13}C$. Current event A marked in orange, other events marked in brown. Yellow and green highlight the horizon markers in this core. All isotope and lipid biomarker data are available in the supplementary file.

Sulfate and methane profiles in core 920GC show that the present-day SMTZ is located at ~150 cm (event A, orange, Fig 4). At ~150 cm, we found a small Ba/Ti peak, light benthic *M. barleeanum* $\delta^{13}C$ value (up to -5.1 ‰), increasing concentrations of archaeal and bacterial lipid biomarkers, and decreasing carbon isotope values of these biomarkers. The straight-line shape of the sulfate profile indicated that the pore water geochemistry reached a steady condition, and the small Ba/Ti peak implies a recent establishment of the steady-state conditions.

We observed depleted $\delta^{13}C$-values of foraminiferal tests in the three intervals named events B, C, and D. Those negative signals are due to secondary MDAC overgrowth on foraminiferal tests (Panieri et al., 2016; Schneider et al., 2018). The $\delta^{13}C$ of foraminifera is a sensitive and stable proxy to infer a past event; however, due to the secondary overgrowth, it is difficult to determine the exact precipitation timing of the depleted carbonate. In events B and C, the benthic foraminifera carbonate shells (- 10.72 ‰ and -13.7 ‰ for *C. neoteretis*, -8.63 ‰ and -8.5 ‰ for *M. barleeanum* in event B and C, respectively) were more depleted than the planktonic one (-5.49 ‰ and -10.85 ‰ for *N. pachyderma*). In addition to the depleted foraminiferal $\delta^{13}C$-values, event C was characterized by high abundance of the lipid biomarkers archaeol and the fatty acid (FA) C16:1ω5c, both of which also displayed low $\delta^{13}C$-values.

No Ba/Ti peak was observed in event B. A possible scenario for the absence of a barite front could be that event B was a rapid and short-lasting methane-release. It was not long enough to influence the barite dissolution and precipitation equilibrium substantially as the time needed to produce a barium peak at the SMTZ could be at least thousands of years (Riedinger et al., 2006).

Event C was characterized by two peaks in Ba/Ti of different intensities. The upper larger Ba/Ti peak suggested a period of enhanced fluid flow, in agreement with the appearance of Mg-calcite MDAC nodules with an average $\delta^{13}C$ value of ca -24.6 ‰. The Mg-calcite indicates that the precipitation of MDACs occurred within the sediment because the high sulfate concentration occurring close to the seafloor inhibits the formation of Mg-calcite (Burton, 1993; Bohrmann et al., 1998). We believe that the exclusive presence of MDACs in event C, and their absence in other events, indicate pervasive and high methane flux during event C (see also our interpretations for the missing barite front in event B). At the sediment layer corresponding to event C, the archaeal lipid concentrations were high and coupled to the most depleted $\delta^{13}C$-values (up to -100 ‰) in this horizon.

The bacterial FA C16:1ω5c showed the highest level in this event in this core, while the corresponding $\delta^{13}C$ was only moderately depleted to -50 ‰. We can only speculate that ANME-related lipid signals were better preserved in the geological record. One reason for this phenomenon might be the overprint from other non-AOM processes, such as methanogenesis or organic matter degradation (Elvert et al., 2003). Yet both archaeal and bacterial biomarkers indicate the presence of AOM communities in this event in the past.

Event D was below the current SMTZ and was characterized by highest archaeol and relatively high FA C16:1ω5c abundances coupled to low $\delta^{13}C$-values. Similar to event B, a barium front was also absent in event D. However, in this event, it could likely be that a barite front was initially present but dissolved when the methane flux increased during event B or C. Therefore, it seems likely that event D is the oldest recorded in core 920 GC, followed by an increased methane flux (event B and C). After event C, the methane flux decreased to current conditions to form the current SMTZ (event A) where the $\delta^{13}C$ of SRB lipids were depleted up to -70 ‰. Because of the limitation of the proxies, we cannot assess the precise timing of paleo methane emissions, but we hypothesized the timing for event D as discussed later.

Core 1070GC, as 920 GC, was recovered from the inactive GHM 5 revealed only two major seeping events. The current SMTZ (event A at ca 60 cm) was accompanied by a large Ba/Ti peak above it. We have also observed a biofilm 10cm below the current SMTZ in the sediment, which is composed of the AOM-related microbes (Gründger et al., 2019). This indicates a steady flux that was able to sustain high biomass of AOM microbes but was too low to escape the sediments. This is confirmed by the absence of active gas bubbling at the ‘inactive’ GHM5 and the ‘bright spot’ found in seismic profiles, which act as traps for the gas supply migrating from deeper sediments (Waage et al., 2019).

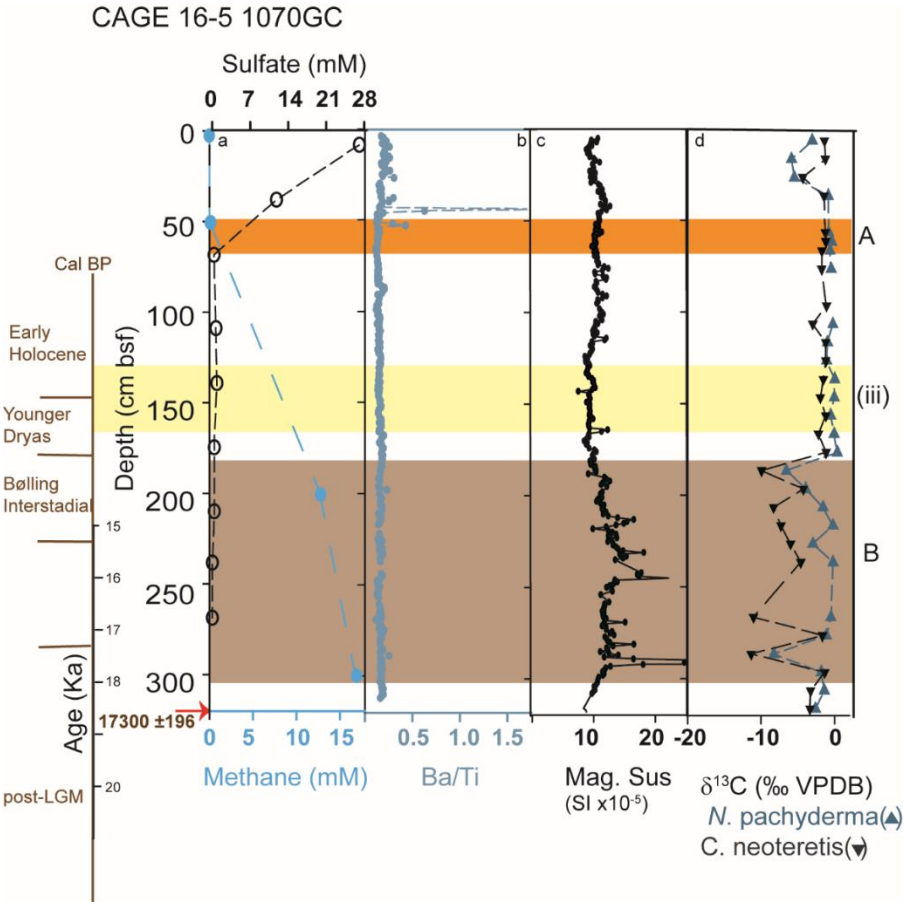

Figure 5. Core 1070GC, from a to d, pore water sulfate and methane from Gründger et al., 2019, sediment elemental ratio Ba/Ti, magnetic susceptibility, $\delta^{13}C$ of planktonic foraminifera *N. pachyderma* and benthic *C. neoteretis*. Current event A marked in orange, other events marked in brown. Yellow and green highlight the horizon markers in this core. All isotope data are available in the supplementary file.

The almost background $\delta^{13}C$ -values of foraminifera at the current SMTZ (-0.35 ‰ for *N. pachyderma* and -1.18 ‰ for *C. neoteretis*) raises the question as to why AOM activity (so far) did not lead to precipitation of MDAC on these foraminifera shells. The pore water sulfate and methane profiles imply steady-state condition, and the AOM-biofilm indicates that the steady-state has been stable for an extended period (at least decades) (Nauhaus et al., 2007; Gründger et al., 2019). The slightly depleted values of foraminifera at 26 cm could be related to a short event not long ago or could indicate that benthic living foraminifera record presence of methane during their lifetime, ingesting methanotrophic bacteria (Bernhard and Panieri, 2018) or using DIC (Wollenburg et al., 2015). The alternative explanation maybe the timing of all these signals. The formation of biofilm may need decades to hundreds of years with steady methane flux (Nauhaus et al., 2007; Puglini et al., 2019); the biomineralization of the foraminiferal tests may take longer also depending on different calcite test of the species. Smooth and imperforate test of *C. neoteretis* is less likely to accommodate contamination and crystalline overgrowth than the *N. pachyderma* with a test with higher porosity and surface area, as already observed by

Cook et al. (2011) and Consolaro et al. (2015). The presence of biofilm at the 'inactive' GHM5 implies that it does not necessarily occur at high methane flux site, but rather a place where methane flux could be low but persistent.

The event B is characterized by negative $\delta^{13}C$ excursions of foraminifera in a sizeable sediment interval (185 – 280 cm). The $\delta^{13}C$ of foraminifera was -2.8 ‰ (planktonic), and -7.15 ‰ (benthic) on average and could indicate both a diffuse steady-state and long-lived focused fluid upflow. The depth of the current SMTZ means that event B is the earlier event, after which an increase in the methane flux shifted the SMTZ upward.

The proxies from the two cores from the inactive GHM 5 show a complex methane seepage history, characterized by significant variability in space and time of methane discharge.

Coring site 920GC experienced a high and intense flux in the past, and then lower and fluctuating fluxes (Figure 6) like in a methane diffusion system. On the other hand, site 1070GC seemingly became slightly more active as the SMTZ shifted upward.

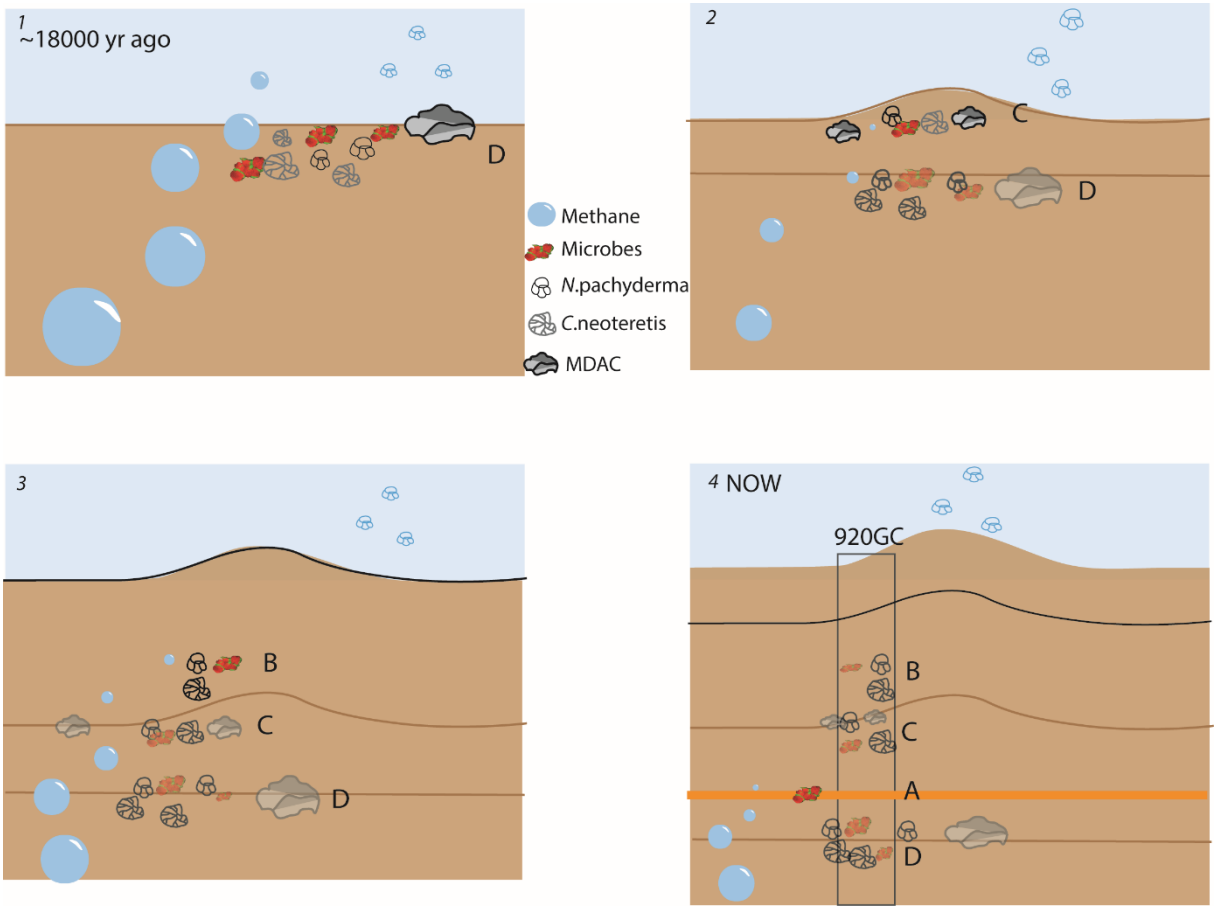

Figure 6. An illustrative summary of 920GC methane emission history. Core 920GC was used for the illustration as this core had a complete profile of all the proxies used in this paper. Current event A marked in orange, other events in light brown.

Core 920GC from GHM5 was investigated with all the proxies available; therefore, we illustrate the history of methane emission of this core in Figure 6 to show the interpretations of the multi-proxy approach. This GHM was active in the past (Figure 6-1 and 2), the high methane flux through conduits/chimneys, the possible formation of gas hydrate, and the accumulation of carbonate nodules and crusts at the time generated the hill-like GHM shape. Assessing the timing of seepage events is challenging, because the host sediment age at the past SMTZ depth does not necessarily translate to the age of one seeping event, but the age of event D is <18,000. The host sediment in the event D here in 920GC and event B in 1070GC ranged from 17 to 12 Ka, which is consistent with the suggested high fluid activity in the Barents Sea (Crémière et al., 2016a), and the local deglaciation started at 18 Ka (Serov et al., 2017). Serov et al. (2017) put forward the methane expulsion in the area started for over 18, 000 yrs based on the GHSZ and glacial isostatic modeling. From our interpretation, we showed that after event D, the methane flux increased in 920GC, lacking small carbonate nodules could be speculated as large carbonate crusts were formed. Therefore, with the co-occurrence of the same age host sediment, we hypothesize that our oldest events in both cores could be associated with the deglaciation and ice stream retreatment. The deglaciation and isostatic adjustment caused the changes in the gas hydrate stability zone, and therefore the methane expulsion occurred. Based on the overview of the methane history in this mound, we could see methane flux increased only from event D in 920GC, and event B in 1070GC, after these events, the methane flux decreased gradually. This trend of methane flux is also supporting the association between the deglaciation timing to the major seeping events in this mound.

4.3 Multi-proxy approach on active mound GHM 3

GHM3 is an active methane seeping site as documented by acoustic flares (cruise report CAGE 15-2,16-5, Serov et al., 2017) and gas hydrate layers interbedded in sediments recovered from 1522GC and 1520GC (at 150 cm bsf). The multi-proxy approach on the three cores collected at GHM3 (1522, 1520 and 920GC) confirms the active methane system, characterized by highly complex heterogeneous fluid and gas dynamics.

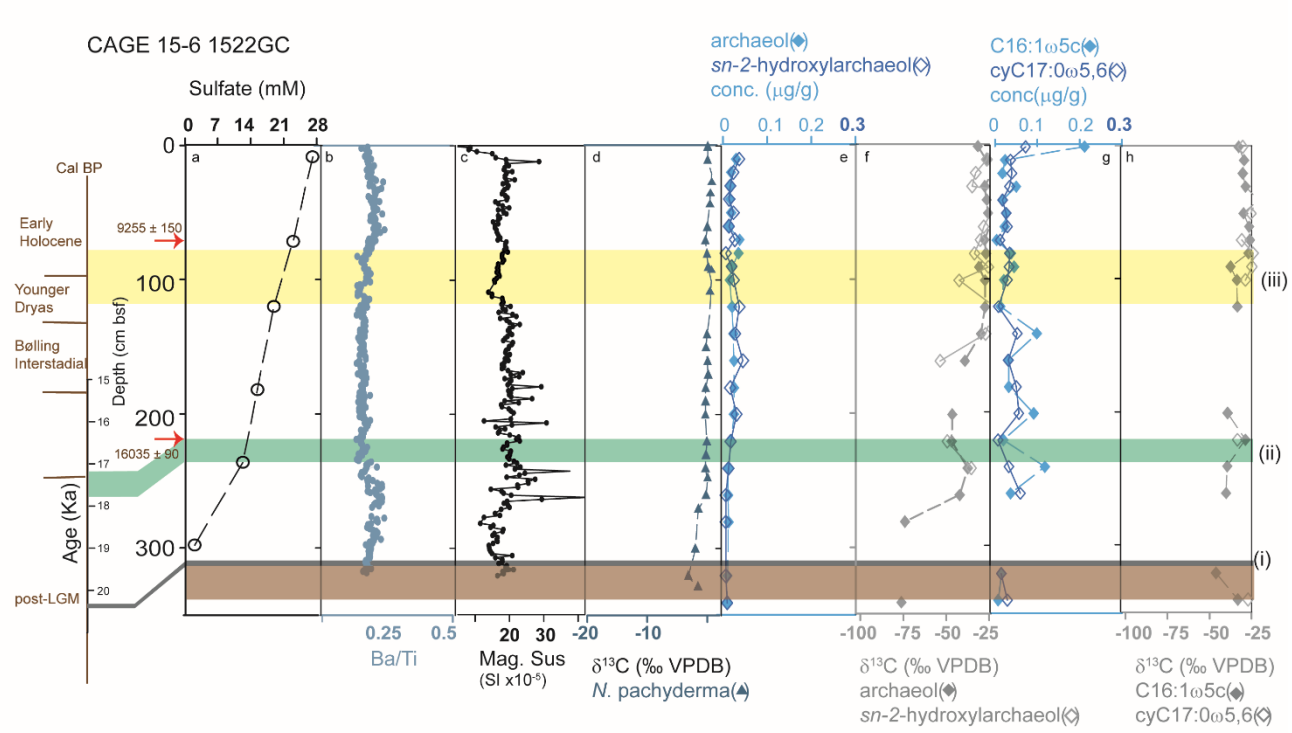

Figure 7. Core 1522GC, from a to h, pore water sulfate from Hong et al., 2017, sediment elemental ratio Ba/Ti, magnetic susceptibility, $\delta^{13}C$ of planktonic foraminifera (*N. pachyderma*), archaeal and bacterial lipid biomarker concentration and $\delta^{13}C$. A tentative event in brown. Yellow and green highlight the horizon markers in this core. All isotope and lipid biomarker data are available in the supplementary file.

The core (1522GC, 320 cm in length), retrieved from the western rim of GHM3, covered a period of 20000 yrs. The trend of the pore water sulfate suggested the SMTZ located at the bottom of the core (~320cm) or slightly below, indicating a very low methane flux (Hong et al., 2017). It is assigned as 'low flux core,' to establish background concentrations and $\delta^{13}C$-values of archaeal and bacterial lipid biomarkers in very low or no flux settings. No barium peak was observed in the Ba/Ti profile, and the $\delta^{13}C$-values of *N. pachyderma* were in the range of normal marine environment (-0.5 ‰ to 0.5 ‰) in the Barents Sea (Knies and Stein, 1998). The concentrations of archaeal lipids archaeol and sn2-hydroxyarchaeol were below 0.1 µg/g of dry sediment but showed a $\delta^{13}C$-minimum in the bottom of the core (280 to 320 cm), providing indications for AOM-related archaea at the SMTZ at the base of the core. In the lower section at 300-320cm, we observed a depletion of the $\delta^{13}C$ of *N. pachyderma* to -3.5 ‰ and of archaeal lipid biomarkers to -75 ‰ together with no significant increase in the abundance of both archaeal and SRB lipid biomarkers. The background $\delta^{13}C$-values of foraminifera, low concentration of both archaeal and bacterial lipid biomarkers, and the heavy carbon isotope all indicate that coring site 1522GC does not experience a substantial influence from methane in the top 300cm.

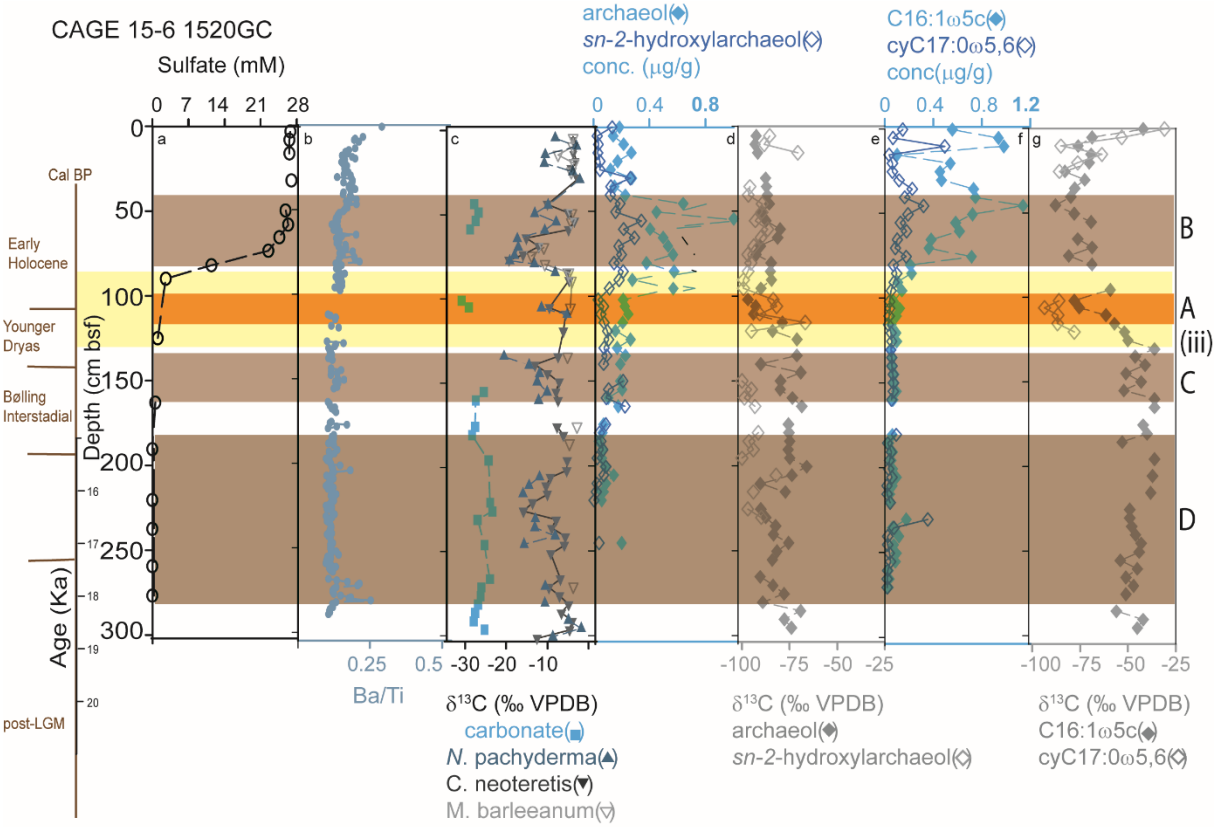

Figure 8. Core 1520GC, from a to g, pore water sulfate from Hong et al., 2017, sediment elemental ratio Ba/Ti, $\delta^{13}C$ of carbonate nodules, planktonic foraminifera (*N. pachyderma*), and benthic foraminifera; archaeal and bacterial lipid biomarker concentration and $\delta^{13}C$. Current event A marked in orange, other events marked in brown. The yellow marker highlights the horizon marker in this core. All isotope and lipid biomarker data are available in the supplementary file.

The general overview of the geochemical profiles of core 1520 collected at the southern rim of GHM3 indicates where respect to the GHM5 (rim) revealed four past methane emission events. The pore water sulfate depletion identifies the current discharge of methane to be located at a sediment depth of ~100cm (event A). The authigenic carbonate nodules appeared throughout the entire core, indicate that the coring site has been affected by continuous, pervasive, diffuse methane emissions for a long time, at least from 18,000 yrs, time span covered by the core. This is confirmed by the lack of prominent Ba/Ti peaks due to highly dynamic methane flux that does not leave enough time to generate a stable barite front. Although unlikely, the missing peak can be also due to the lack of proper contact between the sensor and the sediment core during the XRF acquirement because of the abundant dispersed carbonate nodules. Even if this core has been subject to a continuous and pervasive methane seepage since the LGM, we could still recognize three distinct events (B, C, and D) in addition to the present-day SMTZ, that might indicate advective methane dynamic.

The event B above the current SMTZ shows high concentrations of both archaeal (up to 1 μg/g dry sediment) and SRB (up to 1.2 μg/g dry sediment) lipid biomarkers, $\delta^{13}C$ excursions in planktonic and benthic foraminifera up to -18 ‰, and presence of abundant carbonate nodules. The events C and D below the SMTZ were characterized by numerous carbonate nodules, $\delta^{13}C$ excursions of benthic and planktonic foraminifera, and depleted archaeal lipid biomarkers. The archaeal and SRB lipid biomarkers were in much lower concentration in event C and D, and the $\delta^{13}C$ of SRB lipid biomarkers were not as depleted as in event A or B. We believe that this may suggest that events C and D were older than B, due to degradation of the lipid biomarkers, or the AOM lipid signal was overwritten by another process such as methanogenesis or organic matter degradation (Niemann et al., 2013).

The sequence of event C/D, event B, and A suggest the methane flux was higher in the past and has decreased recently. On the other hand, Hong et al. (2017), modeled the methane flux based on the pore water profile and suggested that in core 1520GC it took 290 years of increasing flux to achieve the current geochemical profiles. This is not contradicted to our interpretation, as the time scale is very likely different. The time scale in the modeled result from Hong et al., are in hundreds of years, whereas the time scale for generating event A and B could be thousands of years. The methane flux wane and waxed in these thousands of years to produce even smaller events that cannot be resolved by our approach due to sampling resolution (every 5 cm).

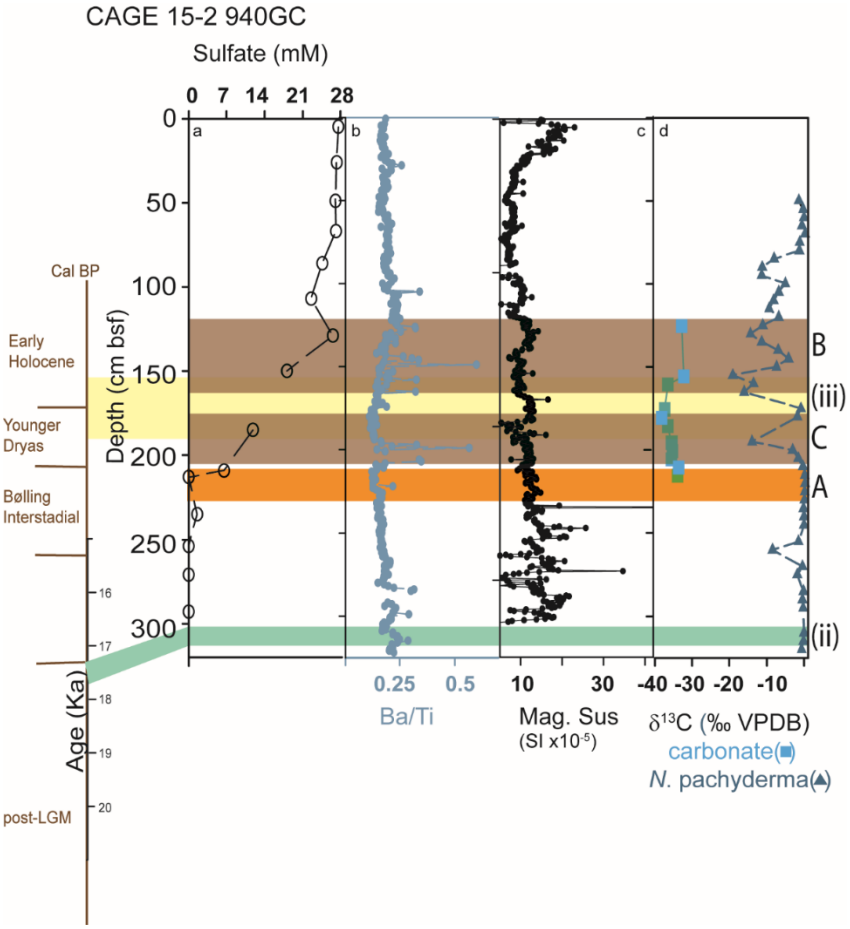

Figure 9. From a to d, pore water sulfate from Hong et al., 2017, sediment elemental ratio Ba/Ti, magnetic susceptibility, $\delta^{13}C$ of carbonate nodules, planktonic foraminifera (*N. pachyderma*). Current event A marked in orange, other events marked in brown. Yellow and green highlight the horizon markers in this core. All isotope data are available in the supplementary file.

In core 940GC, from the eastern rim of GHM3, we could apply the Ba/Ti sediment ratio, magnetic susceptibility, and $\delta^{13}C$ of carbonate nodules and planktonic foraminifera due to sampling availability. The pore water sulfate profile depleted at 210 cm of the core, set the current SMTZ, and labeled as event A while the excellent preservation of the Ba/Ti peaks suggests a continuous decreasing methane flux at this coring site.

Two major Ba/Ti peaks were recognized and determine the events B and C. In both events B and C, authigenic carbonate nodules co-occur with the $\delta^{13}C$ excursion of planktonic foraminifera. The $\delta^{13}C$ of *N. pachyderma* were depleted to -19 ‰ in event B and -16 ‰ in event C. However, the $\delta^{13}C$ of *N. pachyderma* was -0.3 ‰ at the current SMTZ (event A), co-occur with some carbonate nodules with $\delta^{13}C$ of -33.5 ‰. One of the possible reasons for the discrepancy could be due to sample preparation. When the foraminifera was picked for isotopic investigation, the 'glassy' specimens were likely to be picked compared to the 'frosty' ones. Even though glassy appearance does not guarantee any diagenetic influence (Panieri et al., 2017;

Schneider et al., 2017), the possibility of picking ten 'clean' specimens in the profoundly affected sediment could be low.

From both mounds, we revealed a major methane flux increasing phase, e.g. event D in 920GC, event B in 1070GC, and event D in 1520GC. We speculate an association of our major seeping events with the deglaciation triggered changes in the GHSZ (Serov et al., 2017). The increased or decreased fluid flow within the mounds was controlled by the GHSZ and the hydrate dissociation, whereas due to spatial heterogeneity generated by carbonate precipitation, gas hydrates, each core experienced different fluid discharge.

Summary

A profound understanding of methane emissions from Arctic Ocean sediments in the (geological) past and associated drivers and trigger mechanisms can be the key to understand present-day and, more importantly, to predict methane emission scenarios in an Arctic future-ocean impacted by climate change. This can be achieved by tracing evidence for past methane dynamics preserved in fossil records – i.e., proxy indicators. In this paper, we provide an overview of a set of (bio) geochemical proxies (pore water sulfate and methane; sedimentary XRF ratios of Ba/Ti; magnetic susceptibility, $\delta^{13}C$ records from benthic and planktic foraminifera; mineralogy and $\delta^{13}C$ of authigenic carbonate; abundance and $\delta^{13}C$ of AOM signature lipid biomarkers) to investigate benthic methane dynamics. We applied these proxies (multi-proxy approach) to the case of a shallow water gas hydrate area, Storfjordrenna, to reconstruct the emission history of this Arctic cold seep. ^{14}C dating of 20609 cal BP in our reference core showed that deglaciation started at that time in the Storfjordrenna region. Stratigraphy correlation based on Zr/Rb (also Fe/Ca) of the reference and the other cores allowed us to establish a stratigraphic context. Using the multi-proxy approach, we identified several major and smaller venting phases in each core from both the active and inactive GHMs allowing a better definition and an estimation of the chronology of these seeping events. The methane history in the GHMs revealed a major methane venting phase in both of the mounds. Based on the local deglaciation timing and previous investigation, ice sheet retreat in Storfjordrenna started around 22,500 yrs ago and the active ice stream retreated from the GHMs area ~21,000 yrs ago, until it attained a stable position 40 km farther upstream around 18,000 yr ago and retreated to inner Storfjorden by 14,500 yrs ago (Serov et al., 2017). It is tempting to assign the same dates to past emission events recorded in our cores, but we are aware that methane emissions might not be coeval to the age of the hosted sediments. The deglaciation triggered changes in the GHSZ and hydrate dissociation, and the hydrate system in the area

experienced repeated cycles of emergence and dissociation during the late glacial and Holocene periods driven by changes in the oceanographic conditions and gradual glacio-isostatic recovery. The changes in the GHSZ forced distinct phases of seafloor methane venting as our identified events, due to its episodic nature (Serov et al., 2017). Therefore, we associated the major seeping events with hydrate dissociation caused by the GHSZ changes triggered by isostatic adjustment right after the onset of the LGM. The multi-proxy approach highlights the complexity and heterogeneity of the methane system. Even across the same GHM (hundreds of meters), the methane flux history could be different and contrasting.

Lastly, we reviewed and evaluated the use of the most common proxies related to AOM to reconstruct the paleo methane seepage based on their relationship with AOM, and considering their preservation in the sedimentary record as summarized in Table 2.

Table 2. Summary of conventional proxies used for methane seepage reconstruction and applied in this study.

	Proxy		**Indication/Information**	**Pros**	**Cons**
Abiotic	Sulfate and methane concentration in pore water		Sulfate and methane profiles indicate the current activity of AOM	Identify the current SMTZ	No past seepage information
	Barite front (in the form of Ba/Ti ratio, or Ba counts)		Past and present SMTZs	Easy to access, non-destructive	Complicate with changing flux intensity, sometimes missing
	Magnetic susceptibility (Mag. Sus)		Abrupt drop of Mag.sus implies the location of paleo-SMTZ, due to formation of pyrite.	easy to access, non-destructive	need background value to compare
	Methane-Derived Authigenic Carbonate	$\delta^{13}C$ and $\delta^{18}O$	Fluid source and environmental conditions during precipitation	Well established, robust proxy, easy to measure	Not always present
		Mineralogy	Diagenetic environment		
Biotic	Foraminifera	$\delta^{13}C$	Incorporation of methane-derived carbon, primary and secondary signal	well established, easy to measure	the discrepancy at the current SMTZ
		Abundances and species distribution	High abundance of endobenthic foram and high absolute abundance of benthic foram were interpreted as indicating methane seepage.		
		Shell preservation	Diagenetically altered shells indicate precipitation of authigenic phases at a depth of the SMTZ at sites of methane seepage		

Lipid biomarkers	lipid biomarker concentration	Indicate the presence of AOM related microbial communities	well established, indirect evidence for AOM microbial community	the signal can be mixed with other sedimentary processes
	$\delta^{13}C$ of lipid biomarker	inherit isotope signal from source methane and isotopic fractionation of AOM	distinguish signal from AOM to other sedimentary processes	easily overwrote by other processes
Biofilm		Associated with fractures in the sediment that represent the location of AOM	strong evidence for AOM	serendipity

The combination of our findings provides a base and directions for future investigation in cold seep sites and thus can provide insights and guidance for choosing the appropriate proxy to use depending on the environmental conditions.

Competing interests
We declare no conflict of competing interest for the co-authors

Acknowledgments

This work was supported by the Research Council of Norway through its Centre of Excellence funding scheme for CAGE, project number 223259, and partially by the NORCRUST project, grant number 255150. We thank Prof. Simon Belt for hosting the IP_{25} analyses. We thank the captain, crew members, and scientific team of R/V Helmer Hanssen for their contribution during the research cruises CAGE15-2, CAGE 15-6, and CAGE16-5.

Reference

Aloisi, G., Pierre, C., Rouchy, J.-M., Foucher, J.-P., and Woodside, J.: Methane-related authigenic carbonates of eastern Mediterranean Sea mud volcanoes and their possible relation to gas hydrate destabilisation, Earth and Planetary Science Letters, 184, 321-338, https://doi.org/10.1016/S0012-821X(00)00322-8, 2000.
Aloisi, G., Bouloubassi, I., Heijis, S. K., Pancost, R. D., Pierre, C., Sinninghe Damsté, J. S., Gottschal, J. C., Forney, L. J., and Rouchy, J.-M.: CH4-consuming microorganisms and the formation of carbonate crusts at cold seeps, Earth and Planetary Science Letters, 203, 195-203, 2002.
Andreassen, K., Nilssen, E. G., and Ødegaard, C. M.: Analysis of shallow gas and fluid migration within the Plio-Pleistocene sedimentary succession of the SW Barents Sea

continental margin using 3D seismic data, Geo-Marine Letters, 27, 155-171, 10.1007/s00367-007-0071-5, 2007.
Bernhard, J. M., and Panieri, G.: Keystone Arctic paleoceanographic proxy association with putative methanotrophic bacteria, Sci Rep, 8, 10610, 10.1038/s41598-018-28871-3, 2018.
Berndt, C., Feseker, T., Treude, T., Krastel, S., Liebetrau, V., Niemann, H., Bertics, V. J., Dumke, I., Dunnbier, K., Ferre, B., Graves, C., Gross, F., Hissmann, K., Huhnerbach, V., Krause, S., Lieser, K., Schauer, J., and Steinle, L.: Temporal constraints on hydrate-controlled methane seepage off Svalbard, Science, 343, 284-287, 10.1126/science.1246298, 2014.
Birgel, D., and Peckmann, J.: Aerobic methanotrophy at ancient marine methane seeps: A synthesis, Organic Geochemistry, 39, 1659-1667, 10.1016/j.orggeochem.2008.01.023, 2008.
Blees, J., Niemann, H., Wenk, C. B., Zopfi, J., Schubert, C. J., Jenzer, J. S., Veronesi, M., and Lehman, M. F.: Bacterial methanotrophs drive the formation of a seasonal anoxic benthic nepheloid layer in an alpine lake, Limnology and Oceanography, 59, 1410-1420, 10.4319/lo.2014.59.4.141E, 2014.
Blumenberg, M., Seifert, R., Reitner, J., Pape, T., and Michaelis, W.: Membrane lipid patterns typify distinct anaerobic methanotrophic consortia, PNAS, 101, 11111–11116, 2004.
Blumenberg, M.: Microbial Chemofossils in Specific Marine Hydrothermal and Methane Cold Seep Settings, in: The Vent and Seep Biota, Topics in Geobiology, 73-106, 2010.
Boetius, A., Ravenschlag, K., Schubert, C. J., Rickert, D., Widdel, F., Gieseke, A., Amann, R., Jørgensen, B., Witte, U., and Pfannkuche, O.: A marine microbial consortium apparentlymediating anaerobic oxidation of methane, Nature, 407, 623-626, 2000.
Bohrmann, G., Greinert, J., Suess, E., and Torres, M.: Authigenic carbonates from the Cascadia subduction zone and their relation to gas hydrate stability, Geology, 26, 647-650, 10.1130/0091-7613(1998)026<0647:ACFTCS>2.3.CO;2 %J Geology, 1998.
Bohrmann, G., and Torres, M. E.: Marine Gas Hydrates, in: Encyclopedia of Marine Geosciences, edited by: Harff, J., Meschede, M., Petersen, S., and Thiede, J., Springer Netherlands, Dordrecht, 1-7, 2013.
Borowski, W. S., Paull, C. K., and Ussler III, W.: Carbon cycling within the upper methanogenic zone of continental rise sediments: An example from the methane-rich sediments overlying the Blake Ridge gas hydrate deposits, Marine Chemistry, 57, 299-311, 1997.
Bouloubassi, I., Aloisi, G., Pancost, R. D., Hopmans, E., Pierre, C., and Sinninghe Damsté, J. S.: Archaeal and bacterial lipids in authigenic carbonate crusts from eastern Mediterranean mud volcanoes, Organic Geochemistry, 37, 484-500, 10.1016/j.orggeochem.2005.11.005, 2006.
Briggs, B. R., Pohlman, J. W., Torres, M., Riedel, M., Brodie, E. L., and Colwell, F. S.: Macroscopic biofilms in fracture-dominated sediment that anaerobically oxidize methane, Appl Environ Microbiol, 77, 6780-6787, 10.1128/AEM.00288-11, 2011.
Burton, E. A.: Controls on marine carbonate cement mineralogy: review and reassessment, Chemical Geology, 105, 163-179, https://doi.org/10.1016/0009-2541(93)90124-2, 1993.
Canfield, D. E., and Berner, R. A.: Dissolution and pyritization of magnetite in anoxic marine sediments, Geochimica et Cosmochimica Acta, 51, 645-659, https://doi.org/10.1016/0016-7037(87)90076-7, 1987.
Cartwright, J.: The impact of 3D seismic data on the understanding of compaction, fluid flow and diagenesis in sedimentary basins, Journal of the Geological Society, 164, 881-893, 10.1144/0016-76492006-143, 2007.
Chand, S., Thorsnes, T., Rise, L., Brunstad, H., Stoddart, D., Bøe, R., Lågstad, P., and Svolsbru, T.: Multiple episodes of fluid flow in the SW Barents Sea (Loppa High) evidenced by gas flares, pockmarks and gas hydrate accumulation, Earth and Planetary Science Letters, 331-332, 305-314, 10.1016/j.epsl.2012.03.021, 2012.

Consolaro, C., Rasmussen, T. L., Panieri, G., Mienert, J., Bünz, S., and Sztybor, K.: Carbon isotope (δ¹³C) excursions suggest times of major methane release during the last 14 kyr in Fram Strait, the deep-water gateway to the Arctic, Climate of the Past, 11, 669-685, 10.5194/cp-11-669-2015, 2015.
Cook, M. S., Keigwin, L. D., Birgel, D., and Hinrichs, K.-U.: Repeated pulses of vertical methane flux recorded in glacial sediments from the southeast Bering Sea, Paleoceanography, 26, n/a-n/a, 10.1029/2010pa001993, 2011.
Crémière, A., Lepland, A., Chand, S., Sahy, D., Condon, D. J., Noble, S. R., Martma, T., Thorsnes, T., Sauer, S., and Brunstad, H.: Timescales of methane seepage on the Norwegian margin following collapse of the Scandinavian Ice Sheet, Nat Commun, 7, 11509, 10.1038/ncomms11509, 2016a.
Crémière, A., Lepland, A., Chand, S., Sahy, D., Kirsimäe, K., Bau, M., Whitehouse, M. J., Noble, S. R., Martma, T., Thorsnes, T., and Brunstad, H.: Fluid source and methane-related diagenetic processes recorded in cold seep carbonates from the Alvheim channel, central North Sea, Chemical Geology, 432, 16-33, https://doi.org/10.1016/j.chemgeo.2016.03.019, 2016b.
Dessandier, P.-A., Borrelli, C., Kalenitchenko, D., and Panieri, G.: Benthic Foraminifera in Arctic Methane Hydrate Bearing Sediments, Frontiers in Marine Science, 6, 10.3389/fmars.2019.00765, 2019.
Dewangan, P., Basavaiah, N., Badesab, F. K., Usapkar, A., Mazumdar, A., Joshi, R., and Ramprasad, T.: Diagenesis of magnetic minerals in a gas hydrate/cold seep environment off the Krishna–Godavari basin, Bay of Bengal, Marine Geology, 340, 57-70, https://doi.org/10.1016/j.margeo.2013.04.016, 2013.
Dickens, G. R.: Sulfate profiles and barium fronts in sediment on the Blake Ridge: present and past methane fluxes through a large gas hydrate reservoir, Geochimica et Cosmochimica Acta, 65, 529-543, https://doi.org/10.1016/S0016-7037(00)00556-1, 2001.
Dickens, G. R.: Rethinking the global carbon cycle with a large, dynamic and microbially mediated gas hydrate capacitor, Earth and Planetary Science Letters, 213, 169-183, 10.1016/s0012-821x(03)00325-x, 2003.
Dowdeswell, J. A., and Elverhoi, A.: The timing of initiation of fast-£owing ice streams during a glacial cycle inferred from glacimarine sedimentation, Marine Geology, 188, 3-14, 2002.
Dypvik, H., and Harris, N. B.: Geochemical facies analysis of fine-grained siliciclastics using Th/U, Zr/Rb and (Zr+Rb) /Sr ratios, Chemical Geology, 181, 131–146, 2001.
Elvert, M., Boetius, A., Knittel, K., and Jørgensen, B. B.: Characterization of Specific Membrane Fatty Acids as Chemotaxonomic Markers for Sulfate-Reducing Bacteria Involved in Anaerobic Oxidation of Methane, Geomicrobiology Journal, 20, 403-419, 10.1080/01490450303894, 2003.
Etiope, G., and Sherwood Lollar, B.: ABIOTIC METHANE ON EARTH, Reviews of Geophysics, 51, 276-299, 10.1002/rog.20011, 2013.
Goldsmith, J. R., Graf, D. L., Chodos, A. A., Joensuu, O. I., and Mcvicker, L. D.: Relation between lattice constants and composition of Ca-Mg carbonates, American Mineralogist, 43, 84-101, 1958.
Ferré, B., Jansson, P. G., Moser, M., Serov, P., Portnov, A., Graves, C. A., Panieri, G., Gründger, F., Berndt, C., Lehmann, M. F., and Niemann, H.: Reduced methane seepage from Arctic sediments during cold bottom-water conditions, Nature Geoscience, 10.1038/s41561-019-0515-3, 2020.
Gründger, F., Carrier, V., Svenning, M. M., Panieri, G., Vonnahme, T. R., Klasek, S., and Niemann, H.: Methane-fuelled biofilms predominantly composed of methanotrophic ANME-

1 in Arctic gas hydrate-related sediments, Sci Rep, 9, 9725, 10.1038/s41598-019-46209-5, 2019.
Han, Y.-J., and Aizenberg, J.: Effect of Magnesium Ions on Oriented Growth of Calcite on Carboxylic Acid Functionalized Self-Assembled Monolayer, Journal of the American Chemical Society, 125, 4032-4033, 10.1021/ja034094z, 2003.
Hill, T. M., Kennett, J. P., and Valentine, D. L.: Isotopic evidence for the incorporation of methane-derived carbon into foraminifera from modern methane seeps, Hydrate Ridge, Northeast Pacific, Geochimica et Cosmochimica Acta, 68, 4619-4627, 10.1016/j.gca.2004.07.012, 2004.
Himmler, T., Sahy, D., Martma, T., Bohrmann, G., Plaza-Faverola, A., Bünz, S., Condon, D. J., Knies, J., and Lepland, A.: A 160,000-year-old history of tectonically controlled methane seepage in the Arctic, Science Advances, 5, eaaw1450, 10.1126/sciadv.aaw1450, 2019.
Hinrichs, K.-U., Summons, R. E., Orphan, V., Sylva, S. P., and Hayes, J. M.: Molecular and isotopic analysis of anaerobic methane-oxidizing communities in marine sediments, Organic Geochemistry, 31, 1685-1701, https://doi.org/10.1016/S0146-6380(00)00106-6, 2000.
Hinrichs, K. U., Hayes, J. M., Sylva, S. P., Brewer, P. G., and Delong, E. F.: Methane-consuming archaebacteria in marinesediments, Nature, 398, 802-805, 1999.
Holler, T., Wegener, G., Knittel, K., Boetius, A., Brunner, B., Kuypers, M. M., and Widdel, F.: Substantial (13) C/(12) C and D/H fractionation during anaerobic oxidation of methane by marine consortia enriched in vitro, Environ Microbiol Rep, 1, 370-376, 10.1111/j.1758-2229.2009.00074.x, 2009.
Holmes, C. D., Prather, M. J., Søvde, O. A., and Myhre, G.: Future methane, hydroxyl, and their uncertainties: key climate and emission parameters for future predictions, Atmos. Chem. Phys., 13, 285-302, 10.5194/acp-13-285-2013, 2013.
Hong, W. L., Torres, M. E., Carroll, J., Cremiere, A., Panieri, G., Yao, H., and Serov, P.: Seepage from an arctic shallow marine gas hydrate reservoir is insensitive to momentary ocean warming, Nat Commun, 8, 15745, 10.1038/ncomms15745, 2017.
Hong, W. L., Torres, M. E., Portnov, A., Waage, M., Haley, B., and Lepland, A.: Variations in Gas and Water Pulses at an Arctic Seep: Fluid Sources and Methane Transport, Geophysical Research Letters, 10.1029/2018gl077309, 2018.
Jessen, S. P., Rasmussen, T. L., Nielsen, T., and Solheim, A.: A new Late Weichselian and Holocene marine chronology for the western Svalbard slope 30,000–0 cal years BP, Quaternary Science Reviews, 29, 1301-1312, 10.1016/j.quascirev.2010.02.020, 2010.
Joye, S. B., Boetius, A., Orcutt, B. N., Montoya, J. P., Schulz, H. N., Erickson, M. J., and Lugo, S. K.: The anaerobic oxidation of methane and sulfate reduction in sediments from Gulf of Mexico cold seeps, Chemical Geology, 205, 219-238, https://doi.org/10.1016/j.chemgeo.2003.12.019, 2004.
Judd, A., and Hovland, M.: Seabed Fluid Flow: The Impact on Geology, Biology and the Marine Environment, Cambridge University Press, Cambridge, 2007.
Kasten, S., Nöthen, K., Hensen, C., Spieß, V., Blumenberg, M., and Schneider, R. R. J. G.-M. L.: Gas hydrate decomposition recorded by authigenic barite at pockmark sites of the northern Congo Fan, 32, 515-524, 10.1007/s00367-012-0288-9, 2012.
Kaneko, M., Naraoka, H., Takano, Y., and Ohkouchi, N.: Distribution and isotopic signatures of archaeal lipid biomarkers associated with gas hydrate occurrences on the northern Cascadia Margin, Chemical Geology, 343, 76-84, 10.1016/j.chemgeo.2013.02.003, 2013.

Knies, J., and Stein, R.: New aspects of organic carbon deposition and its paleoceanographic implications along the Northern Barents Sea Margin during the last 30,000 years, Paleoceanography, 13, 384-394, 10.1029/98pa01501, 1998.

Knies, J., Koseoglu, D., Rise, L., Baeten, N., Bellec, V. K., Boe, R., Klug, M., Panieri, G., Jernas, P. E., and Belt, S. T.: Nordic Seas polynyas and their role in preconditioning marine productivity during the Last Glacial Maximum, Nat Commun, 9, 3959, 10.1038/s41467-018-06252-8, 2018.
Knittel, K., and Boetius, A.: Anaerobic oxidation of methane: progress with an unknown process, Annu Rev Microbiol, 63, 311-334, 10.1146/annurev.micro.61.080706.093130, 2009.
Lee, D. H., Kim, J. H., Lee, Y. M., Stadnitskaia, A., Jin, Y. K., Niemann, H., Kim, Y. G., and Shin, K. H.: Biogeochemical evidence of anaerobic methane oxidation on active submarine mud volcanoes on the continental slope of the Canadian Beaufort Sea, Biogeosciences, 15, 7419-7433, 10.5194/bg-15-7419-2018, 2018.
Lim, K. L. H., Pancost, R. D., Hornibrook, E. R. C., Maxfield, P. J., and Evershed, R. P.: Archaeol: An indicator of methanogenesis in water-saturated soils, Archaea, 2012, 10.1155/2012/896727, 2012.
Lucchi, R. G., Pedrosa, M. T., Camerlenghi, A., Urgeles, R., De Mol, B., and Rebesco, M.: Recent Submarine Landslides on the Continental Slope of Storfjorden and Kveithola Trough-Mouth Fans (North West Barents Sea), 735-745, 10.1007/978-94-007-2162-3_65, 2012.
Lucchi, R. G., Camerlenghi, A., Rebesco, M., Colmenero-Hidalgo, E., Sierro, F. J., Sagnotti, L., Urgeles, R., Melis, R., Morigi, C., Bárcena, M. A., Giorgetti, G., Villa, G., Persico, D., Flores, J. A., Rigual-Hernández, A. S., Pedrosa, M. T., Macri, P., and Caburlotto, A.: Postglacial sedimentary processes on the Storfjorden and Kveithola trough mouth fans: Significance of extreme glacimarine sedimentation, Global and Planetary Change, 111, 309-326, 10.1016/j.gloplacha.2013.10.008, 2013.
Luff, R., Wallmann, K., and Aloisi, G.: Numerical modeling of carbonate crust formation at cold vent sites: significance for fluid and methane budgets and chemosynthetic biological communities, Earth and Planetary Science Letters, 221, 337-353, 10.1016/s0012-821x(04)00107-4, 2004.
MacLeod, M. K.: Gas hydrates in ocean bottom sediments, AAPG Bulletin, 66, 2649-2662, 1982.
Mangerud, J., Bondevik, S., Gulliksen, S., Karin Hufthammer, A., and Høisæter, T.: Marine 14C reservoir ages for 19th century whales and molluscs from the North Atlantic, Quaternary Science Reviews, 25, 3228-3245, https://doi.org/10.1016/j.quascirev.2006.03.010, 2006.
Martin, R. A., Nesbitt, E. A., and Campbell, K. A.: The effects of anaerobic methane oxidation on benthic foraminiferal assemblages and stable isotopes on the Hikurangi Margin of eastern New Zealand, Marine Geology, 272, 270-284, 10.1016/j.margeo.2009.03.024, 2010.
Mazzini, A., Ivanov, M. K., Parnell, J., Stadnitskaia, A., Cronin, B. T., Poludetkina, E., Mazurenko, L., and van Weering, T. C. E.: Methane-related authigenic carbonates from the Black Sea: geochemical characterisation and relation to seeping fluids, Marine Geology, 212, 153-181, 10.1016/j.margeo.2004.08.001, 2004.
Nauhaus, K., Albrecht, M., Elvert, M., Boetius, A., and Widdel, F.: In vitro cell growth of marine archaeal-bacterial consortia during anaerobic oxidation of methane with sulfate, Environ Microbiol, 9, 187-196, 10.1111/j.1462-2920.2006.01127.x, 2007.
Niemann, H., Elvert, M., Hovland, M., Orcutt, B., Judd, A., Suck, I., Gutt, J., Joye, S., Damm, E., Finster, K., and Boetius, A.: Methane emission and consumption at a North Sea gas seep (Tommeliten area), Biogeosciences, 2, 335-351, 2005.
Niemann, H., Duarte, J., Hensen, C., Omoregie, E., Magalhães, V. H., Elvert, M., Pinheiro, L. M., Kopf, A., and Boetius, A.: Microbial methane turnover at mud volcanoes of the Gulf of Cadiz, Geochimica et Cosmochimica Acta, 70, 5336-5355, 10.1016/j.gca.2006.08.010, 2006a.
Niemann, H., Losekann, T., de Beer, D., Elvert, M., Nadalig, T., Knittel, K., Amann, R., Sauter, E. J., Schluter, M., Klages, M., Foucher, J. P., and Boetius, A.: Novel microbial

communities of the Haakon Mosby mud volcano and their role as a methane sink, Nature, 443, 854-858, 10.1038/nature05227, 2006b.
Niemann, H., and Elvert, M.: Diagnostic lipid biomarker and stable carbon isotope signatures of microbial communities mediating the anaerobic oxidation of methane with sulphate, Organic Geochemistry, 39, 1668-1677, 10.1016/j.orggeochem.2007.11.003, 2008.
Niemann, H., Linke, P., Knittel, K., MacPherson, E., Boetius, A., Bruckmann, W., Larvik, G., Wallmann, K., Schacht, U., Omoregie, E., Hilton, D., Brown, K., and Rehder, G.: Methane-carbon flow into the benthic food web at cold seeps--a case study from the Costa Rica subduction zone, PLoS One, 8, e74894, 10.1371/journal.pone.0074894, 2013.
Pancost, R. D., Damste, J. S., De Lint, S., Van Der Maarel, M. J. E. C., and Gottchal, J. C.: Biomarker Evidence for Widespread Anaerobic Methane Oxidation in Mediterranean Sediments by a Consortium of Methanogenic Archaea and Bacteria, Appl Environ Microbiol, 66, 1126–1132, 2000.
Pancost, R. D., Hopmans, E. C., and Sinninghe Damsté, J. S.: Archaeal lipids in Mediterranean Cold Seeps: Molecular proxies for anaerobic methane oxidation, Geochimica et Cosmochimica Acta, 65, 1611–1627, 2001.
Panieri, G.: Foraminiferal response to an active methane seep environment: A case study from the Adriatic Sea, Marine Micropaleontology, 61, 116-130, 10.1016/j.marmicro.2006.05.008, 2006.
Panieri, G., and Sen Gupta, B. K.: Benthic Foraminifera of the Blake Ridge hydrate mound, Western North Atlantic Ocean, Marine Micropaleontology, 66, 91-102, https://doi.org/10.1016/j.marmicro.2007.08.002, 2008.
Panieri, G., Camerlenghi, A., Conti, S., Pini, G. A., and Cacho, I.: Methane seepages recorded in benthic foraminifera from Miocene seep carbonates, Northern Apennines (Italy), Palaeogeography, Palaeoclimatology, Palaeoecology, 284, 271-282, https://doi.org/10.1016/j.palaeo.2009.10.006, 2009.
Panieri, G., Graves, C. A., and James, R. H.: Paleo-methane emissions recorded in foraminifera near the landward limit of the gas hydrate stability zone offshore western Svalbard, Geochemistry, Geophysics, Geosystems, 17, 521-537, 10.1002/, 2016.
Panieri, G., Lepland, A., Whitehouse, M. J., Wirth, R., Raanes, M. P., James, R. H., Graves, C. A., Crémière, A., and Schneider, A.: Diagenetic Mg-calcite overgrowths on foraminiferal tests in the vicinity of methane seeps, Earth and Planetary Science Letters, 458, 203-212, 10.1016/j.epsl.2016.10.024, 2017.
Patton, H., Andreassen, K., Bjarnadóttir, L. R., Dowdeswell, J. A., Winsborrow, M. C. M., Noormets, R., Polyak, L., Auriac, A., and Hubbard, A.: Geophysical constraints on the dynamics and retreat of the Barents Sea ice sheet as a paleobenchmark for models of marine ice sheet deglaciation, Reviews of Geophysics, 53, 1051-1098, 10.1002/2015rg000495, 2015.
Peckmann, J., Reimer, A., Luth, U., Luth, C., Hansen, B. T., Heinicke, C., Hoefs, J., and Reitner, J.: Methane-derived carbonates and authigenic pyrite from the northwestern Black Sea, Marine Geology, 177, 129-150, https://doi.org/10.1016/S0025-3227(01)00128-1, 2001.
Peckmann, J., and Thiel, V.: Carbon cycling at ancient methane-seeps, Chemical Geology, 205, 443-467, 10.1016/j.chemgeo.2003.12.025, 2004.
Puglini, M., Brovkin, V., Regnier, P., and Arndt, S.: Assessing the potential for non-turbulent methane escape from the East Siberian Arctic Shelf, Biogeosciences Discussions, 1-44, 10.5194/bg-2019-264, 2019.
Reeburgh, W. S.: Oceanic Methane Biogeochemistry, Chem. Rev, 107, 486-513, 2007.
Reimer, P. J., Bard, E., Bayliss, A., Beck, J. W., Blackwell, P. G., Ramsey, C. B., Buck, C. E., Cheng, H., Edwards, R. L., Friedrich, M., Grootes, P. M., Guilderson, T. P., Haflidason, H., Hajdas, I., Hatté, C., Heaton, T. J., Hoffmann, D. L., Hogg, A. G., Hughen, K. A., Kaiser, K. F., Kromer, B., Manning, S. W., Niu, M., Reimer, R. W., Richards, D. A., Scott, E. M.,

Southon, J. R., Staff, R. A., Turney, C. S. M., and van der Plicht, J.: IntCal13 and Marine13 Radiocarbon Age Calibration Curves 0–50,000 Years cal BP, Radiocarbon, 55, 1869-1887, 10.2458/azu_js_rc.55.16947, 2013.
Riedinger, N., Kasten, S., Gröger, J., Franke, C., and Pfeifer, K.: Active and buried authigenic barite fronts in sediments from the Eastern Cape Basin, Earth and Planetary Science Letters, 241, 876-887, 10.1016/j.epsl.2005.10.032, 2006.
Ruppel, C. D., and Kessler, J. D.: The interaction of climate change and methane hydrates, Reviews of Geophysics, 55, 126-168, 10.1002/2016rg000534, 2017.
Sauer, S., Hong, W.-L., Knies, J., Lepland, A., Forwick, M., Klug, M., Eichinger, F., Baranwal, S., Crémière, A., Chand, S., and Schubert, C. J.: Sources and turnover of organic carbon and methane in fjord and shelf sediments off northern Norway, Geochemistry, Geophysics, Geosystems, 17, 4011-4031, 10.1002/2016gc006296, 2016.
Sauer, S., Crémière, A., Knies, J., Lepland, A., Sahy, D., Martma, T., Noble, S. R., Schönenberger, J., Klug, M., and Schubert, C. J.: U-Th chronology and formation controls of methane-derived authigenic carbonates from the Hola trough seep area, northern Norway, Chemical Geology, 470, 164-179, 10.1016/j.chemgeo.2017.09.004, 2017.
Schneider, A., Crémière, A., Panieri, G., Lepland, A., and Knies, J.: Diagenetic alteration of benthic foraminifera from a methane seep site on Vestnesa Ridge (NW Svalbard), Deep Sea Research Part I: Oceanographic Research Papers, 123, 22-34, https://doi.org/10.1016/j.dsr.2017.03.001, 2017.
Schneider, A., Panieri, G., Lepland, A., Consolaro, C., Crémière, A., Forwick, M., Johnson, J. E., Plaza-Faverola, A., Sauer, S., and Knies, J.: Methane seepage at Vestnesa Ridge (NW Svalbard) since the Last Glacial Maximum, Quaternary Science Reviews, 193, 98-117, 10.1016/j.quascirev.2018.06.006, 2018.
Sen, A., Åström, E. K. L., Hong, W.-L., Portnov, A., Waage, M., Serov, P., Carroll, M. L., and Carroll, J.: Geophysical and geochemical controls on the megafaunal community of a high Arctic cold seep, Biogeosciences Discussions, 1-52, 10.5194/bg-2017-540, 2018.
Serov, P., Vadakkepuliyambatta, S., Mienert, J., Patton, H., Portnov, A., Silyakova, A., Panieri, G., Carroll, M. L., Carroll, J., Andreassen, K., and Hubbard, A.: Postglacial response of Arctic Ocean gas hydrates to climatic amelioration, Proc Natl Acad Sci U S A, 10.1073/pnas.1619288114, 2017.
Solomon, E. A., and Kastner, M.: Progressive barite dissolution in the Costa Rica forearc – Implications for global fluxes of Ba to the volcanic arc and mantle, Geochimica et Cosmochimica Acta, 83, 110-124, 10.1016/j.gca.2011.12.021, 2012.
Stuiver, M., Reimer, P. J., and Braziunas, T. F.: High-Precision Radiocarbon Age Calibration for Terrestrial and Marine Samples, Radiocarbon, 40, 1127-1151, 10.1017/S0033822200019172, 1998.
Suess, E., Torres, M. E., Bohrmann, G., Collier, R. W., Rickert, D., Goldfinger, C., Linke, P., Heuser, A., Sahling, H., Heeschen, K., Jung, C., Nakamura, K., Greinert, J., Pfannkuche, O., Trehu, A., Klinkhammer, G., Whiticar, M. J., Eisenhauer, A., Teichert, B., and Elver, M.: Sea Floor Methane Hydrates at Hydrate Ridge, Cascadia Margin, in: Natural Gas Hydrates: Occurrence, Distribution, and Detection, 87-98, 2001.
Torres, M. E., Brumsack, H. J., Bohrmann, G., and Emeis, K. C.: Barite fronts in continental margin sediments: a new look at barium remobilization in the zone of sulfate reduction and formation of heavy barites in diagenetic fronts, Chemical Geology, 127, 125-139, https://doi.org/10.1016/0009-2541(95)00090-9, 1996.
Torres, M. E., McManus, J., Hammond, D. E., De Angelis, M. A., Heeschen, K. U., Colbert, S. L., Tryon, M. D., Brown, K. M., and Suess, E.: Fluid and chemical £uxes in and out of sediments hosting methane hydrate deposits on Hydrate Ridge, OR, I: Hydrological provinces, Earth and Planetary Science Letters, 201, 525-540, 2002.

Torres, M. E., Bohrmann, G., Dubé, T. E., and Poole, F. G.: Formation of modern and Paleozoic stratiform barite at cold methane seeps on continental margins, Geology, 31, 897-900, 10.1130/G19652.1 %J Geology, 2003a.
Torres, M. E., Mix, A. C., Kinports, K., Haley, B., Klinkhammer, G. P., McManus, J., and de Angelis, M. A.: Is methane venting at the seafloor recorded by δ13C of benthic foraminifera shells?, Paleoceanography, 18, n/a-n/a, 10.1029/2002pa000824, 2003b.
Valentine, D. L., and Reeburgh, W. S.: New perspectives on anaerobic methane oxidation, Environmental Microbiology, 2, 477-484, 2000.
Volkman, J. K., and Smittenberg, R. H.: Lipid Biomarkers as Organic Geochemical Proxies for the Paleoenvironmental Reconstruction of Estuarine Environments, in: Applications of Paleoenvironmental Techniques in Estuarine Studies, edited by: Weckström, K., Saunders, K. M., Gell, P. A., and Skilbeck, C. G., Springer Netherlands, Dordrecht, 173-212, 2017.
Vorren, T. O., Laberg, J. S., BLAUME, F., Dowdeswell, J. A., KENYON, H. H., Mienert, J., RUMOHR, J., and WERNER, F.: THE NORWEGIAN–GREENLAND SEA CONTINENTAL MARGINS: MORPHOLOGY AND LATE QUATERNARY SEDIMENTARY PROCESSES AND ENVIRONMENT, Quaternary Science Reviews, 17, 273-302, 1998.
Waage, M., Portnov, A., Serov, P., Bünz, S., Waghorn, K. A., Vadakkepuliyambatta, S., Mienert, J., and Andreassen, K.: Geological Controls on Fluid Flow and Gas Hydrate Pingo Development on the Barents Sea Margin, Geochemistry, Geophysics, Geosystems, 20, doi:10.1029/2018GC007930, 2019.
Wallmann, K., Riedel, M., Hong, W. L., Patton, H., Hubbard, A., Pape, T., Hsu, C. W., Schmidt, C., Johnson, J. E., Torres, M. E., Andreassen, K., Berndt, C., and Bohrmann, G.: Gas hydrate dissociation off Svalbard induced by isostatic rebound rather than global warming, Nat Commun, 9, 83, 10.1038/s41467-017-02550-9, 2018.
Wefer, G., Berger, W. H., Bijma, J., and Fischer, G.: Clues to Ocean History: a Brief Overview of Proxies, in: Use of Proxies in Paleoceanography: Examples from the South Atlantic, edited by: Fischer, G., and Wefer, G., Springer Berlin Heidelberg, Berlin, Heidelberg, 1-68, 1999.
Wegener, G., Niemann, H., Elvert, M., Hinrichs, K. U., and Boetius, A.: Assimilation of methane and inorganic carbon by microbial communities mediating the anaerobic oxidation of methane, Environmental Microbiology, 10, 2287–2298, 2008.
Whiticar, M.: Carbon and hydrogen isotope systematics of bacterial formation and oxidation of methane, Chemical Geology 161, 291-314, 1999.
Wollenburg, J. E., Kuhnt, W., and Mackensen, A.: Changes in Arctic Ocean paleoproductivity and hydrography during the last 145 kyr: The benthic foraminiferal record, Paleoceanography, 16, 65-77, 10.1029/1999pa000454, 2001.
Wollenburg, J. E., Raitzsch, M., and Tiedemann, R.: Novel high-pressure culture experiments on deep-sea benthic foraminifera — Evidence for methane seepage-related δ13C of Cibicides wuellerstorfi, Marine Micropaleontology, 117, 47-64, 10.1016/j.marmicro.2015.04.003, 2015.
Yao, H., Hong, W. L., Panieri, G., Sauer, S., Torres, M. E., Lehmann, M. F., Gründger, F., and Niemann, H.: Fracture-controlled fluid transport supports microbial methane-oxidizing communities at Vestnesa Ridge, Biogeosciences, 16, 2221-2232, 10.5194/bg-16-2221-2019, 2019.
Zhang, C. L.: Lipid and carbon isotopic evidence of methane-oxidizing and sulfate-reducing bacteria in association with gas hydrates from the Gulf of Mexico, Geology, 30, 239–242, 2002.

Data
Foraminifera

921GC	N. Pachyderma		1522GC	N. Pachyderma	
depth	921 $\delta^{13}C$	921 $\delta^{18}O$	depth	1522 $\delta^{13}C$	1522 $\delta^{18}O$
cmbsf	permil,VPDB	permil,VPDB	cmbsf	permil,VPDB	permil,VPDB
0	-0.08	2.89	1	0.05	2.97
2.5	-0.35	2.69	11	0.04	2.81
6.5	-0.34	2.89	21	0.73	3.23
15.5	0.41	2.94	31	0.51	2.92
20.5	0.37	2.92	41	0.42	2.92
25.5	0.62	3.12	61	-0.02	2.73
30.5	0.42	2.89	71	-0.35	2.66
35.5	0.51	2.97	81	-0.05	2.89
40.5	0.41	2.97	91	0.13	3.32
45.5	0.10	2.98	101	0.67	3.49
50.5	0.00	2.72	121	0.45	3.70
55.5	0.27	3.02	141	-0.06	3.77
60.5	0.18	3.09	151	-0.23	3.47
65.5	0.12	3.11	161	0.04	4.25
75.5	0.26	3.91	171	0.13	3.94
80.5	0.25	3.38	181	-0.27	3.60
85.5	0.09	3.66	191	-0.29	3.74
90.5	0.47	3.51	201	-0.34	3.66
95.5	0.62	3.41	221	-0.10	3.93
100.5	0.44	3.27	231	-0.22	3.93
101.5	0.55	3.32	241	-0.32	4.69
105.5	0.25	3.91	248	0.02	4.81
110.5	0.18	3.71	261	-0.21	4.50
115.5	0.41	3.90	271	-1.52	4.45
120.5	0.46	3.65	301	-2.00	4.85
126.5	0.10	3.85	321	-3.18	4.88
130.5	0.24	3.95	329	-1.58	4.71
135.5	0.28	3.99			
140.5	0.03	4.04			
160.5	0.25	4.06			
165.5	0.08	4.00			
175.5	-0.17	3.89			
180.5	-0.14	3.85			
185.5	-0.37	3.78			
190.5	-0.20	3.81			
202.5	-0.35	3.66			
205.5	0.07	3.67			
210.5	-0.16	3.47			
215.5	0.20	4.52			
220.5	-0.10	2.43			
225.5	-0.32	4.28			

235.5	-0.08	4.88
240.5	-0.17	4.92
245.5	-0.05	5.00
250.5	-0.07	4.88
255.5	-0.49	4.84
270.5	-0.40	4.72
275.5	-0.39	4.68
280.5	-0.88	4.90
285.5	-0.64	4.91
290.5	-0.77	4.91
295.5	-0.67	4.91
302.5	-0.71	4.94
305.5	-0.28	4.94
310.5	-0.52	4.91
315.5	-0.11	4.83
320.5	-0.19	4.83
325.5	0.10	4.80
330.5	0.04	4.84
335.5	-0.02	4.81
340.5	0.03	4.94
345.5	0.03	4.87
350.5	-0.01	4.90

1520GC	Cassidulina neoteretis		Melonis Barleeanum		N. Pachyderma	
depth cmbsf	$\delta^{13}C$	$\delta^{18}O$	$\delta^{13}C$	$\delta^{18}O$	$\delta^{13}C$	$\delta^{18}O$
6.5	-1.67	4.16	-1.69	3.61	-6.42	3.41
11.5	-0.69	4.41	-1.80		-0.79	
16.5	-1.44	4.33	-5.65	3.84	-9.02	3.65
21.5	-0.76	4.25	-1.37	3.69	-9.27	3.59
26.5	-2.47	4.45	-2.18	3.84	-1.82	
31.5	-0.34	4.21	-1.63	3.74	0.08	
46.5	-8.42	4.62			-8.24	3.52
51.5	-3.01	4.36	-2.04	3.57	-11.822	3.85
56.5	-1.36	4.35	-2.17	3.77	-6.16	3.69
61.5	-2.92	4.29			-9.11	3.50
66.5	-13.88	4.69			-16.3603	4.35
71.5	-10.53	4.64	-9.34	4.20	-16.1116	4.22
76.5	-14.63	4.84	-12.60	4.55	-17.11	4.50
79.5	-18.33	5.00			-18.3118	5.10
81.5			-9.08		-11.83	3.88
86.5	-3.22	4.55	-2.79		-6.34	
91.5	-2.75		-2.08	3.27		
107.5	-7.81	4.65	-2.44	3.85	-10.04	3.73
111.5	-3.59	4.61			-3.26	3.53
121.5	-4.24	4.45				

136.5	-5.56	4.48	-3.14		-19.80	4.45
141.5	-11.55	4.63			-13.28	3.80
146.5	-8.30	4.57			-10.45	3.65
151.5	-5.30	4.72			-11.12	4.06
157.5	-6.17	4.72			-8.55	
162.5	-5.57	4.77			-10.74	
227.5	-5.89	4.91	-0.71			
232.5	-4.26	4.64				
237.5			-2.64			
241.5						
247.5	-3.24	4.63				
253.5	-3.36					
257.5	-7.62	4.70			-10.48	3.94
262.5	-8.66	4.85			-13.30	4.39
267.5	-8.40	4.72			-14.82	4.57
272.5	-12.19	4.84				
277.5	-14.60	5.00				
282.5	-6.13	4.69			-11.64	4.28
287.5	-7.28	4.72			-11.76	4.05
292.5	-3.75	4.70			-6.35	3.86
297.5	-3.99	4.61			-14.58	4.19
302.5	-7.43	4.73				
317.5	-5.05	4.59				
322.5	-7.98	4.68	-1.59	3.92	-8.97	3.94
327.5	-5.25	4.74				
332.5	-2.87	5.07			-9.10	4.25
337.5	-4.74	4.75				
342.5	-2.01	4.34			-2.96	3.69
347.5	-2.56	4.40			0.45	
352.5	-11.03	4.26			-7.05	3.84

920GC	N. Pachyderma		Melonis Barleeanum		Cassidulina neoteretis	
depth cmbsf	920 $\delta^{13}C$	$\delta^{18}O$	$\delta^{13}C$	$\delta^{18}O$	$\delta^{13}C$	$\delta^{18}O$
0.5	-0.12	2.86	-1.94	3.81	-0.71	4.18
10.5	0.21	3.57	-1.82	3.55	-0.34	4.20
15.5	-0.08	2.78			0.34	4.41
20.5	-0.16	2.55	-1.97	3.64	-0.39	4.15
25.5	-0.39	2.73			-1.09	4.16
30.5	-0.43	2.91			-0.88	4.40
73.5	-5.50	3.52	-8.64		-10.73	4.09
79.5	-4.03	3.61	-2.76	3.23		
93.5	-8.94	4.20	-5.10	4.11	-8.40	4.59

100.5	-5.56	3.85	-2.45	3.79	-11.68	4.72
105.5	-14.05	4.54			-10.79	4.70
125.5	-12.95	4.79	-13.42	4.39	-18.63	4.58
130	-15.91	4.38	-3.61	3.80		
145			-5.10	3.92		
150			-3.35	3.88		
155.5	-8.23	4.18	-2.93	3.76		
165	-10.68	4.78	-7.57	4.50		
173	-13.56	4.29			-8.88	4.42
181			-0.16	3.42		
190	-0.26	4.36	-2.17	3.65		
196.5	-0.49	3.27	-1.85	4.55	-0.78	4.44
210.5	-1.56	3.11				
215.5	-0.43	4.48	-1.04	4.05	-0.86	4.90
222.5	-0.53	4.72	-2.21	4.64	-0.81	4.75
243.5	-1.44	4.30				

1070GC	N. Pachyderma		Cassidulina neoteretis	
depth cmbsf	$\delta^{13}C$	$\delta^{18}O$	$\delta^{13}C$	$\delta^{18}O$
6.5	-3.02	3.29	-1.40	4.24
16.5	-5.87	3.59	-1.25	3.96
26.5	-5.49	3.41	-4.34	4.25
36.5	-0.87	3.59	-1.45	4.24
56.5	-0.79	3.66	-1.24	4.36
61.5	-0.35	3.49	-1.18	4.42
66.5	-0.60	3.88	-1.72	4.41
76.5	-0.46	3.49	-1.77	4.89
96.5			-1.10	4.61
106.5	-0.24	3.18	-2.98	4.39
116.5	-0.96	2.96	-1.22	4.28
126.5	-1.08	3.74	-1.21	4.34
136.5	0.01	3.47	-1.53	4.28
146.5	-0.04	3.63	-1.95	4.50
156.5	-0.52	3.59	-1.20	4.23
166.5	-0.08	3.52	-2.18	4.34
176.5	0.37	3.88	-1.14	4.61
186.5	-6.56	3.73	-9.92	4.16
196.5	-3.94	3.95	-4.25	4.50
206.5	-1.57	3.49	-8.30	4.88
216.5	-0.21	3.77	-7.28	4.61
226.5	-2.94	4.06	-5.99	4.57
236.5	-0.22	4.66	-4.61	4.74
266.5	-0.50	3.97	-11.03	3.48

276.5	-1.11	3.93	-1.65	4.64
286.5	-8.26	4.11	-11.34	4.76
296.5	-1.82	3.94	-1.36	4.66
306.5	-1.40	4.12	-3.26	4.27
316.5	-2.60	4.36	-3.34	3.52

940GC	N. Pachyderma	
depth cmbsf	$\delta^{13}C$	$\delta^{18}O$
50	-1.40	2.48
55	-0.25	2.81
60	-0.01	2.99
65	-0.55	3.06
70	0.20	2.94
75	-1.20	3.18
80	-1.30	3.29
85	-8.07	3.72
90	-11.30	3.97
95	-11.33	3.92
100	-5.06	3.57
105	-6.81	3.11
110	-8.20	3.40
115	-9.39	3.59
120	-6.80	3.41
125	-11.06	3.91
130	-14.35	3.67
135	-11.32	3.69
140	-6.96	2.99
145	-4.16	2.91
150	-7.44	3.41
155	-19.06	4.33
160	-13.52	3.46
165	-16.03	4.31
175	-0.93	2.49
180	-1.85	3.36
195	-13.95	4.07
200	-3.14	3.72
205	-1.57	3.81
210	-0.33	3.46
215	0.15	3.52
220	0.19	3.42
225	0.16	3.84
230	0.05	3.77
235	-0.17	3.82
240	-0.04	3.93
245	-0.06	3.88

255	-1.51	4.21
260	-8.51	4.84
270	-0.45	3.72
275	-1.78	3.73
285	-0.17	3.52
290	-0.49	3.25
295	-0.25	3.90
310	-0.02	4.87
315	-0.16	4.58
320	-0.70	4.92

Lipid biomarkers

1520GC

depth	Archeol (μg/g)	SnAr (μg/g)	δ^{13}C Ar	δ^{13}C SnAr	C16:ω5c (μg/g)	CyC17 (μg/g)	δ^{13}C16	δ^{13}CyC17
0.5	0.1884	0.1347			0.5771	0.1516	-41.93	-30.768
5.5	0.1432	0.0258	-92.518	-85.499	0.9725	0.0692	-68.742	-53.223
10.5	0.2205	0.0335	-93.128	-88.342	1.0199	0.513	-76.025	-85.005
15.5	0.2775	0.0303	-91.764	-70.578	0.1031	0.0372	-69.221	-63.602
20.5	0.1752	0.0453			0.5605	0.0653	-70.147	-76.242
25.5	0.124	0.0455			0.4708	0.0645	-82.903	-85.842
30.5	0.2813	0.2702	-87.606		0.485	0.1214	-72.5	
35.5	0.1517	0.1265	-87.159	-95.789	0.7599	0.2351	-77.752	
40.5	0.233	0.1213	-86.663	-96.639	0.7737	0.169	-79.859	
45.5	0.6624	0.1949	-85.642	-89.294	1.1822	0.331	-87.861	
50.5	0.464	0.1606	-89.07	-89.605	0.7498	0.1979	-78.018	
55.5	1.0652	0.3512	-87.321	-92.972	0.6057	0.1325	-69.191	
60.5	0.4165	0.2193	-79.839	-86.502	0.6386	0.185		
65.5	0.5141	0.3017	-81.291	-90.015	0.3959	0.1055	-76.235	
70.5	0.5487	0.1842	-90.269	-93.753	0.3772	0.0909	-68.649	
75.5	0.5866	0.2046	-92.588	-96.911	0.7424	0.1839	-80.928	
80.5	0.3897	0.1488	-84.602	-95.273	0.2173	0.0738	-68.823	
85.5	0.5949	0.2171	-85.12	-96.724	0.2286	0.0998		
90.5	0.2854	0.1877	-84.424	-99.223	0.1098	0.0788		
95.5	0.588	0.1146	-90	-99.135	0.146	0.0542	-59.176	
102	0.2164	0.0317	-96.859	-83.532	0.0761	0.039	-78.084	-86
106	0.2291	0.0723	-92.802	-81.805	0.1267	0.0425	-75.34	-93.644
110.5	0.2549	0.0509	-93.929	-90.623	0.099	0.0352	-61.449	-86.671
115.5	0.214	0.0756	-78.817	-66.82	0.0553	0.0294	-56.917	-86.802
120.5	0.1585	0.1006	-83.968	-95.025	0.0954	0.0537	-51.776	-78
125.5	0.2726	0.1103	-71.098		0.1016	0.0588	-49.9	
130.5	0.1719	0.0762			0.0478	0.0509	-36	
135	0.2336	0.097	-71.128		0.0614	0.0592	-46.137	
140	0.1952	0.0713	-90.108		0.0626	0.0604	-41	
145			-69.119		0.0796	0.0702	-51	
150	0.1969	0.2158	-79.753	-100	0.0799	0.0736	-43	

155	0.2088	0.1082	-79.834	-95.034	0.0991	0.0733	-52
160	0.1063	0.0922	-73.466	-98.702	0.068	0.0571	-36
165	0.1809	0.232	-68.593	-93.208			-36
170							
225	0.0723	0.0873	-75.564				-42
230	0.0634	0.0407	-75.381	-91.48	0.064	0.099	-40
235	0.0373	0.051	-74.923	-96.387	0.0329	0.023	-53
240	0.0684	0.0668	-75.767	-94.066	0.066	0.0546	
245	0.0579	0.025	-74.902	-100	0.0539	0.0376	-36
250	0.0815	0.0897	-66		0.0664	0.0306	
255	0.1468	0.0734	-73.806	-82.071	0.0988	0.0613	-37
260	0.0897	0.0227	-90.391		0.0635	0.0175	
265	0.0437	0.0188	-77.191	-94.059	0.0406	0.0185	-38
270	0.0569	0			0.048	0.0451	
275			-90.151	-96.878			-49
280			-87.414	-89.785	0.1831	0.3669	-49
285			-82.359		0.065	0.0754	-48
290			-83.442		0.1197	0.0248	-46
295	0.206	0.0382	-75.509		0.0762	0.0247	-43
300			-81.64		0.0959	0.0384	-44
305			-84.075		0.0908	0.0494	-54
310					0.029	0.0219	-45
315			-90.468		0.0358	0.0195	-51
320			-83.657		0.0302	0.0186	-47
325			-77.843				-51
330			-89.043				
335			-69.239				-56
340			-77.782				-42
345			-74.029				-45

920GC

depth	Archeol (μg/g)	SnAr (μg/g)	δ^{13}C Ar	δ^{13}C SnAr	C16:ω5c (μg/g)	CyC17 (μg/g)	δ^{13}C16	δ^{13}CyC17
2.5	0.0597	0.0392	-26.333	-26.167	0.3204		-32.5	-27
11.5	0.0784	0.0559	-27.206		0.2037	0.0179	-50.2	-30
16.5	0.0528	0.0269	-26.161		0.1068	0.0151	-34.7	-38
21.5	0.1108	0.0269	-27.412		0.157	0.0504	-33	-32
26.5	0.0298	0	-47.04		0.0914	9.30E-03	-44	-50
31.5	0.0415	0	-55.386		0.0913	5.15E-03	-39	-31
36.5	0.0465	0	-75.735		0.0683	2.46E-03	-40	-32
43	0.0465	0.0217	-51.884		0.0524	6.77E-03	-38	-30
47	0.0667	0.0241	-45.68		0.0681	0.0262	-40	-33
52	0.0666	0	-60.95		0.0659	0.0719	-41	-31
57	0.0535	0	-69.09		0.095	0.0936	-44	
63	0.0408	0	-60.838		0.1033	0.1168	-41	
69	0.0513	0	-67.849		0.06	0.0476	-50	-35
75	0.089	0	-74.613		0.0718	0.0513	-43	-32

81	0.1665	0	-78.06		0.0717	0.0536	-48	-39
87	0.0317	0	-57.077		0.0199	0.0189	-45	
95	0.036	0.0306	-58.399		0.0259	0.0262	-46	-36
103	0.0627	0.0453	-59.84	-84.888	0.0666	0.0352	-49	
107	0.0766	0.028	-64.372	-75.904	0.1248	0.0166	-50	
112	0.1186	0.1083	-72.958		0.13	0.1389	-54	
117	0.1734	0.0855	-92.095	-99.67			-47	
122	0.1051	0.0516	-87.899	-89.585			-50	
127	0.0971	0.0551	-79.454	-92.386	0.0669	0.0167	-44	
132	0.0691	0.0348	-75.798		0.0533	0.0582	-42	
137	0.0422	0	-76.636		0.0516	0.0564	-37	
142	0.106	0	-82.472		0.0359	0.0445	-58	
147	0.0968	0	-80.043				-60	
152	0.1675	0.0168	-86.629		0.0542	0.0256	-59	-42
157	0.2542	0.143	-86.195	-92.951	0.0683	0.093		
162	0.2113	0.0633	-80.448		0.0724	0.0679	-37	
168	0.053	0	-79.143		0.1181	0.0626	-44	
175	0.0484	0	-88.382		0.0922	0.0709	-58	
183	0.0138	0	-63.213		0.092	0.1047	-48	
192	0.0162	0	-43.8		0.0361	0.0243	-40	
198	0.0111	0	-57.859		0.031	0	-44	
204	9.93E-03		-71.024		0.0307	0.0252	-53	
212	0.0103		-53.232		0.0276	9.91E-03		
217	5.91E-03		-37.543		6.17E-03	5.65E-03		
224	7.52E-03		-31.732		0.0624	0.033		
230	5.51E-03				0	0.0343		
235								
240	4.83E-03				0.0469	0.0302		
245								

1522GC

depth	Archeol (μg/g)	SnAr (μg/g)	δ^{13}C Ar	δ^{13}C SnAr	C16:ω5c (μg/g)	CyC17 (μg/g)	δ^{13}C C16	δ^{13}C CyC17
1			-31.087	-23.841	0.2147	0.081	-33.421	-31.091
11	0.0238	0.0305	-26.263	-25.884	0.0346	0.0468	-30.286	
21	0.0123	0.0178	-22.791	-32.357	0.0287	0.0497	-31	
31	0.0115	0.0104	-27.071	-34.339	0.0599	0.0451	-29.338	-24.7
41	0.0104	7.68E-03	-26	26	0.0288	0.0293	-22	-23
51	0.0127	0.018	-25.183	-23.549	0.0379	0.0375	-30.6	-26.2
61	7.82E-03	7.04E-03	-24.194	-27.795	0.034	0.0399	-27.308	
71	0.0315	0.0206	-27.184	-29.633	0.0159	0.0236	-26.81	-31.6
81	0.029	0	-26.344	-33.083	0.048	0.0454	-27.65	-25
91	0.0153	0.0135	-30.439	-25	0.0552	0.0438	-38.09	-25.7
101	9.43E-03	0.0184	-27	-42	0.0324	0.0402	-34.4	-29.5
121	0.0143	0.031	-27	-21	0.0244	0.0194	-34.16	
141	0.0174	0.0215	-29.226	-26.7	0.1068	0.0626		

161	0.019	0.0391	-38.66	-53	0.0428	0.0424		
181	0.0192	0.0101			0.0435	0.0603		
201	0.0186	0.0246	-46		0.0995	0.0658	-39.8	
221	0.0122	0.0112	-46.324	-48.814	0.031	0.019	-29.5	-34
241	5.79E-03	6.20E-03	-37	-35	0.1248	0.0434	-40	
261	5.29E-03	0	-41.7		0.0474	0.0694	-40.638	
281	6.59E-03	0	-73.5					
321	3.99E-03	0			0.0272	0.0261	-46.535	
341	3.23E-03	3.63E-03	-75.48		0.0192	0.0398	-33.8	-28

Paper III

Biomarker and isotopic composition of seep carbonates record environmental conditions in two Arctic methane seeps

Haoyi Yao, Giuliana Panieri, Moritz Lehmann, Tobias Himmler, Helge Niemann
to be submitted to Deep Sea Research

Biomarker and isotopic composition of seep carbonates record environmental conditions in two Arctic methane seeps

Haoyi Yao[1], Giuliana Panieri[1], Moritz Lehmann[2], Tobias Himmler[1,3], Helge Niemann [1, 2,4,5]

[1] CAGE - Centre for Arctic Gas Hydrate, Environment and Climate, Department of Geosciences, UiT The Arctic University of Norway in Tromsø, Norway

[2] Department of Environmental Sciences, University of Basel, Bernoullistrasse 30, CH-4056 Basel, Switzerland

[3] Geological Survey of Norway, Trondheim, Norway

[4] NIOZ Royal Institute for Sea Research, Department of Marine Microbiology and Biogeochemistry, and Utrecht University, P.O. Box 59, 1790 AB Den Burg, Texel, The Netherlands

[5] Department of Earth Sciences, Faculty of Geosciences, Utrecht University, 3584 CD Utrecht, the Netherlands

Abstract

We investigated methane-seep associated carbonate crusts and nodules from two Arctic cold seep sites at Vestnesa Ridge (ca. 1200 m water depth) and Storfjordrenna (ca. 380m water depth) to determine the biogeochemical parameters at the time of carbonate formation. Gas bubbling were observed during remotely operated vehicle (ROV)-assisted sampling at both sites revealed ongoing seep activity. Seep carbonates were present, both as outcropping crusts at the seafloor and as centimeter-size carbonate-cemented nodules at both study sites. The aragonite-dominated mineralogy of all except one seep carbonates suggests precipitation close to the seafloor in an environment characterized by high rates of sulfate-dependent anaerobic oxidation of methane (AOM). In contrast, Mg-calcite rich nodules sampled in the Storfjordrenna sediment core appear to have formed at the sulfate-methane-transition zone deeper within the sediment at lower rates of AOM. Evidence for AOM activity at the time of carbonate precipitaton is provided by high concentrations of ^{13}C-depleted lipid biomarkers diagnostic for anaerobic methanotrophic archaea (archaeol and *sn2*-hydroxyarchaeol) and sulfate-reducing bacteria (iso and anteiso-C15:0 fatty acids) in the crusts. We also found lipid biomarkers (diploptene and a 4α-methyl sterol) related to the aerobic oxidation of methane (MOx), suggesting that the spatial separation between AOM and MOx zones was very low at the time of carbonate precipitation. The δ^{13}C carbonate values of bulk rock and micro-drilled samples vary between −36 ‰ and −20 ‰ (VPDB) as is typical range for AOM-induced seep carbonate

precipitation. Relatively high $\delta^{18}O$ carbonate values indicate significant contribution of ^{18}O-enrichd gas hydrate-derived water during carbonate formation. We infer the seafloor seep carbonates were formed during intensive methane seepage, which probably caused methane ebullition from the sea floor into the water column at both investigated sites.

1. Introduction

In the marine sediments, methane is stored in the form of free-, dissolved- or gas hydrate. Significant concern exists that a warmer Arctic ocean will facilitate higher methane emission rates from the sea floor to the water column and potentially to the atmosphere. Gas hydrates are particularly susceptible to dissociation if bottom water heat efficiently penetrates into the seafloor (MacDonald et al., 1994;Dickens et al., 1995; Kennett, 2000;Dickens, 2003). Several gas seep and hydrate sites have been recognized in the Arctic ocean, for example at the Vestnesa Ridge (~1200 m water depth; Bünz et al., 2012;Plaza-Faverola et al., 2015;Panieri et al., 2017), the Prins Karls Forland (~400 m water depth; Berndt et al., 2014), and at the Storfjordrenna gas hydrate mound (~ 380m water depth; Serov et al., 2017; Hong et al., 2017;). It is expected that environmental temperatures rise more strongly in the Arctic than in lower latitudes (Collins et al., 2013; Bintanja, 2018). Bottom-water warming may thus be more severe in the Arctic, makes Arctic gas hydrate deposits in sediments in shallow waters particularly vulnerable to global warming. Knowledge on the emission history of Arctic seep systems is thus crucial in order to understand which are the environmental parameters, for example temperature, that have affected methane emisisons.

Traces of past vent activity can be deciphered from relicts of microbial communities that are dependend on methane. At present, most methane in the marine sediments is consumed through microbially mediated sulfate-dependent anaerobic oxidation of methane – AOM (e.g. Reeburgh, 2007):

$CH_4 + SO_4^{2-} \leftrightarrow HS^- + HCO_3^- + H_2O$ (eq. 1)

The oxidation of methane and reduction of sulfate forms a zone in sediments where both species are consumed, the sulfate-methane transition zone (SMTZ). AOM is mediated by anaerobic methanotrophic archaea (ANME), typically forming syntrophic partnerships with sulfate-reducing bacteria (SRB) (Knittel and Boetius, 2009). Methane bypassing the AOM filter can then be oxidised by aerobic methanotrophs at the sediment surface or in the water column. At highly active gas seeps, the spatial distance between the horizons that are dominated by AOM and sediment layers that primarily host aerobic methanotrophy (MOx) can be on the cm to mm scale (Niemann et al., 2006; Elvert and Niemann, 2008). The AOM end-products HS^- and HCO_3^-result in increased alkalinity in the sediment

pore waters, which in turn, facilitates precipitation of authigenic carbonates that then often encase the methanotrophic community that was present in the sediments at the time of carbonate precipitation. Molecular fossils such as lipid biomarkers of aerobic and anaerobic methanotrophic microbes have high preservation potential in seep carbonates (Niemann et al., 2005; Birgel et al., 2008;Birgel et al., 2011), thus allowing to reconstruct past microbial communities at the seep site (Niemann and Elvert, 2008). Seep carbonates can form nodules, slabs, chimneys and sometimes massive pavements at cold seeps (Aloisi et al., 2000;Reitner et al., 2005;Blumenberg, 2010). Seep carbonates are preserved at the seafloor or within sediments at seep sites even after the methane flux has diminished and thus constitute a geological record of past seepage (e.g. Peckmann and Thiel, 2004;Feng et al., 2010;Crémière et al., 2016a;Sauer et al., 2017). More precisely, the mineralogy and isotopic signatures of seep carbonates, as well as its biomarker ccontent/composition provide information on the environmental conditions and microbial communities during past seepage episodes, and potential changes of the ascending fluids over time (Greinert et al., 2001;Pierre and Fouquet, 2007).

Seep carbonates typically display low δ^{13}C-carbonate values reflecting the incorporation of methane-derived carbon (Aloisi et al., 2000;Crémière et al., 2016b). The δ^{18}O values of carbonates have been used as a proxy to determine the origin of fluids with differential ^{18}O-signatures, e.g., gas hydrate derived water, water from clay dehydration, or seawater (Bohrmann et al., 1998;Aloisi et al., 2000;Han and Aizenberg, 2003;Feng et al., 2014). The mineralogy of seep carbonates (aragonite vs. calcite or dolomite) indicates whether they were formed close to the seafloor (aragonite) or in deeper sediments (calcite/high-Mg and calcite/dolomite) (Bohrmann et al.,1998; Aloisi et al., 2000; Haas et al., 2010).

In this study, we investigated seep carbonates sampled from the seafloor and from sediment cores obtained at two active seeps sites in the Arctic with underlying gas hydrates: (i) the deep water Vestnesa Ridge and the more shallow water (ii) Storfjordenna gas hydrate mound (Table 1, Figure 1) (Bünz et al., 2012;Panieri et al., 2017;Serov et al., 2017). We studied the carbonate petrography and geochemistry to elucidate the history of hydrocarbon seepage at these systems, and to reveal potential factors influencing the fluid discharge at the different settings in the past. We used carbonate-carbon and -oxygen isotope ratio measurements to constrain the carbon sources and to assess the possible influence of seawater and/or fluid from gas hydrate in the carbonate precipitation environment. Seep carbonate-associated lipid biomarkers were analyzed to determine the methanotrophic communities that were present at the time of carbonate precipitation and were encased in the carbonate matrix. In this context, one of the prime objectives was to compare the isotope- and biomarker-geochemical imprint of carbonates formed at the seafloor versus those formed in deeper sediments, in order to gain the potential links between carbonate formation, methanotrophic communities and differential methane-seepage activity.

Table 1. List of studied seep carbonates, detailed sample locations and remarks indicating the main characteristic of the samples and where they were collected, at the seabed or at different depothin the sediment cores; GC = gravity core; cmbsf = centimeters below seafloor.

Name	Sample ID	Location	Water depth(m)	Coordinates	Remarks
S-1	HH 1029	Storfjordrenna	378	76.1069 °N 15. 9679 °E	Seabed crust
S-2	HH1077	Storfjordrenna	378	76.1070 °N 15. 9694 °E	Seabed crust
S-3	1520GC	Storfjordrenna	380	76. 1057 °N 15. 9661 °E	Weakly lithified nodular in sediment; 282 cmbsf
V-1	P1606002	Vestnesa Ridge	1204	79.0026 °N 6.9213 °E	Seabed crust (P002 in Fig.1)
V-2	P1606011	Vestnesa Ridge	1207	79.0076 °N 6.8993 °E	Seabed crust (P011 in Fig.1)
V-3	P1606012	Vestnesa Ridge	1207	79.0077 °N 6.8992 °E	Seabed crust (P012 in Fig.1)
V-4	GeoB21616-1-2R-1E	Vestnesa Ridge	1210	79.0069 °N 6.9041 °E	Cored crust; MeBo core 127, ~590 - 595 cmbsf (Mebo 127 in Fig. 1)

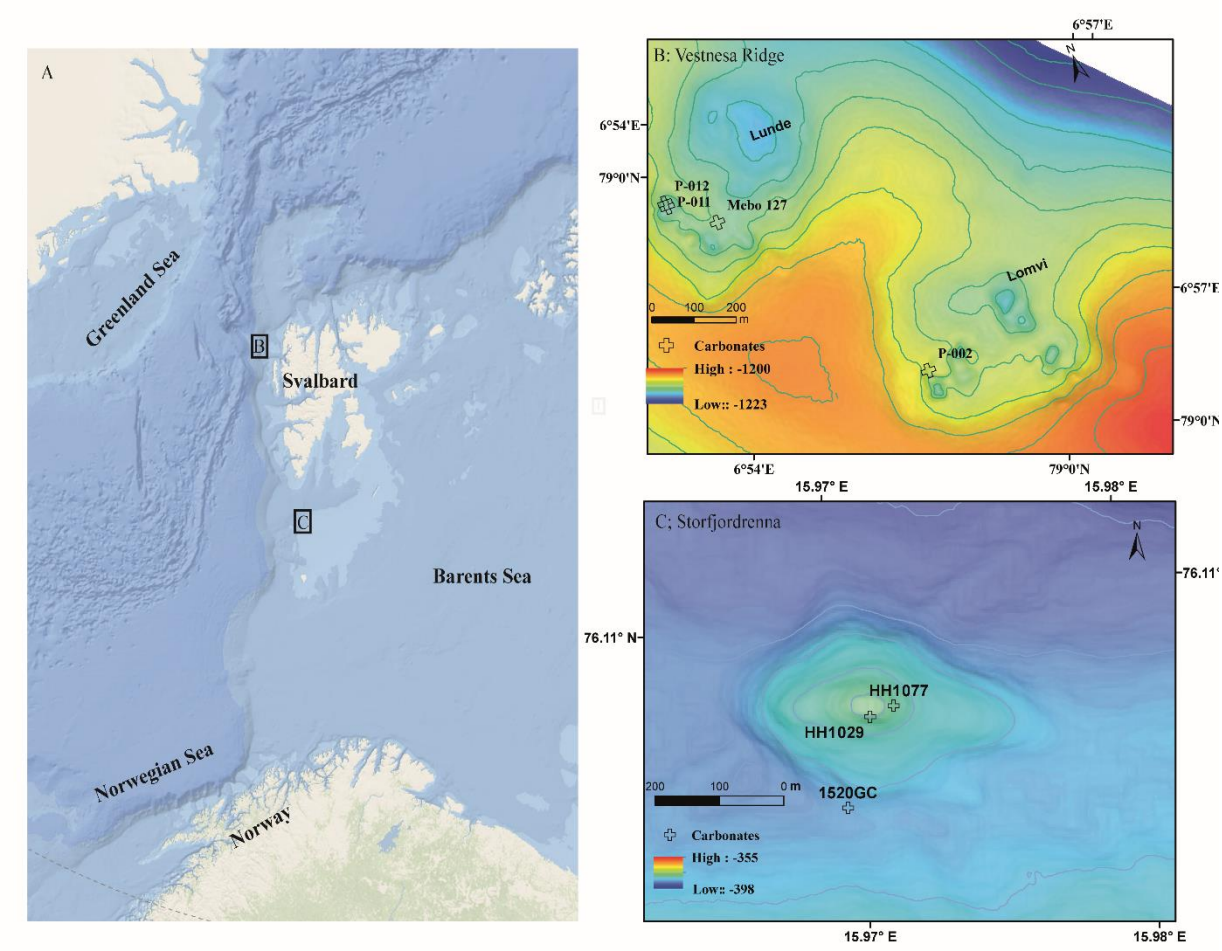

Figure 1. A) Overview of sampling locations Vestnesa Ridge off NW Svalbard, and Storfjordrenna gas hydrate mound in the NW Barents Sea. B) and C) Detailed bathymetry maps and respective seep carbonate sample locations.

2. Study areas

Vestnesa Ridge (~1200 m water depth) is a NW - SE trending sediment drift off NW Svalbard. Whereas the Storfjordenna area was affected directly by the pressure release after the retreat of the grounded Scandinavian Ice Sheet, causing the destabilization of gas hydrate (Serov et al., 2017), the deep-water Vestnesa Ridge gas hydrate system was only indirectly influenced by ice-sheet dynamics (Schneider et al., 2018; Himmler et al., 2019). The eastern ridge segment is characterized by numerous pockmarks actively releasing a mixture of biogenic and thermogentic methane from the seafloor (e.g., Panieri et al., 2017; Pape et al., 2020). Previous investigations showed that the pockmarks cluster along sub-vertical faults (Plaza-Faverola et al., 2015), and that seepage has likely been ongoing since the early Pleistocene (Knies et al., 2018).

Storfjordrenna is a trough mouth fan south of Svalbard, NW Barents Sea, and the bathymetry (~380 m water depth) is highly influenced by the repeated growth and retreat of grounding glaciers. Methane

release from several seafloor mounds was previously found (Serov et al., 2017). Shallow gas hydrates were recovered from various mounds, including the studied site (Hong et al., 2017;Serov et al., 2017). The seabed gas hydrate mounds are up to 500 m in diameter and 10 m high. The gas hydrate system of Storfjordrenna has been proposed to have existed for at least the last 33, 000 years (Serov et al., 2017), but there are both active and inactive mounds, reflecting the spatio-temporal heterogeneity with regards to the activities of methane transport and fluid seepage (Hong et al., 2018;Sen et al., 2018).

3. Methods

3.1 Sample collection

At the Strofjordrenna mound, seep carbonates were sampled from the seabed (S-1 and S-2, Tab. 1) using a remotely operated vehicle (ROV) by NTNU AMOS (Norwegian University of Science and Technology, Centre for Autonomous Marine Operations and Systems), and from the subsurface using gravity coring (S-3) during expedition CAGE 16-5 on board of R/V Helmer Hanssen in 2016. At Vestnesa Ridge, seafloor samples (V-1, V-2, and V-3) were collected with ROV Ægir 6000 during the R/V G.O. Sars cruise P1606 in 2016. The core sample (V-4) was retrieved during cruise with R/V Maria S. Merian, expedition MSM 57, with the deep-sea drill rig MARUM-MeBo 70 in 2016. The carbonate piece analysed here was recovered from core Mebo 127 (V-4) from a sediment depth of ~ 5m (Freudenthal and Wefer, 2013;Himmler et al., 2019).

3.2 Carbonate carbon and oxygen isotopes

Subsamples for stable carbon and oxygen isotopes ratio analyses of samples S1, S2, and V1-V3, were obtained from freshly cut surfaces with a hand-held microdrill. Powders were reacted with anhydrous phosphoric acid in a GasBench II preparation line at University of Tartu, Estonia. For stable carbon and oxygen isotopes of samples S-3 and V-4, subsamples were pulverized using an agate mortar and pestle. Other carbonate samples' were grounded, and the powders were placed in specific vials and flushed with helium gas. Afterwards, five drops of anhydrous phosphoric acid were added manually. After equilibration (>3 hours at 50°C), the liberated gas was analyzed on a Gasbench II and MAT253 Isotope Ratio Mass Spectrometer. The $\delta^{13}C$ and $\delta^{18}O$ values are reported in per mill (‰) relative to the Vienna Pee Dee belemnite (VPDB) standard. Normalization to the VPDB for carbon and oxygen isotopes was done using in-house standards. Analytical precision was estimated to be better than 0.07 ‰ for $\delta^{13}C$ and 0.08 ‰ for $\delta^{18}O$ by measuring the certified standard NBS-19. The sample reproducibility for drilled samples were ± 0.2‰ for both $\delta^{13}C$ and $\delta^{18}O$.

δ^{18}O-fluid values were calculated using the fractionation factor-temperature relationship after Kim et al. (2007b) (eq.2), and Grossman and Ku (1986) (eq. 3), assuming O-isotope equilibrium with the ambient water during carbonate formation:

$$1000 \ln a_{aragonite-water} = 17.88 \times \frac{103}{T(Kelvin)} - 31.14 \quad \text{(eq.2)}$$

$$\delta^{18}O_{water}\ (SMOW) = \delta^{18}O_{aragonite}\ (PDB) - \frac{19.7 - t\,(℃)}{4.34} \quad \text{(eq.3)}$$

3.3 Mineralogical compositions of carboantes

Mineralogical compositions were determined by X-ray diffraction (XRD) on homogenized bulk-rock powders. All samples were measured on a Bruker D8 Advance X-ray diffractometer (Cu Kα radiation in 3-75° 2θ range)(Sauer et al., 2017). Quantitative data were obtained with the Rietveld algorithm-based code, Topas-4, provided by Bruker. The displacement correction of the spectrum was made on the main quartz peak, the displacement of calcite d104 was used to estimate the amount of $MgCO_3$ mol% (mole percentage)(Goldsmith et al., 1958).

3.4 Lipid biomarker

Crust samples were crushed into centimeter-sized chips and thoroughly washed with deionized (DI) water. Loose sediment was removed from the weakly lithified carbonate nodules by washing with Milli-Q water. The cleaned chips and nodules were placed with sanitized stainless-steel tweezers into a glass beaker before slowly adding 37% HCl to dissolve the carbonate matrix. The resulting solution was extracted with organic solvents, and lipids were analyzed according to previously reported protocols (Elvert et al., 2003) with modification for alcohol derivatization and instrument setup (Niemann et al., 2005;Blees et al., 2014). Briefly, a total lipid extract (TLE) was obtained by four-step solvent extraction with decreasing polarity of the carbonate solution: dichloromethane (DCM)/methanol (MeOH) 1:2; DCM/MeOH 2:1; and two times DCM. The TLE was then saponified with 12% KOH in MeOH for 3h at 80 °C. A neutral fraction was extracted with hexane before methylation with BF_3/MeOH of the fatty acids, yielding fatty acid methyl esters (FAMEs) for gas-chromatographic (GC) analysis. Concentrations of the different fractions were examined with GC with flame ionization detection (FID) (Thermo Scientific TRACE™ Ultra, Rxi-5ms column). The identification of the individual compounds was made by gas-chromatographic mass spectrometry GC-MS (Thermo Scientific DSQ II). Similarly, compound-specific stable carbon isotope ratios were determined using an isotope ratio mass spectrometry (IRMS) unit (Thermo Scientific Delta V Advantage) coupled to a GC setup with the above-outlined specification.

Concentrations and stable carbon isotope values were verified with internal standards. $\delta^{13}C$ values are reported with an analytical error of ± 1.5 ‰.

4. Results

4.1 Mineralogy and stable carbon and oxygen isotopes

Table 2. Mineralogical compositions (weight-%) of the carbonates; Mg-calcite = magnesium-calcite.

Sample	Aragonite	Mg-calcite	Dolomite	Quartz	Plagioclase
HH 1029 (S-1)	55	23		10	3
HH 1077 (S-2)	75	10		7	2
1520GC (S-3)		60	1	23	4
P1606002 (V-1)	61	11	Trace	12	5
P1606011 (V-2)	40	2		23	11
P1606012 (V-3)	70				
Mebo 127 (V-4)	77	2		10	4

Aragonite and magnesium calcite dominate the carbonate mineralogy of the seafloor samples from both Storfjordrenna (S1-S2) and Vestnesa Ridge (V1-V3). The subseafloor sample from Storfjordrenna was comprised mainly of High-Mg-calcite, whereas the MeBo core sample from 590- 595 cmbsf was mostly aragonitic. Quartz and plagioclase comprised the main non-carbonate minerals.

The carbonate $\delta^{13}C$ values of all investigated samples ranged from −36 to −20‰, and the $\delta^{18}O$ values from 4 to 7‰ (Fig. 2).

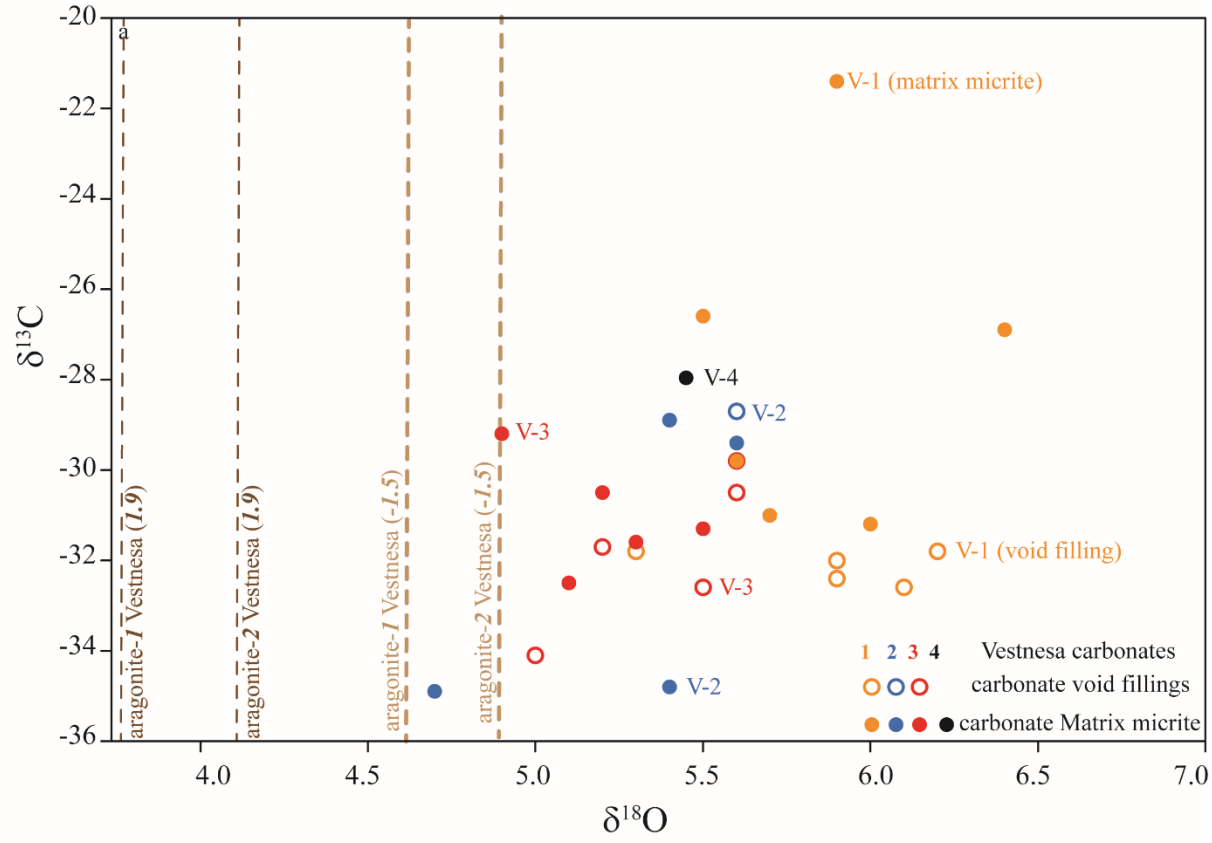
a
V-1 (matrix micrite)
V-4
V-2
V-3
V-1 (void filling)
V-3
V-2
aragonite-1 Vestnesa (-1.9)
aragonite-2 Vestnesa (-1.9)
aragonite-1 Vestnesa (-1.5)
aragonite-2 Vestnesa (-1.5)
1 2 3 4 Vestnesa carbonates
carbonate void fillings
carbonate Matrix micrite
δ13C
δ18O

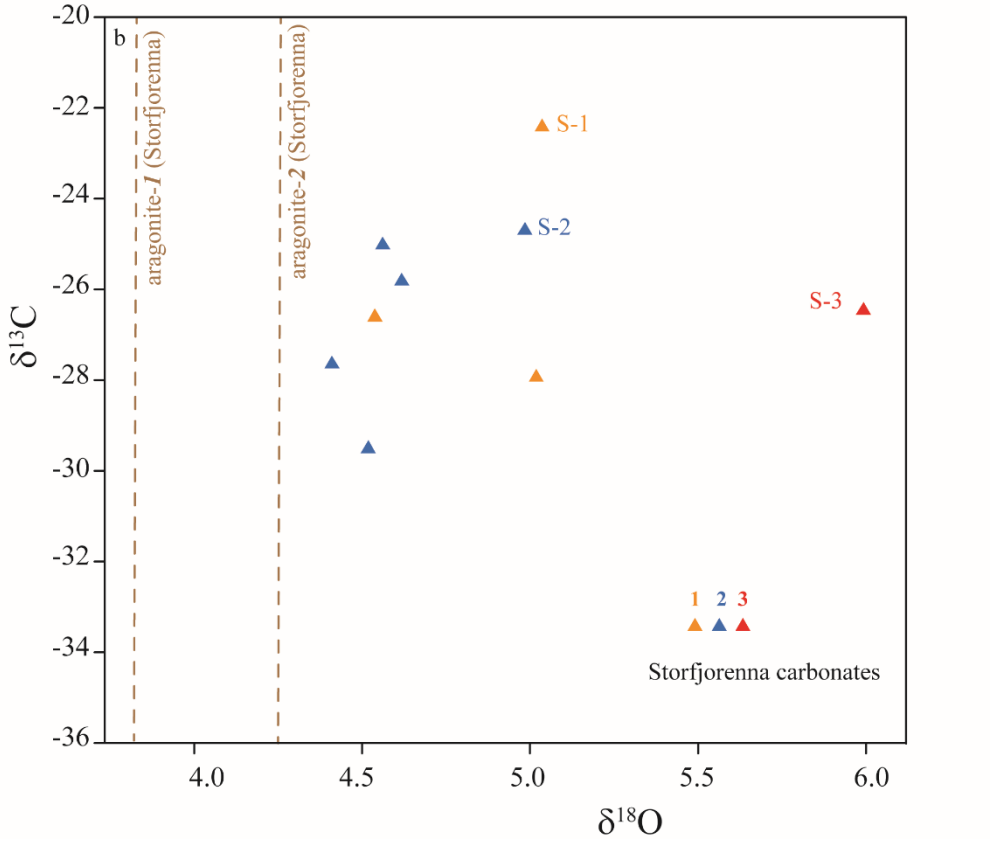
b
S-1
S-2
S-3
aragonite-1 (Storfjorenna)
aragonite-2 (Storfjorenna)
1 2 3
Storfjorenna carbonates
δ13C
δ18O

Figure 2. Carbonate stable carbon and oxygen isotope compositions. The dashed lines indicate the theoretical $\delta^{18}O$ values of aragonite-1 (Kim et al., 2007), aragonite-2 (Grossman and Ku, 1986) expected for precipitation in equilibrium with bottom water temperature.

4.2 Lipid biomarker inventory

Table 3. Lipid biomarkers contents (μg g^{-1} rock) and $\delta^{13}C$ values. (FA: fatty acids; PMI: pentamethyleicosane; Ar: archaeol; OH-Ar: sn2-hydroxylarchaeol; n.d.: not determined, content too low for accurate analysis)

	HH 1029 (S-1)		HH 1077 (S-2)		1520GC (S-3)		P1606002 (V-1)		P1606011 (V-2)		P1606012 (V-3)		Mebo 127 (V-4)	
	Contents (μg/g carbonate)	$\delta^{13}C$ (‰)	Contents (μg/g carbonate)	$\delta^{13}C$ (‰)	Contents (μg/g carbonate)	$\delta^{13}C$ (‰)	Contents (μg/g carbonate)	$\delta^{13}C$ (‰)	Contents (μg/g carbonate)	$\delta^{13}C$ (‰)	Contents (μg/g carbonate)	$\delta^{13}C$ (‰)	Contents (μg/g carbonate)	$\delta^{13}C$ (‰)
i-15-FA	0.30	-62	0.31	-76	0.42	-39	0.85	-74	0.40	-83	2.79	-91	0.76	-99
ai-15-FA	0.35	-64	0.45	-76	0.34	-33	0.85	-71	0.40	-70	0.35	-78	0.87	-90
Ar	1.00	-102	3.64	-99	0.49	-90	0.71	-99	0.67	-104	0.82	-105	11.37	-109
OH-Ar	0.16	-95	0.94	-101	0.07	-93	0.13	n.d.	0.13	-103	0.27	-105	0.49	-83
4α methyl sterol	0.04	-45	0.14	-57	0.29	-64	0.02	-52	0.03	-46	0.02	-61	0.16	-108
Diploptene	0.08	-54	0.36	-52	0.15	-46	0.17	-51	0.18	-52	0.15	n.d.	0.70	-79
crocetane	0.36	-97	1.65	--105	n.d.	n.d.	0.30	-99	0.47	-103	0.05	n.d.	1.76	-115
PMI:0	0.07	-91	0.20	-96	0.09		0.03		0.05	-100	0.03	n.d.	0.14	-113
OH-Ar/Ar	0.2		0.3		0.1		0.2		0.2		0.3		0.04	
ai-15-FA/i-15-FA	1.2		1.4		0.8		0.9		1.0		0.1		1.1	
Δδ13C Ar-OH-Ar	-6		3		3				-1				-27	

Lipid contents and compound-specific $\delta^{13}C$ values are listed in Table 3. In the fatty-acid fractions of all samples, we found the iso-/anteiso-C15:0 fatty acids with low $\delta^{13}C$-values in the range of −60 to −100 ‰. The isoprenoid glycerol diethers archaeol and *sn2*-hydroxyarchaeol were detected in the alcohol fractions of all samples. In all instances, $\delta^{13}C$-values were lower than −83‰, with the most moderate values (-109 ‰) found in sample V-4 (11.37 μg/g carbonate). The irregular isoprenoid hydrocarbon crocetane was absent in the cored nodule carbonate from Storfjordrenna 1520GC (S-3), and only minor concentrations were found in the seafloor Vestnesa crust (V-3). The irregular isoprenoid hydrocarbon 2,6,10,15,19-pentamethyleicosane (PMI) was present in all samples but concentrations in V-1 and V-2 were low (0.05 and 0.03 μg/g carbonate). The $\delta^{13}C$ of the isoprenoid hydrocarbons was always below −91 ‰.

Typical MOx related lipids such as 4α-methyl sterols and diplotene were also present in all samples, with $\delta^{13}C$ values around −50 ‰. Only the Vestnesa core carbonate (V-4) were these values were substantially lower (-108 and -79 ‰).

5. Discussion

5.1 Lipid biomarker constraints on microbial communities during carbonate precipitation

AOM communities- At cold seeps, a substantial fraction of methane is consumed in sediments by anaerobic methane-oxidizing archaea (ANME-1, -2, -3), often in association with sulfate-reducing partner bacteria of the DSS and DSB clade (Knittel and Boetius, 2009; Milucka et al., 2012; Wegener et al., 2015;Gründger et al., 2019). In oxic sediments and the water column, methane is most often consumed by the aerobic oxidation of methane (MOx) (Niemann et al., 2006; Reeburgh, 2007; Steinle et al., 2015). Specific lipid biomarkers can be used to identify the dominant microbes involved in AOM and MOx (Elvert and Niemann, 2008;Niemann and Elvert, 2008), and to tell the two main modes of methane oxidation appart. Encased in the carbonate matrix, lipids can also be used to assess the biogeochemical environment, in which the carbonates were formed (Blumenberg et al., 2004;Niemann and Elvert, 2008;Birgel et al., 2011;Himmler et al., 2015).

Diagnostic archaeal and bacterial lipids detected here were strongly depleted in ^{13}C, providing conclusive evidence for the occurrence of microbial communities performing AOM (Niemann and Elvert, 2008) as well as MOx (Elvert and Niemann, 2008). Overall, the lipid biomarker inventory is similar to seep carbonates from other seeps, including the Congo fan (Feng et al., 2010), the Gulf of Mexico (Birgel et al., 2011;Feng et al., 2014) and the South China Sea (Guan et al., 2016).

ANME-1/DSS, ANME-2/DSS, and ANME-3/DBB consortia can be distinguished based on their lipid biomarker and isotopic fingerprints (Niemann and Elvert, 2008). E.g., ANME-2/DSS consortia are characterized by the presence of crocetane, while PMIs with 4 and 5 double bonds without any higher saturated homologs were only found in ANME-3. Both ANME-2 and -3 are characterised by an elevated (typically >1.1) *sn2*-hydroxyarchaeol to archaeol (OH-ar/ar) ratio, which distinguishes them from ANME-1/DSS (Niemann and Elvert, 2008). Accordingly, sn2-hydroxyarchaeol to archaeol (OH-ar/ar) ratio of 0.1 to 0.3, such as found here in all the carbonates, suggests the presence of ANME-1/DSS. However, we also observed high concentrations of crocetane in all carbonates except for S-3 and V-3. Crocetane is abundant in ANME-2, but is typically only found in minor amounts, or not at all, in ANME-1 (Niemann and Elvert, 2008 and reference therein). Its absence, while not conclusively diagnostic, is

consistent with a ANME-1/DSS dominated seep environments (Haas et al., 2010). ANME-1 at some ancient seeps has been identified in a similar manner (Peckmann et al., 2009;Natalicchio et al., 2015). We argue that a lower stability of *sn2*-hydroxyarchaeol can explain the finding of low *sn2*-hydroxyarchaeol to archaeol ratios, i.e., *sn2*-hydroxyarchaeol loses its hydroxyl group during (early) diagenesis so that the *sn2*-hydroxyarchaeol to archaeol ratio decreases. On the other hand, the saturated hydrocarbon crocetane is probably more stable, such that its presence in carbonates indicates that the AOM community at the time of precipitation was either ANME-2 dominated or a mixture of ANME-2 and ANME-1. Only carbonate S-3 did not contain detectable amounts of crocetane, pointing to ANME-1 as the dominant AOM microbes in this sample. S-3 carbonate also contained a higher proportion of magnesium calcite, pointing to a lower methane flux at the time of precipitation as discussed in the following session. This is also consistent with a prevalence of ANME-1, which often dominate low methane flux sites (Knittel et al., 2005, Gründger et al., 2019; Yao et al., in review). It was shown previously that the dominant microbial community in relatively deep sediments (70 cmbsf) at this system was ANME-1/Seep-SRB1 (Gründger et al., 2019), which is conform with the lipid biomarker signature of the Mg-calcite dominated nodular seep carbonate (S3) recovered from 282 cmbsf. However, we also found signatures typical for MOx communities in this carbonate (see below), which begs the question whether the carbonate was indeed precipitated in deep anoxic sediments.

In contrast, the surface carbonates (S1, S2, and V1-V3), where the MDACs mineralogy is mostly aragonite, were dominated by ANME-2/DSS, or a mix of ANME-2 and ANME-1. The ANME-2/DSS and aragonite mineralogy together indicate a high methane flux regime. The lipid inventory of the cored carbonate from Vestnesa (V-4) was similar to that in the seabed carbonates, in contrast to the nodular carbonate sampled from a gravity core at Storfjordrenna. Therefore it seems probabale that this core carbonate formed at high methane flux at or close to the seafloor and was later buried by sedimentation.

The terminally branched ai-C15:0 and i-C15:0 fatty acids are diagnostic biomarkers for the SR partner bacteria (Niemann and Elvert, 2008). The ratio of ai-C15:0/i-C15:0 of ~1 in all samples point to ANME-2 associated SEEP-SRB1 or Desulfobulbus associated to ANME-3. However, we could not find the fatty acid cyC17:0ω5,6, which is indicative for the ANME-2 associated SRB, nor could we find n-C17:1ω6, which is indicative for the ANME-3 partner SRB (Niemann and Elvert, 2008 and reference therein). Nevertheless, with respect to the probable prevalence of ANME-2 in the systems (except sample S3), we suggest that the fatty acid pattern is rather indicative for the ANME-2 associated SEEP-SRB1.

MOx-communities: The seep carbonates contained high abundances of ^{13}C-depleted diplotene and 4α-methyl sterol (compound Ib in Elvert and Niemann, 2008), respectively, which were suggested

characteristic markers for Type I aerobic methanotrophs (Elvert and Niemann, 2008). MOx is a strictly aerobic process and is thus unlikely to proceed in deep (anoxic/reduced) sediment layers, but usually occurs at the sediment-water interface or in the water column, where dissolved oxygen and methane are available. Both, the seafloor and core samples at Vestnesa Ridge (V1 to V4) contained diplotene and a 4α-methyl sterol (Ib) with a moderate to substantial ^{13}C-depletion (−108 to −45‰), similar to what is observed in some of the modern seep carbonates (Birgel et al., 2011;Himmler et al., 2015;Guan et al., 2016) and in surface sediments of active cold seeps (Elvert and Niemann, 2008). Their presence in seep carbonates indicates less reducing conditions or intermittent microaerophilic conditions during carbonate precipitation (Birgel et al., 2011). The co-encasing of AOM and MOx derived lipids stronlgy suggests that the spatial distance between AOM and MOx must have been very small. Such conditions are typically found in present day systems where the methane flux rates are very high, preventing sulfate to penetrate deeper into the seafloor and thus limiting AOM to the sediment surface (Niemann et al., 2006; Lösekann et al., 2007; Elvert and Niemann, 2008). We argue that the co-occurrence of AOM and MOx derived lipids furthermore demonstrates that, at the time of carbonate precipitation, the system vigorously vented significant amounts of methane all the way into the water column. Sedimentary MOx communities typically occur when methane bypasses the AOM filter in deeper sediments (Niemann et al., 2006; Birgel et al., 2011). Sedimentary MOx is typically less effective compared to AOM because MOx demands O_2, which restricts MOx communities often to a thin microbial mat/biofilm at the sediment surface. Hence, MOx per se is able to retain only a rather limited methane flux. In contrast, in systems characterized by low methane flux, methane is typically entirely consumed in deeper sediment layers, within a well-defined SMTZ (Knittel and Boetius, 2009), so that MOx communities generally do not develop at the sediment surface. We thus interpret our findings of lipid biomarkers indicating the encapsulation of both aerobic and anaerobic methanotrophs in the same carbonate matrix to reflect past periods of high methane flux. These high-flux periods could have also been related to a non-steady state of methane flux with a not fully developed AOM community, or episodic pulses of high methane fluxes that bypass the AOM barrier and reach oxic surface sediments (Yao et al., 2019)

Our biomarker findings are also consistent with the mineralogical composition (further discussed below). Highest hopanoid contents were found in the aragonite dominated core carbonate in Vestnesa (V-4), with ANME-2/DSS most likely as the dominant consortia. Togehther, the geochemical and mineralogical evidence suggest that carbonate retrieved from the sediment cores in Vestnesa was precipitated very close to the seafloor (Himmler et al., 2019), i.e., a favourable environment for MOx, and was buried later. At this point, however, we cannot sufficiently explain the presence of of MOx-diagnostic hopanoids in sample S3. The mineralogy of this carbonate points to its precipitation in

deeper sediment layers, A persistent anoxic environment there would not support any development of MOx communities. Possibly the Mg-calcite dominated carbonate nodule precipitated in reduced sediments close enough to encase MOx-related lipids

5.2 $\delta^{13}C$ and $\delta^{18}O$ indicate gas hydrate dissociation during precipitation

Sampled carbonates from seabed and core samples from both Storjordrenna and Vestensa have without exception very negative $\delta^{13}C$ values (Fig 2). The $\delta^{13}C$-values in carbonates reflect a mixture of different carbon sources. The latter include dissolved inorganic carbon (DIC) from seawater, oxidized organic matter, and residual DIC affected by methanogenesis in addition to DIC derived from AOM (Peckmann and Thiel, 2004). AOM produces very low-$\delta^{13}C$ carbon isotope signatures because the organisms preferentially utilise a ^{13}C-depleted carbon source (i.e. methane) for biomass production, and additionally discriminate against ^{13}C during methane oxidation (Holler et al., 2009). The methane source at both sampling locations is a mixture between thermogenic and biogenic, with carbon isotope values of −48 ‰ (Serov et al., 2017), and −54 ‰ (Panieri et al., 2017), respectively. Porewater DIC $\delta^{13}C$ values of Storfjordrenna are about −28 ‰, and −32 ‰ at Vestnesa Ridge. The average $\delta^{13}C$ of organic carbon from the investigated Storfjordrenna gas hydrate mound is −26‰ (appendix), and around −25‰ (Sauer et al., in prep Vestnesa), which upon mineralization produces DIC with almost the same carbon isotope composition (Presley and Kaplan, 1968). A quantification of the relative contribution from different carbon sources to the formation of the seep carbonates is difficult based on only the $\delta^{13}C$ values of the two sources. But the $\delta^{13}C$ of the investigated seep carbonates falls into the typical $\delta^{13}C$ range for methane seep carbonates, and we suggest these carbonate have a higher contribution of methane-derived carbon vs. organic matter or seawater carbon.

Information on the oxygen isotopic composition of the fluid from which the carbonates precipitated can be deduced from carbonate $\delta^{18}O$-values (Greinert et al., 2001; Naehr et al., 2007). In turn, information on the ^{18}O-signature of the ambient water can be used to constrain the site of precipitation. Assuming that aragonite formed in isotopic equilibrium with bottom water at temperatures that are similar to those today, and aassuming a $\delta^{18}O$-value of 0 ‰ (V-SMOW) for the seawater, the theoretical $\delta^{18}O$ aragonite values would be 3.8 (Kim, 2007b; eq.2) to 4.3 ‰ (Ku, 1986; eq.3) in Storfjordrenna, and 3.8 (eq.2) or 4.9 ‰ (eq.3) at Vestnesa Ridge. Remarkably, the measured carbonate $\delta^{18}O$-values are higher than the calculated equilibrium values (Fig. 2). The higher $\delta^{18}O$ values of the authigenic carbonates suggest the incorporation of O-atoms from a ^{18}O-enriched fluid during carbonate precipitation. Such ^{18}O-enriched fluid might have different origins, e.g., from gas hydrate dissociation (Hesse and Harrison, 1981;Ussler and Paull, 1995), clay mineral dehydration (Hesse, 2003) or deep-

sourced fluids modified by mineral-water interactions (Giggenbach, 1992). The previous discussion on lipid biomarkers suggest that the most of our samples (except S-3) were formed close to the seafloor as in agreement with the mineralogy composition, the $\delta^{18}O$ did not show seawater values was also due to the ^{18}O rich fluid overwrite the incorporation of seawater $\delta^{18}O$ which is around 0 ‰. Discriminating the fluid sources based on the carbonate $\delta^{18}O$ values alone is ambiguous. Considering that gas hydrates are present in shallow sediments at both sampling areas (Serov et al., 2017;Panieri et al., 2017), it is reasonable to suggest that at least some of the ^{18}O-enrichment of the carbonate originates from fluids derived from gas hydrate dissociation.

5.3 Seep carbonate mineralogy

The carbonates recovered from the seafloor and the core, which we sampled from Vestnesa Ridge, are predominantly composed of aragonite, whereas the nodular carbonate from Storfjordrenna (S-3) was mostly high-Mg-calcite. This difference in seep carbonate mineralogy has been observed previously (Bohrmann et al., 1998;Crémière et al., 2016b), and was attributed to the formation environment (Burton, 1993;Mazzini et al., 2004). Formation of aragonite is favoured over Mg-calcite at high-sulfate and low-sulfide concentrations, and high Mg/Ca ratios (Burton, 1993;Bayon et al., 2007). Therefore, aragonite-dominated seep carbonates are expected to form closer to the seafloor because of the higher sulfate concentration in seawater compared to the deeper sediments, where sulfate is generally depleted and where calcite is preferentially formed (Bohrmann et al., 1998;Aloisi et al., 2000;Feng et al., 2014;Crémière et al., 2016b). Magnesium- calcite formation thus indicates more reducing conditions during precipitation.

Most of our samples from Vestnesa Ridge were rich in aragonite, indicating that the precipitation took place close to the seafloor. Seep carbonate precipitation at the seafloor requires a relatively high methane flux, because AOM efficiently consumes methane in deeper sediment layers in low methane flux regimes (Niemann et al., 2009;Knittel and Boetius, 2009;Yao et al., 2019). On the contrary, Mg-calcite rich samples rom Storfjordrenna formed likely at a relatively lower methane flux.

Summary and conclusion

In this study, six seep carbonate crusts and one nodule sample from two active Arctic gas hydrate sites, Storfjordrenna gas hydrate mounds and Vestnesa Ridge were investigated. The carbonate carbon and oxygen isotope ratios, mineralogy, and lipid biomarker patterns within the carbonates provided a consistent picture as to where and under which environmental conditions the carbonates were formed.

More precisely, seafloor crusts from both areas featured a ^{13}C-depleted carbon signature and elevated-$\delta^{18}O$ fluid flow during the formation. We interpreted the low carbonate $\delta^{13}C$ values in both areas to reflect mainly DIC derived from AOM, with minor contributions from organic matter degradation and water column background DIC. We attribute the relatively high carbonate $\delta^{18}O$ values to significant ^{18}O-enrichment of the carbonate precipitating fluid deriving from gas hydrate dissociation.

As revealed by the patterns of ^{13}C-depleted biomarkers, remnants of ANME-2/DSS microbial consortia were observed in all carbonate crusts, including the core carbonate from Vestnesa. Furthermore, we also found lipid biomarkers of aerobic methanotrophs in the carbonates indicating high methane fluxes, probabaly methane ebolution to the water column at the time when these carbponates were precipitated. Only in the nodular carbonate from Storfjordrenna, we observed biomarker signatures that rather point to ANME-1/DSS. In combination with the Mg-calcite dominated carbonate lattice, this implies a relatively low and diffusive fluid flow during the precipitation of these carbonates in deeper, more reduced sediments at this site. However, we also found lipids of aerobic methanotrophs in this carbonate, which appears contradictory to carbonate precipitation in deeper sediments.

Competing interests

We declare no conflict of competing interest for the co-authors

Acknowledgments

This work was supported by the Research Council of Norway through its Centre of Excellence funding scheme for CAGE, project number 223259, and partially by the NORCRUST project, grant number 255150. We thank. We thank Tõnu Martma from Univesity of Tartu for the stable isotope analysis, Schoenenberger Jasmin from NGU for the XRD analysis, the captain, crew members, and scientific team of R/V Helmer Hanssen, R/V G.O. Sars, R/V Maria S.Merian for their contribution during the research cruises CAGE16-5, P1606 and MSM57.

Reference

Aloisi, G., Pierre, C., Rouchy, J.-M., Foucher, J.-P., and Woodside, J.: Methane-related authigenic carbonates of eastern Mediterranean Sea mud volcanoes and their possible relation to gas hydrate destabilisation, Earth and Planetary Science Letters, 184, 321-338, https://doi.org/10.1016/S0012-821X(00)00322-8, 2000.

Bayon, G., Pierre, C., Etoubleau, J., Voisset, M., Cauquil, E., Marsset, T., Sultan, N., Le Drezen, E., and Fouquet, Y.: Sr/Ca and Mg/Ca ratios in Niger Delta sediments: Implications for authigenic carbonate

genesis in cold seep environments, Marine Geology, 241, 93-109, 10.1016/j.margeo.2007.03.007, 2007.
Berndt, C., Feseker, T., Treude, T., Krastel, S., Liebetrau, V., Niemann, H., Bertics, V. J., Dumke, I., Dunnbier, K., Ferre, B., Graves, C., Gross, F., Hissmann, K., Huhnerbach, V., Krause, S., Lieser, K., Schauer, J., and Steinle, L.: Temporal constraints on hydrate-controlled methane seepage off Svalbard, Science, 343, 284-287, 10.1126/science.1246298, 2014.
Bintanja, R.: The impact of Arctic warming on increased rainfall, Scientific Reports, 8, 16001, 10.1038/s41598-018-34450-3, 2018.
Birgel, D., Himmler, T., Freiwald, A., and Peckmann, J.: A new constraint on the antiquity of anaerobic oxidation of methane: Late Pennsylvanian seep limestones from southern Namibia, Geology, 36, 543, 10.1130/g24690a.1, 2008.
Birgel, D., Feng, D., Roberts, H. H., and Peckmann, J.: Changing redox conditions at cold seeps as revealed by authigenic carbonates from Alaminos Canyon, northern Gulf of Mexico, Chemical Geology, 285, 82-96, https://doi.org/10.1016/j.chemgeo.2011.03.004, 2011.
Blees, J., Niemann, H., Wenk, C. B., Zopfi, J., Schubert, C. J., Jenzer, J. S., Veronesi, M., and Lehman, M. F.: Bacterial methanotrophs drive the formation of a seasonal anoxic benthic nepheloid layer in an alpine lake, Limnology and Oceanography, 59, 1410-1420, 10.4319/lo.2014.59.4.141E, 2014.
Blumenberg, M., Seifert, R., Reitner, J., Pape, T., and Michaelis, W.: Membrane lipid patterns typify distinct anaerobic methanotrophic consortia, PNAS, 101, 11111–11116, 2004.
Blumenberg, M.: Microbial Chemofossils in Specific Marine Hydrothermal and Methane Cold Seep Settings, in: The Vent and Seep Biota, Topics in Geobiology, 73-106, 2010.
Bohrmann, G., Greinert, J., Suess, E., and Torres, M.: Authigenic carbonates from the Cascadia subduction zone and their relation to gas hydrate stability, Geology, 26, 647-650, 10.1130/0091-7613(1998)026<0647:ACFTCS>2.3.CO;2 %J Geology, 1998.
Bünz, S., Polyanov, S., Vadakkepuliyambatta, S., Consolaro, C., and Mienert, J.: Active gas venting through hydrate-bearing sediments on the Vestnesa Ridge, offshore W-Svalbard, Marine Geology, 332-334, 189-197, 10.1016/j.margeo.2012.09.012, 2012.
Burton, E. A.: Controls on marine carbonate cement mineralogy: review and reassessment, Chemical Geology, 105, 163-179, https://doi.org/10.1016/0009-2541(93)90124-2, 1993.
Chen, Y., Ussler, W., Haflidason, H., Lepland, A., Rise, L., Hovland, M., and Hjelstuen, B. O.: Sources of methane inferred from pore-water δ13C of dissolved inorganic carbon in Pockmark G11, offshore Mid-Norway, Chemical Geology, 275, 127-138, https://doi.org/10.1016/j.chemgeo.2010.04.013, 2010.
Collins, M. *et al*. In Climate Change 2013: *The PhysicalScience Basis. Contribution of working group I to the fifth assessment report of the Intergovernmental Panel on Climate Change* (eds Stocker, T. F. *et al*.)1029–1136 (Cambridge Univ. Press, 2013).
Crémière, A., Lepland, A., Chand, S., Sahy, D., Condon, D. J., Noble, S. R., Martma, T., Thorsnes, T., Sauer, S., and Brunstad, H.: Timescales of methane seepage on the Norwegian margin following collapse of the Scandinavian Ice Sheet, Nat Commun, 7, 11509, 10.1038/ncomms11509, 2016a.
Crémière, A., Lepland, A., Chand, S., Sahy, D., Kirsimäe, K., Bau, M., Whitehouse, M. J., Noble, S. R., Martma, T., Thorsnes, T., and Brunstad, H.: Fluid source and methane-related diagenetic processes recorded in cold seep carbonates from the Alvheim channel, central North Sea, Chemical Geology, 432, 16-33, https://doi.org/10.1016/j.chemgeo.2016.03.019, 2016b.
Dickens, G. R., O'Neil, J. R., Rea, D. K., and Owen, R. M.: Dissociation of oceanic methane hydrate as a cause of the carbon isotope excursion at the end of the Paleocene, Paleoceanography, 10, 965-971, 10.1029/95pa02087, 1995.

Dickens, G. R.: Rethinking the global carbon cycle with a large, dynamic and microbially mediated gas hydrate capacitor, Earth and Planetary Science Letters, 213, 169-183, 10.1016/s0012-821x(03)00325-x, 2003.
Elvert, M., Boetius, A., Knittel, K., and Jørgensen, B. B.: Characterization of Specific Membrane Fatty Acids as Chemotaxonomic Markers for Sulfate-Reducing Bacteria Involved in Anaerobic Oxidation of Methane, Geomicrobiology Journal, 20, 403-419, 10.1080/01490450303894, 2003.
Elvert, M., and Niemann, H.: Occurrence of unusual steroids and hopanoids derived from aerobic methanotrophs at an active marine mud volcano, Organic Geochemistry, 39, 167-177, 10.1016/j.orggeochem.2007.11.006, 2008.
Feng, D., Chen, D., Peckmann, J., and Bohrmann, G.: Authigenic carbonates from methane seeps of the northern Congo fan: Microbial formation mechanism, Marine and Petroleum Geology, 27, 748-756, 10.1016/j.marpetgeo.2009.08.006, 2010.
Feng, D., Birgel, D., Peckmann, J., Roberts, H. H., Joye, S. B., Sassen, R., Liu, X. L., Hinrichs, K. U., and Chen, D.: Time integrated variation of sources of fluids and seepage dynamics archived in authigenic carbonates from Gulf of Mexico Gas Hydrate Seafloor Observatory, Chemical Geology, 385, 129-139, 10.1016/j.chemgeo.2014.07.020, 2014.
Freudenthal, T., and Wefer, G.: Drilling cores on the sea floor with the remote-controlled sea floor drilling rig MeBo, Geosci. Instrum. Method. Data Syst., 2, 329-337, 10.5194/gi-2-329-2013, 2013.
Giggenbach, W. F.: Isotopic shifts in waters from geothermal and volcanic systems along convergent plate boundaries and their origin, Earth and Planetary Science Letters, 113, 495-510, https://doi.org/10.1016/0012-821X(92)90127-H, 1992.
Goldsmith, J. R., Graf, D. L., Chodos, A. A., Joensuu, O. I., and Mcvicker, L. D.: Relation between lattice constants and composition of Ca-Mg carbonates, American Mineralogist, 43, 84-101, 1958.
Greinert, J., Bohrmann, G., and Suess, E.: Gas Hydrate-Associated Carbonates and Methane-Venting at Hydrate Ridge: Classification, Distribution, and Origin of Authigenic Lithologies, in: Natural Gas Hydrates: Occurrence, Distribution, and Detection, 99-113, 2001.
Grossman, E. L., and Ku, T.-L.: Oxygen and carbon isotope fractionation in biogenic aragonite: Temperature effects, Chemical Geology: Isotope Geoscience section, 59, 59-74, https://doi.org/10.1016/0168-9622(86)90057-6, 1986.
Gründger, F., Carrier, V., Svenning, M. M., Panieri, G., Vonnahme, T. R., Klasek, S., and Niemann, H.: Methane-fuelled biofilms predominantly composed of methanotrophic ANME-1 in Arctic gas hydrate-related sediments, Sci Rep, 9, 9725, 10.1038/s41598-019-46209-5, 2019.
Guan, H., Feng, D., Wu, N., and Chen, D.: Methane seepage intensities traced by biomarker patterns in authigenic carbonates from the South China Sea, Organic Geochemistry, 91, 109-119, https://doi.org/10.1016/j.orggeochem.2015.11.007, 2016.
Haas, A., Peckmann, J., Elvert, M., Sahling, H., and Bohrmann, G.: Patterns of carbonate authigenesis at the Kouilou pockmarks on the Congo deep-sea fan, Marine Geology, 268, 129-136, 10.1016/j.margeo.2009.10.027, 2010
Han, Y.-J., and Aizenberg, J.: Effect of Magnesium Ions on Oriented Growth of Calcite on Carboxylic Acid Functionalized Self-Assembled Monolayer, Journal of the American Chemical Society, 125, 4032-4033, 10.1021/ja034094z, 2003.
Hesse, R., and Harrison, W. E.: Gas hydrates (clathrates) causing pore-water freshening and oxygen isotope fractionation in deep-water sedimentary sections of terrigenous continental margins, Earth and Planetary Science Letters, 55, 453-462, https://doi.org/10.1016/0012-821X(81)90172-2, 1981.

Hesse, R.: Pore water anomalies of submarine gas-hydrate zones as tool to assess hydrate abundance and distribution in the subsurface: What have we learned in the past decade?, Earth-Science Reviews, 61, 149-179, https://doi.org/10.1016/S0012-8252(02)00117-4, 2003.
Himmler, T., Birgel, D., Bayon, G., Pape, T., Ge, L., Bohrmann, G., and Peckmann, J.: Formation of seep carbonates along the Makran convergent margin, northern Arabian Sea and a molecular and isotopic approach to constrain the carbon isotopic composition of parent methane, Chemical Geology, 415, 102-117, 10.1016/j.chemgeo.2015.09.016, 2015.
Himmler, T., Sahy, D., Martma, T., Bohrmann, G., Plaza-Faverola, A., Bünz, S., Condon, D. J., Knies, J., and Lepland, A.: A 160,000-year-old history of tectonically controlled methane seepage in the Arctic, Science Advances, 5, eaaw1450, 10.1126/sciadv.aaw1450, 2019.
Holler, T., Wegener, G., Knittel, K., Boetius, A., Brunner, B., Kuypers, M. M., and Widdel, F.: Substantial (13) C/(12) C and D/H fractionation during anaerobic oxidation of methane by marine consortia enriched in vitro, Environ Microbiol Rep, 1, 370-376, 10.1111/j.1758-2229.2009.00074.x, 2009.
Hong, W. L., Torres, M. E., Carroll, J., Cremiere, A., Panieri, G., Yao, H., and Serov, P.: Seepage from an arctic shallow marine gas hydrate reservoir is insensitive to momentary ocean warming, Nat Commun, 8, 15745, 10.1038/ncomms15745, 2017.
Hong, W. L., Torres, M. E., Portnov, A., Waage, M., Haley, B., and Lepland, A.: Variations in Gas and Water Pulses at an Arctic Seep: Fluid Sources and Methane Transport, Geophysical Research Letters, 10.1029/2018gl077309, 2018.
Kennett, J. P.: Carbon isotopic evidence for methane hydrate instability during quaternary interstadials, Science, 288, 128-133, 10.1126/science.288.5463.128, 2000.
Kim, S.-T., O'Neil, J. R., Hillaire-Marcel, C., and Mucci, A.: Oxygen isotope fractionation between synthetic aragonite and water: Influence of temperature and Mg2+ concentration, Geochimica et Cosmochimica Acta, 71, 4704-4715, 10.1016/j.gca.2007.04.019, 2007.
Knies, J., Daszinnies, M., Plaza-Faverola, A., Chand, S., Sylta, Ø., Bünz, S., Johnson, J. E., Mattingsdal, R., and Mienert, J.: Modelling persistent methane seepage offshore western Svalbard since early Pleistocene, Marine and Petroleum Geology, 91, 800-811, 10.1016/j.marpetgeo.2018.01.020, 2018.
Knittel, K., Lösekann, T., Boetius, A., Kort, R. and Amann, R.: Diversity and distribution of methanotrophic archaea at cold seeps, Appl. Environ. Microbiol., 71(1), 467–479, 2005.
Knittel, K., and Boetius, A.: Anaerobic oxidation of methane: progress with an unknown process, Annu Rev Microbiol, 63, 311-334, 10.1146/annurev.micro.61.080706.093130, 2009.
MacDonald, I. R., Guinasso , N. L., Jr., Sassen, R., Brooks, J. M., Lee, L., and Scott, K. T.: Gas hydrate that breaches the sea floor on the continental slope of the Gulf of Mexico, Geology, 22, 699-702, 10.1130/0091-7613(1994)022<0699:Ghtbts>2.3.Co;2, 1994.
Mazzini, A., Ivanov, M. K., Parnell, J., Stadnitskaia, A., Cronin, B. T., Poludetkina, E., Mazurenko, L., and van Weering, T. C. E.: Methane-related authigenic carbonates from the Black Sea: geochemical characterisation and relation to seeping fluids, Marine Geology, 212, 153-181, 10.1016/j.margeo.2004.08.001, 2004.
Milucka, J., Ferdelman, T. G., Polerecky, L., Franzke, D., Wegener, G., Schmid, M., Lieberwirth, I., Wagner, M., Widdel, F., and Kuypers, M. M.: Zero-valent sulphur is a key intermediate in marine methane oxidation, Nature, 491, 541-546, 10.1038/nature11656, 2012.
Naehr, T. H., Eichhubl, P., Orphan, V. J., Hovland, M., Paull, C. K., Ussler, W., Lorenson, T. D., and Greene, H. G.: Authigenic carbonate formation at hydrocarbon seeps in continental margin sediments: A comparative study, Deep Sea Research Part II: Topical Studies in Oceanography, 54, 1268-1291, https://doi.org/10.1016/j.dsr2.2007.04.010, 2007.

Natalicchio, M., Peckmann, J., Birgel, D., and Kiel, S.: Seep deposits from northern Istria, Croatia: A first glimpse into the Eocene seep fauna of the Tethys region, Geological Magazine, 152, 444-459, 10.1017/S0016756814000466, 2015.
Niemann, H., Elvert, M., Hovland, M., Orcutt, B., Judd, A., Suck, I., Gutt, J., Joye, S., Damm, E., Finster, K., and Boetius, A.: Methane emission and consumption at a North Sea gas seep (Tommeliten area), Biogeosciences, 2, 335-351, 2005.
Niemann, H., and Elvert, M.: Diagnostic lipid biomarker and stable carbon isotope signatures of microbial communities mediating the anaerobic oxidation of methane with sulphate, Organic Geochemistry, 39, 1668-1677, 10.1016/j.orggeochem.2007.11.003, 2008.
Niemann, H., Fischer, D., Graffe, D., Knittel, K., Montiel, A., Heilmayer, O., Nothen, K., Pape, T., Kasten, S., Bohrmann, G., Boetius, A., and Gutt, J.: Biogeochemistry of a low-activity cold seep in the Larsen B area, western Weddell Sea, Antarctica, Biogeosciences, 6, 2383-2395, 10.1594/PANGAEA.702077, 2009.
Panieri, G., Bünz, S., Fornari, D. J., Escartin, J., Serov, P., Jansson, P., Torres, M. E., Johnson, J. E., Hong, W., Sauer, S., Garcia, R., and Gracias, N.: An integrated view of the methane system in the pockmarks at Vestnesa Ridge, 79°N, Marine Geology, 390, 282-300, 10.1016/j.margeo.2017.06.006, 2017.
Pape, T., Bünz, S., Hong, W.-L., Torres, M. E., Riedel, M., Panieri, G., Lepland, A., Hsu, C.-W., Wintersteller, P., Wallmann, K., Schmidt, C., Yao, H., and Bohrmann, G.: Origin and Transformation of Light Hydrocarbons Ascending at an Active Pockmark on Vestnesa Ridge, Arctic Ocean, Journal of Geophysical Research: Solid Earth, 125, e2018JB016679, 10.1029/2018jb016679, 2020.
Peckmann, J., and Thiel, V.: Carbon cycling at ancient methane-seeps, Chemical Geology, 205, 443-467, 10.1016/j.chemgeo.2003.12.025, 2004.
Peckmann, J., Birgel, D., and Kiel, S.: Molecular fossils reveal fluid composition and flow intensity at a Cretaceous seep, Geology, 37, 847-850, 10.1130/G25658A.1, 2009.
Pierre, C., and Fouquet, Y.: Authigenic carbonates from methane seeps of the Congo deep-sea fan, Geo-Marine Letters, 27, 249-257, 10.1007/s00367-007-0081-3, 2007.
Plaza-Faverola, A., Bünz, S., Johnson, J. E., Chand, S., Knies, J., Mienert, J., and Franek, P.: Role of tectonic stress in seepage evolution along the gas hydrate-charged Vestnesa Ridge, Fram Strait, Geophysical Research Letters, 42, 733-742, 10.1002/2014gl062474, 2015.
Presley, B. J., and Kaplan, I. R.: Changes in dissolved sulfate, calcium and carbonate from interstitial water of near-shore sediments, Geochimica et Cosmochimica Acta, 32, 1037-1048, https://doi.org/10.1016/0016-7037(68)90106-3, 1968.
Reitner, J., Peckmann, J., Blumenberg, M., Michaelis, W., Reimer, A., and Thiel, V.: Concretionary methane-seep carbonates and associated microbial communities in Black Sea sediments, Palaeogeography, Palaeoclimatology, Palaeoecology, 227, 18-30, 10.1016/j.palaeo.2005.04.033, 2005.
Sauer, S., Crémière, A., Knies, J., Lepland, A., Sahy, D., Martma, T., Noble, S. R., Schönenberger, J., Klug, M., and Schubert, C. J.: U-Th chronology and formation controls of methane-derived authigenic carbonates from the Hola trough seep area, northern Norway, Chemical Geology, 470, 164-179, 10.1016/j.chemgeo.2017.09.004, 2017.
Sauer, S., Hong, W. L., Yao., H., Knies, J., Lepalnd, A., Klug, M., Eichinger, F., Himmler, T., Panieri, G., Schubert, C. J.: Methane transport and sources in shallow sediments at an Active Cold seep site on Vestnesa Ridge, 79N-insights from carbonat isotopes of methane, dissolved inorganic carbon, total organic carbon and lipid biomarkers, in prep.

Schneider, A., Panieri, G., Lepland, A., Consolaro, C., Crémière, A., Forwick, M., Johnson, J. E., Plaza-Faverola, A., Sauer, S., and Knies, J.: Methane seepage at Vestnesa Ridge (NW Svalbard) since the Last Glacial Maximum, Quaternary Science Reviews, 193, 98-117, 10.1016/j.quascirev.2018.06.006, 2018.
Sen, A., Åström, E. K. L., Hong, W.-L., Portnov, A., Waage, M., Serov, P., Carroll, M. L., and Carroll, J.: Geophysical and geochemical controls on the megafaunal community of a high Arctic cold seep, Biogeosciences Discussions, 1-52, 10.5194/bg-2017-540, 2018.
Serov, P., Vadakkepuliyambatta, S., Mienert, J., Patton, H., Portnov, A., Silyakova, A., Panieri, G., Carroll, M. L., Carroll, J., Andreassen, K., and Hubbard, A.: Postglacial response of Arctic Ocean gas hydrates to climatic amelioration, Proc Natl Acad Sci U S A, 10.1073/pnas.1619288114, 2017.
Ussler, W., and Paull, C. K.: Effects of ion exclusion and isotopic fractionation on pore water geochemistry during gas hydrate formation and decomposition, Geo-Marine Letters, 15, 37-44, 10.1007/BF01204496, 1995.
Wegener, G., Krukenberg, V., Riedel, D., Tegetmeyer, H. E., and Boetius, A.: Intercellular wiring enables electron transfer between methanotrophic archaea and bacteria, Nature, 526, 587-590, 10.1038/nature15733, 2015.
Yao, H., Hong, W. L., Panieri, G., Sauer, S., Torres, M. E., Lehmann, M. F., Gründger, F., and Niemann, H.: Fracture-controlled fluid transport supports microbial methane-oxidizing communities at Vestnesa Ridge, Biogeosciences, 16, 2221-2232, 10.5194/bg-16-2221-2019, 2019.

Yao, H., Niemann, H., Panieri, G.: Multi-proxy aproach to unravel methane emission history of an Arctic cold seep, Quaternary Sciences Reviews (in review).

Data

Organic carbon isotope

Sample name core/depth	$\delta^{13}C$ (permil, VPDB)	Amt% C
911 GC 13	-24.72	2.62
911 GC 20	-25.05	1.89
911 GC 30	-25.46	1.57
911 GC 39	-25.73	1.80
911 GC 48	-26.48	1.51
911 GC 63	-25.82	1.77
911 GC 72	-27.44	1.57
911 GC 83A	-26.32	1.80